Enclosure 2

WEC Non-Proprietary Document: WBT-D-3807 NP-Enclosure, :Watts Bar Unit 2 Evaluation for Tube Vibration Induced Fatigue WCAP 17309-NP,Revision 1" dated February 2012.

Westinghouse Non-Proprietary Class 3

WCAP-17309-NP
Revision 1

February 2012

WATTS BAR UNIT 2 EVALUATION FOR TUBE VIBRATION INDUCED FATIGUE

WCAP-17309-NP
Revision 1

WATTS BAR UNIT 2 EVALUATION FOR TUBE VIBRATION INDUCED FATIGUE

February 2012

Author: *
D. J. Saffer
Steam Generator Design & Analysis

Reviewer: *
J. M. Hall
Steam Generator Management & Modification Programs

Approved: *
D. Merkovsky, Manager
Steam Generator Design & Analysis

**Electronically approved records are authenticated in the electronic document management system*

Westinghouse Electric Company LLC
1000 Westinghouse Drive
Cranberry Township, PA 16066

TABLE OF CONTENTS

LIST OF TABLES

LIST OF FIGURES

ABSTRACT

On July 15, 1987, a steam generator tube rupture event occurred at the North Anna Unit 1 plant. The cause of the tube rupture has been determined to be high cycle fatigue. The source of the loads associated with the fatigue mechanism is a combination of a mean stress level in the tube with a superimposed alternating stress. The mean stress is the result of applied loading, manufacturing-induced residual stress and denting, such that the denting causes a fixed boundary condition, of the tube at the top tube support plate, while the alternating stress is due to out-of-plane deflection of the tube U-bend attributed to flow-induced vibration. For tubes without AVB support, local flow peaking effects are a significant contributor to tube vibration amplitudes.

This report documents the evaluation for tube vibration-induced fatigue for the Westinghouse Model D3 steam generators at Watts Bar Unit 2 for susceptibility to fatigue-induced cracking of the type experienced at North Anna Unit 1. The evaluation utilizes design operating conditions specific to Watts Bar Unit 2 to account for the plant-specific nature of the tube loading and response. The evaluation also includes reviews of eddy current test data for Watts Bar Unit 2 to establish AVB locations. This report provides background of the event which occurred at North Anna Unit 1, the criteria for fatigue assessment, a summary of test data which support the analytical approach, field measurement results showing AVB positions, thermal-hydraulic analysis results, and calculations to determine tube mean stress, stability ratio, tube stress ratio, and accumulated fatigue usage. This evaluation concludes that four of the Watts Bar Unit 2 tubes are potentially susceptible to fatigue, and have been recommended for corrective action.

SUMMARY OF ABBREVIATIONS

ASME	-	American Society of Mechanical Engineers
ATHOS	-	Analysis of the Thermal Hydraulics of Steam Generators
AVB	-	Anti-Vibration Bar
AVT	-	All Volatile Treatment
ECT	-	Eddy Current Test
EPRI	-	Electric Power Research Institute
FFT	-	Fast Fourier Transform
FLOVIB	-	Flow-Induced Vibrations
MEVF	-	Modal Effective Void Fraction
OD	-	Outside Diameter
RMS	-	Root Mean Square
SR	-	Stability Ratio
TSP	-	Tube Support Plate
°F	-	degrees Fahrenheit
hr	-	hour
ksi	-	measure of stress - 1000 pounds per square inch
lb	-	pound force
mil	-	0.001 inch
MW	-	megawatt
psi	-	measure of stress - pounds per square inch
psia	-	measure of pressure – absolute

1 INTRODUCTION

This report documents the evaluation for tube vibration induced fatigue for the Westinghouse Model D3 steam generators at Watts Bar Unit 2 for susceptibility to fatigue-induced cracking of the type experienced at North Anna Unit 1 in July, 1987. The evaluation includes three-dimensional flow analysis of the tube bundle, air tests performed to support the vibration analytical procedure, field measurements to establish AVB locations, structural and vibration analysis of selected tubes, and fatigue usage calculations to predict cumulative usage for critical tubes. The evaluation utilizes operating conditions specific to Watts Bar Unit 2 in order to account for plant-specific features of the tube loading and response.

Section 2 of the report provides a summary of the Watts Bar Unit 2 evaluation results and overall conclusions. Section 3 provides background of the tube rupture event, which occurred at North Anna Unit 1 including results of the examination of the ruptured tube and a discussion of the rupture mechanism. The criteria for predicting the fatigue usage for tubes having an environment conducive to this type of rupture are discussed in Section 4. Section 5 provides a summary of test data, which supports the analytical vibration evaluation of the candidate tubes. A summary of field measurements used to determine AVB locations and to identify unsupported tubes is provided in Section 6. Section 7 provides the results of a thermal-hydraulic analysis to establish flow field characteristics at the top support plate which are subsequently used to assist in identifying tubes which may be dynamically unstable. Section 8 presents an update of the methodology originally used to evaluate the tube rupture at North Anna Unit 1 specifically addressing flow peaking considerations. The final section, Section 9, presents results of the structural and vibration assessment. This section describes tube mean stress, stability ratio and stress ratio distributions, and accumulated fatigue usage for the Watts Bar Unit 2 steam generator small radius U-tubes. The conclusion of this evaluation is that four tubes in Steam Generator 4 at Watts Bar Unit 2 are potentially susceptible to fatigue, and have been recommended for corrective action.

This report, WCAP-17309-NP Revision 1, is the non-proprietary version of WCAP-17309-P Revision 1. The non-proprietary version of WCAP-17309-P Revision 0 was never published.

1.1 RECORD OF REVISIONS

Revision	Date	Description
0	N/A	This report was never published.
1	February 2012	This is the first issue of WCAP-17309-NP based on WCAP-17309-P Revision 1.

2 SUMMARY AND CONCLUSIONS

The four Westinghouse Model D3 steam generators at Watts Bar Unit 2 have been evaluated for the susceptibility to a fatigue rupture of the type experienced at North Anna Unit 1 in Steam Generator C at the tube located in Row 9 Column 51 (R9C51). The evaluation used Eddy Current Test (ECT) data acquired during the February 2010 pre-service inspection and interpreted by Westinghouse.

2.1 BACKGROUND

The initiation of the circumferential crack in the tube at the top of the top tube support plate at North Anna 1 has been attributed to limited displacement, fluid elastic instability. This condition is believed to have prevailed in the R9C51 tube since the tube experienced denting, such that the denting causes a fixed boundary condition, at the support plate. A combination of the conditions present was concluded to have led to the rupture. The tube was not supported by an anti-vibration bar (AVB), had a higher flow field due to local flow peaking as a result of non-uniform insertion depths of AVBs, had reduced damping due to denting at the top support plate, and had reduced fatigue properties due to the environment of the all volatile treatment (AVT) chemistry of the secondary water and the additional mean stress from the denting.

2.2 EVALUATION CRITERIA

The criteria established to provide a fatigue usage less than 1.0 for a finite period of time (i.e., 40 years) is a 10% reduction in stability ratio that provides at least a 58% reduction in stress amplitude (to < 4.0 ksi) for a Row 9 tube in the North Anna 1 steam generators (SG's). This reduction is required to produce a fatigue usage of < 0.021 per year for a Row 9 tube in North Anna and therefore is greater than the 40 year fatigue design basis. This same fatigue criteria is applied as the principal criteria in the evaluation of the Watts Bar Unit 2 tubing.

The fluid elastic stability ratio is the ratio of the effective velocity divided by the critical velocity. A value greater than unity (1.0) indicates instability. The stress ratio is the expected stress amplitude in a Watts Bar Unit 2 tube divided by the stress amplitude for the North Anna 1, R9C51 tube.

Displacements are computed for unsupported U-bend tubes in Rows 8 through 12 using relative stability ratios to R9C51 of North Anna 1 and an appropriate power law relationship based on instability displacement versus flow velocity. Different U-bend radius tubes and tube sizes have different stiffness and frequency and, therefore, different stress and fatigue usage per year than the Row 9 North Anna tube. These effects are accounted for in a stress ratio technique. The stress ratio is formulated so that a stress ratio of 1.0 or less produces acceptable stress amplitudes and fatigue usage for the Watts Bar Unit 2 tubing assuming that the tubing remains in service for the entire plant operating license at the operating conditions for the reference fuel cycle analyzed. Therefore, a stress ratio less than 1.0 provides the next level of acceptance criteria for unsupported tubes for which the relative stability ratio, including flow peaking, exceed 0.9.

The stability ratios for Watts Bar Unit 2 tubing, the corresponding stress and amplitude, and the resulting cumulative fatigue usage must be evaluated relative to the ruptured tube at Row 9 Column 51, North Anna 1, Steam Generator C, for two reasons. The local effect on the flow field due to AVB insertion

depths is not calculable with available analysis techniques and is determined by test as a ratio between two AVB configurations. In addition, an analysis and examination of the ruptured tube at North Anna 1 provided a range of initiating stress amplitudes, but could only bound the possible stability ratios that correspond to these stress amplitudes. Therefore, to minimize the influence of uncertainties, the evaluation of Watts Bar Unit 2 tubing has been based on relative stability ratios, relative flow peaking factors, and relative stress ratios.

The criteria for establishing that a tube has support from an AVB, is that it must have at least one-sided AVB support present at the tube centerline. The criteria are based on test results, which show that one-sided AVB support is sufficient to limit the vibration amplitude for fluid elastic excitation. AVB support is established by analysis of eddy current test (ECT) measurements and is a key factor in determining the local flow peaking factors. The local flow peaking produces increased local velocities, which cause an increase in stability ratio. A small change in the stability ratio causes a significant change in stress amplitude. The relative flow peaking factors of Watts Bar Unit 2 tubing without direct AVB support have been determined by test. These flow peaking factors, normalized to the North Anna R9C51 peaking, are applied to relative stability ratios determined by 3-D tube bundle flow analysis, to obtain the combined relative stability ratio used in the stress ratio determination.

2.3 DENTING EVALUATION

For conservatism in the evaluation, all of the tubes evaluated are postulated to be dented. The effect of denting on the fatigue usage of the tube has been conservatively maximized by assuming the maximum effect of mean stress in the tube fatigue usage evaluation and by incorporating reduced damping in the tube vibration evaluation.

2.4 AVB INSERTION DEPTHS

The Watts Bar Unit 2 SGs have two sets of chrome plated, Alloy 600 AVBs with a square cross section. The design depth of insertion, such that the apex of the AVB is tangent with the tube centerline at the row apex, is Row 10 for the 'inner' or lower AVBs and Row 21 for the 'outer' or upper AVBs. The AVBs provide a nominal total clearance between a tube without ovality and the surrounding AVBs of [ ]^{a,c} inch. Since the purpose of this analysis is to evaluate the potentially unsupported tubes at or near the point of maximum AVB insertion, only the dimensions and ECT data pertaining to the inner AVBs are required.

The ECT data were analyzed by Westinghouse to identify the number of tube/AVB intersections and the location of these intersections relative to the apex of a given tube. This information was used in calculations to determine the deepest penetration of a given AVB into the tube bundle. For the area of interest in the Watts Bar Unit 2 steam generators, the AVB support of the tube can normally be verified if ECT data shows both legs of the lower AVB, one on each side (hot leg - cold leg) of the U-bend. This is the preferred method of establishing tube support.

If only the apex of a Watts Bar Unit 2 AVB assembly is near or touching the apex of a tube U-bend, only one AVB signal may be seen. In this case, adequate tube support cannot be assumed without supplemental input. Support can be determined if 'projection' calculations based on AVB intercepts of higher row number tubes in the same and adjacent columns verify insertion depth to a point below the

tube centerline. Maps of the AVB insertion depths for Watts Bar Unit 2 are shown in Figures 6-1 thru 6-4. The AVB maps list the results of the 'projection' calculations for the column by using each tube in the column for which suitable data exist to make a projection. At tube locations where flow peaking effects could be significant, determination of only tube support conditions may not be sufficient to adequately define flow peaking factors. Flow peaking factor can, in some cases, [

].[a,c]

2.5 FLOW PEAKING FACTORS

Past tests that were performed for the North Anna Unit 1 evaluation are sufficient to model Watts Bar Unit 2 tube and AVB geometries to determine the flow peaking factors for various AVB configurations relative to the North Anna R9C51 peaking factor. The test results were used to define an upper bound of the ratio relative to the R9C51 configuration.

2.6 TUBE VIBRATION EVALUATION

The calculation of relative stability ratios for Watts Bar Unit 2 makes use of detailed tube bundle flow field information computed by the ATHOS steam generator thermal/hydraulic analysis code. Code output includes three-dimensional distributions of secondary side velocity, density, and void fractions, along with primary fluid and tube wall temperatures. Distributions of these parameters have been generated for every tube of interest in the Watts Bar Unit 2 tube bundles based on anticipated full power operating conditions. This information was factored into the tube vibration analysis leading to the relative stability ratios.

Relative stability ratios of Watts Bar Unit 2 (Rows 8 through 12) tubing versus R9C51 of North Anna 1 are plotted in Figure 9-5. These relative stability ratios include relative flow peaking factors and assume the tube is unsupported. The stress ratios for Watts Bar Unit 2 are given in Figure 9-6 for tubes in the dented condition and also assume that the tubes are not supported by the AVBs. These figures include the relative flow peaking effect, and are calculated based on clamped tube conditions with denting (with deformation) at the top tube support plate. Table 9-3 contains a list of tubes with significant flow peaking or large stress ratios. Two Row 12 tubes in SG 4 have stress ratios greater than 1.0 (R12C106 and R12C109). Two other Row 12 tubes in SG 4 have stress ratios that approach 1.0 (R12C107 and R12C108). All four tube of these tubes are recommended for corrective action.

Of the remaining unsupported tubes in all four Unit 2 SGs, the highest stress ratio is 0.863 and occurs at location R11C110 of SG 4. The maximum fatigue usage for this tube is calculated by combining the usage for Unit 2 operating history to date (no usage) plus the projected usage for future operation. Assuming operation at 100% power with the currently defined parameters and plugging values for 100% availability, the maximum calculated fatigue usage is 0.254.

A summary listing of the unsupported critical tubes and pertinent vibration parameters is given in Table 9-3.

2.7 OVERALL CONCLUSION

As a result of the evaluation, four tubes in SG 4 have been recommended for preventive action since the stress ratios and total cumulative fatigue usage of all the unsupported U-bend tubes either approach or exceed the limiting value of 1.0. The rest of the tubes remaining in service in the Watts Bar Unit 2 steam generators are not expected to be susceptible to high-cycle fatigue rupture at the top tube support plate in a manner similar to the rupture which occurred at North Anna Unit 1, assuming that the plugging levels remain at or below 10% when evaluated for either the normal power conditions or the MUR uprate power conditions.

3 BACKGROUND

On July 15, 1987, a steam generator tube rupture occurred at the North Anna Unit 1. The ruptured tube was determined to be the Row 9 Column 51 tube in Steam Generator C. The location of the opening was found to be at the top tube support plate on the cold leg side of the tube and was circumferential in orientation with a 360-degree extent.

3.1 NORTH ANNA UNIT 1 TUBE RUPTURE EVENT

The cause of the tube rupture has been determined to be high cycle fatigue. The source of the loads associated with the fatigue mechanism has been determined to be a combination of a mean stress level in the tube and a superimposed alternating stress. The mean stress has been determined to have been increased to a maximum level as the result of denting of the tube at the top tube support plate and the alternating stress has been determined to be due to out-of-plane deflection of the tube U-bend above the top tube support caused by flow-induced vibration. These loads are consistent with a lower bound fatigue curve for the tube material in an AVT water chemistry environment. The vibration mechanism has been determined to be fluid elastic, based on the magnitude of the alternating stress.

A significant contributor to the occurrence of excessive vibration is the reduction in damping at the tube-to-tube support plate interface caused by the denting. Also, the absence of AVB support has been concluded to be required for vibration to occur. The presence of an AVB support restricts tube motion and thus precludes the deflection amplitude required for fatigue. Inspection data show that an AVB is not present for the Row 9 Column 51 tube but that the actual AVB installation depth exceeded the minimum requirements in all cases with data for AVBs at many other Row 9 tubes. Also contributing significantly to the level of vibration, and thus loading, is the local flow field associated with the detailed geometry of the steam generator, i.e., AVB insertion depths. In addition, the fatigue properties of the tube reflect the lower range of properties expected for an AVT environment. In summary, the prerequisite conditions derived from the evaluations were concluded to be:

Fatigue Requirements		**Prerequisite Conditions**
Alternating stress	→	Tube vibration - Dented support - Flow excitation - Absence of AVB
Mean stress	→	Denting in addition to applied stress
Material fatigue properties	→	AVT environment - Lower range of properties

3.2 TUBE EXAMINATION RESULTS

Fatigue was found to have initiated on the cold leg outside surface of tube R9C51 immediately above the top tube support plate. No indication of significant accompanying intergranular corrosion was observed on the fracture face or on the immediately adjacent OD surfaces. Multiple fatigue initiation sites were found with major sites located at 110°, 120°, 135° and 150°, (see Figure 3-1). The plane of the U-bend is located at 45° with the orientation system used, or approximately 90° from the geometric center of the initiation zone at Section D-D. High cycle fatigue striation spacings approached 1 micro-inch near the origin sites, Figure 3-2. The early crack front is believed to have broken through-wall from approximately 100° to 140°. From this point on, crack growth is believed (as determined by striation spacing, striation direction, and later observations of parabolic dimples followed by equiaxed dimples) to have accelerated and to have changed direction with the resulting crack front running perpendicular to the circumferential direction.

3.3 MECHANISM ASSESSMENT

To address a fatigue mechanism and to identify the cause of the loading, any loading condition that would cause cyclic stress or steady mean stress had to be considered. The analysis of Normal, Upset and Test conditions indicated a relatively low total number of cycles involved and a corresponding low fatigue usage, even when accounting for the dented tube condition at the plate. This analysis also showed an axial tensile stress contribution at the tube OD a short distance above the plate from operating pressure and temperature, thus providing a contribution to mean stress. Combining these effects with denting deflection on the tube demonstrated a high mean stress at the failure location. Vibration analysis for the tube developed the characteristics of first mode, cantilever response of the dented tube to flow-induced vibration for the uncracked tube and for the tube with an increasing crack angle, beginning at 90° to the plane of the tube and progressing around on both sides to complete separation of the tube.

Crack propagation analysis matched cyclic deformation with the stress intensities and striation spacings indicated by the fracture inspection and analysis. Leakage data and crack opening analysis provided the relationship between leak rate and circumferential crack length. Leakage versus time was then predicted from the crack growth analysis and the leakage analysis with initial stress amplitudes of 5, 7, and 9 ksi. The comparison to the estimate of plant leakage (performed after the event) showed good agreement, Figure 3-3.

Based on these results, it followed that the predominant loading mechanism responsible is a flow-induced tube vibration loading mechanism. It was shown that of the two possible flow-induced vibration mechanisms, turbulence and fluid elastic instability, that fluid elastic instability was the most probable cause. Due to the range of expected initiation stress amplitudes (4 to 10 ksi), the fluid elastic instability would be limited in displacement to a range of approximately [ ].[a,c] This is less than the distance between tubes at the apex, [ ].[a,c] It was further confirmed that displacement prior to the rupture was limited since no indication of tube U-bend (apex region) damage was evident in the eddy current signals of adjacent tubes.

Given the likelihood of limited displacement, fluid elastic instability, a means of establishing the change in displacement, and corresponding change in stress amplitude, was developed for a given reduction in stability ratio (SR). Since the rupture was a fatigue mechanism, the change in stress amplitude resulting

from a reduction in stability ratio was converted to a fatigue usage benefit through the use of the fatigue curve developed. Mean stress effects were included due to the presence of denting and applied loadings. The results indicated that a 10% reduction in stability ratio is needed (considering the range of possible initiation stress amplitudes) to reduce the fatigue usage per year to less than 0.02 for a tube similar to Row 9 Column 51 at North Anna Unit 1.

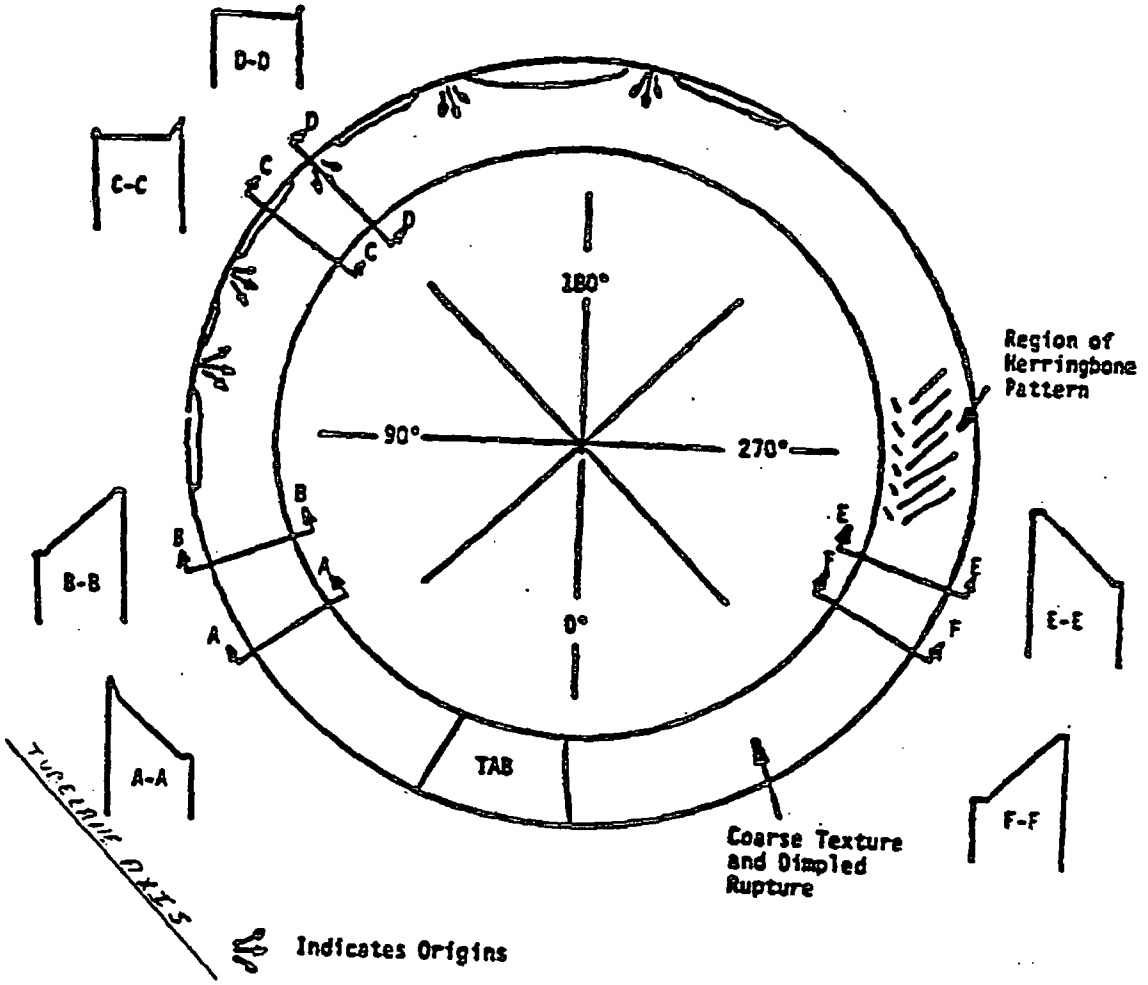

Figure 3-1 Appropriate Mapping of Fracture Surface of Tube R9C51, S/G "C" Cold Leg, North Anna Unit 1

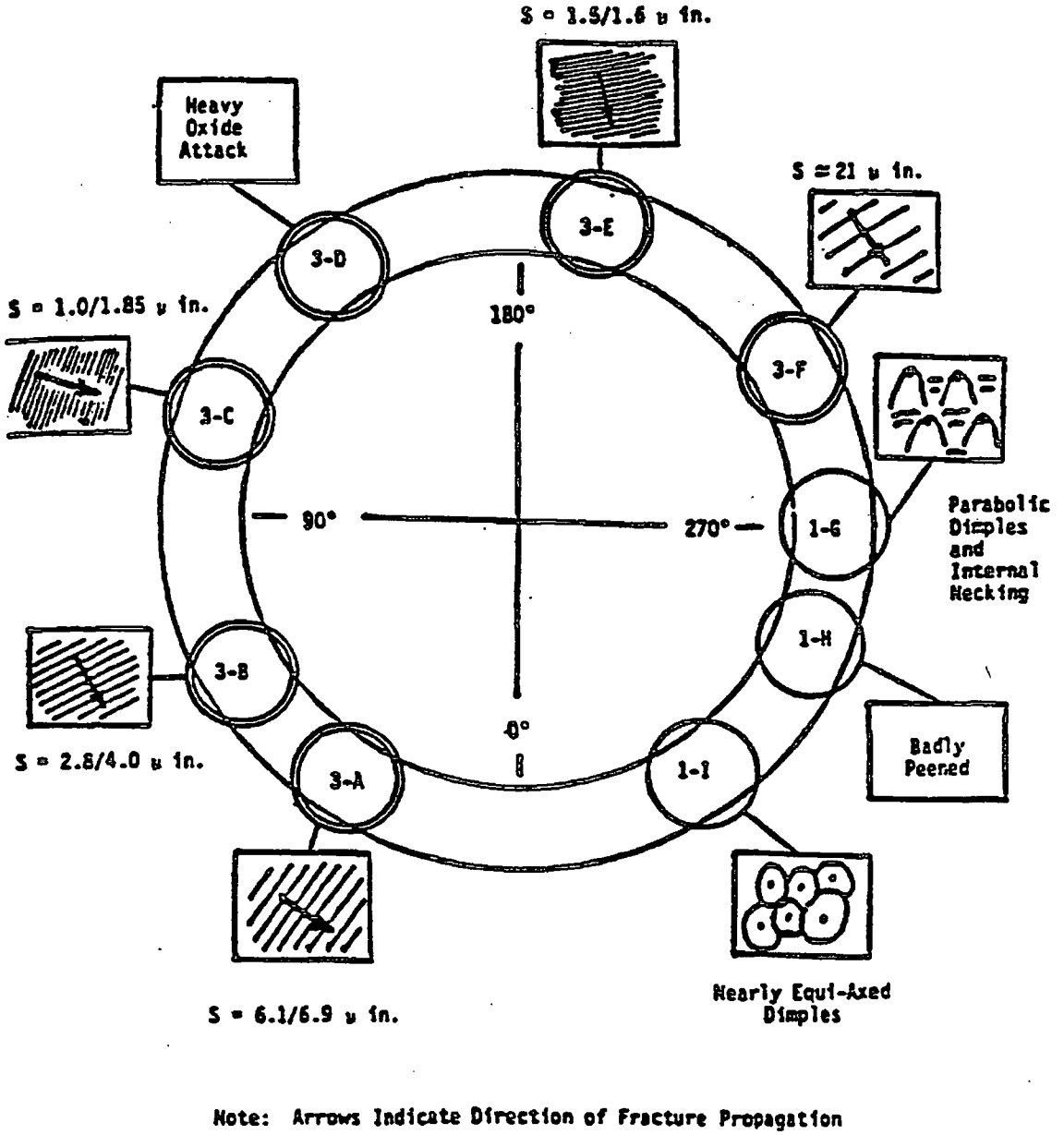

Figure 3-2 Schematic Representation of Features Observed During TEM Fractographic Examination of the Fracture Surface of Tube R9C51, S/G "C" Cold Leg, North Anna Unit 1

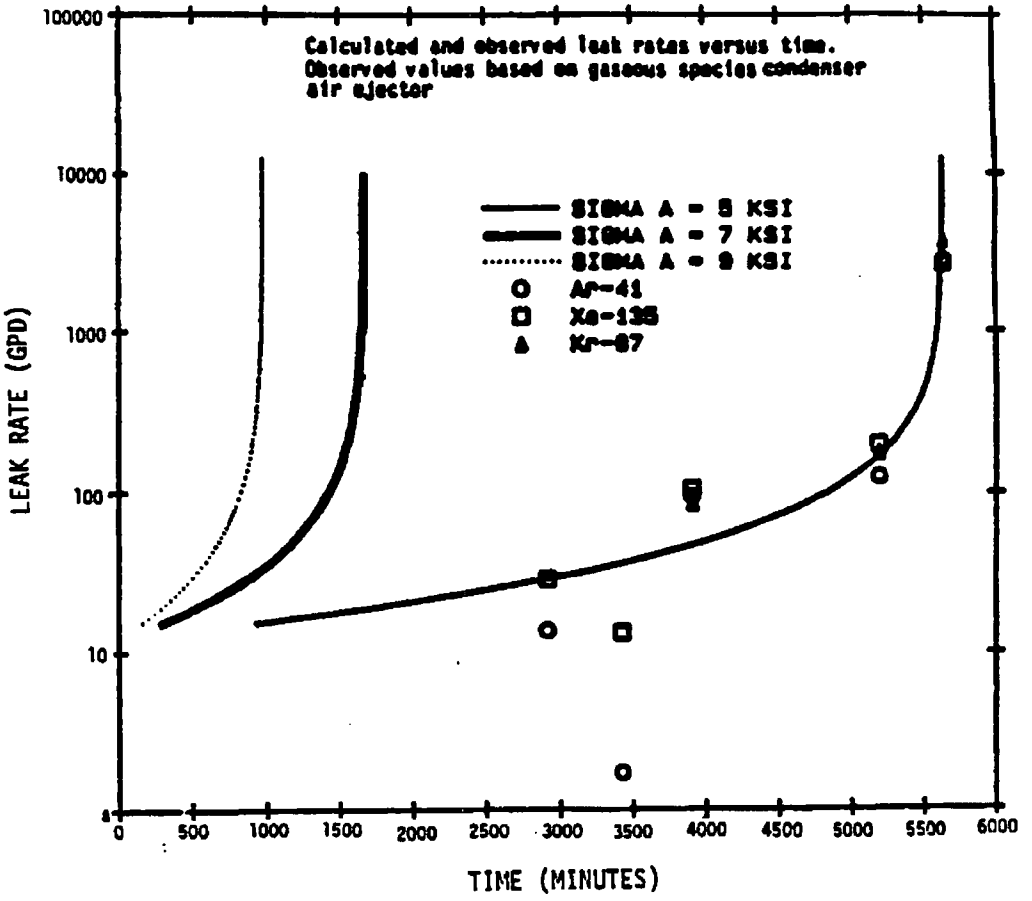

Figure 3-3 Calculated and Observed Leak Rates versus Time

4 CRITERIA FOR FATIGUE ASSESSMENT

The evaluation method and acceptance criteria are based on a relative comparison with the Row 9 Column 51 tube of Steam Generator C, North Anna Unit 1. This approach is necessary because (1) methods for direct analytical prediction of actual stability ratios incorporate greater uncertainties than a relative ratio method, and (2) the stress amplitude (or displacement) associated with a specific value of stability ratio can only be estimated by the analysis of North Anna Unit 1. For these reasons, the North Anna Unit 1 tubing evaluation was done on a relative basis to Row 9 Column 51 and a 10% reduction in the stability ratio criteria was established to demonstrate that tubes left in service would be expected to have sufficiently low vibration stress to preclude future fatigue rupture events.

To accomplish the necessary relative assessment of Watts Bar Unit 2 tubing to Row 9 Column 51 of North Anna Unit 1, several criteria are utilized. First, stability ratios are calculated for Watts Bar Unit 2 tubes based on flow fields predicted by 3-D thermal-hydraulic models and ratioed to the stability ratio for Row 9 Column 51 at North Anna Unit 1 based on a flow field obtained with a 3-D thermal-hydraulic model with the same degree of refinement. These ratios of stability ratio (called relative stability ratios) for each potentially unsupported U-bend in the Watts Bar Unit 2 steam generators should be equivalent to ≤ 0.9 of R9C51, North Anna 1 (meeting the 10% reduction in stability ratio criteria). This provides the first level of screening of susceptible tubes incorporating all tube geometry and flow field differences in the tube dynamic evaluation. It has the inherent assumption, however, that each tube has the same local, high flow condition present at Row 9 Column 51, North Anna Unit 1. To account for these differences, flow peaking factors can be incorporated in the relative stability ratios and the stress ratios.

The next step is to obtain stress ratios, the ratio of stress in the Watts Bar Unit 2 tube of interest to the stress in Row 9 Column 51, North Anna Unit 1, and after incorporating the requirement that the relative stability ratio to Row 9 Column 51 (R9C51) for the tube of interest is equivalent to ≤ 0.9, require the stress ratio to be ≤ 1.0. The stress ratio incorporates the tube geometry differences with R9C51 in relation to the stress calculation and also incorporates the ratio of flow peaking factor for the tube of interest to the flow peaking factor for R9C51 (flow peaking factor is defined in Section 4.2). This should provide that all tubes meeting this criteria have stress amplitudes equivalent to ≤ 4.0 ksi.

Finally, the cumulative fatigue usage for plant operation to date and for continued operation with the same operating parameters is evaluated. A fatigue usage ≤ 1.0 may not be satisfied by meeting the stress ratio criteria using the reference operating cycle evaluation since the reference cycle does not necessarily represent the exact duty cycle to date. Therefore, the time history of operation is evaluated on a normalized basis and used together with the stress ratio to obtain a stress amplitude history. This permits the calculation of current and future fatigue usage for comparison to 1.0. However for the current Unit 2 analysis there is no need to consider past operating history since this unit has not yet been in operation.

4.1 STABILITY RATIO REDUCTION CRITERIA

For fluid elastic evaluation, stability ratios are determined for specific configurations of a tube. These stability ratios represent a measure of the potential for flow-induced tube vibration during service. Values greater than unity (1.0) indicate instability (see Section 5.1).

Motions developed by a tube in the fluid-elastically unstable mode are quite large in comparison to the other known mechanisms. The maximum modal displacement (at the apex of the tube) is linearly related to the bending stress in the tube just above the cold leg top tube support plate. This relationship applies to any vibration in that mode. Thus, it is possible for an unstable, fixed boundary condition tube to deflect an amount in the U-bend, which will produce fatigue-inducing stresses.

The major features of the fluid-elastic mechanism are illustrated in Figure 4-1. This figure shows the displacement response (LOG D) of a tube as a function of stability ratio (LOG SR). A straight-line plot displayed on log-log coordinates implies a relation of the form $y = A(x)^n$, where A is a constant, x is the independent variable, n is the exponent (or power to which x is raised), and y is the dependent variable. Taking logs of both sides of this equation leads to the slope-intercept form of a straight-line equation in log form, $\log y = c + n \log x$, where $c = \log A$ and represents the intercept and n is the slope. In our case the independent variable x is the stability ratio SR, and the dependent variable y is tube (fluid-elastic instability induced) displacement response D, and the slope n is renamed s.

From experimental results, it is known that the turbulence response curve (on log-log coordinates) has a slope of approximately [ ]^{a,b,c} Test results also show that the slope for the fluid-elastic response depends somewhat on the instability displacement (response amplitude). It has been shown by tests that a slope of [ ]^{a,b,c} is a range of values corresponding to displacement amplitudes in the range of [ ]^{a,c} whereas below [ ]^{a,c} are conservative values.

The reduction in response obtained from a stability ratio reduction can be expressed by the following equation:

$$\left[\qquad\qquad\right]^{a,c}$$

where D_1 and SR_1 are the known values at the point corresponding to point 1 of Figure 4-1 and D_2 and SR_2 are values corresponding to any point lower on this curve. Therefore, this equation can be used to determine the reduction in displacement response for any given reduction in stability ratio.

This equation shows that there is benefit derived from even a very small percentage change in the stability ratio. It is this reduction in displacement for a quite small reduction in stability ratio that formed the basis for demonstrating that a 10% reduction in stability ratio would be sufficient to prevent Row 9 Column 51 from rupturing by fatigue.

The fatigue curve developed for the North Anna Unit 1 tube at R9C51 is from [

]^{a,c} Thus,

$$\left[\qquad\right]^{a,c}$$

where, σ'_σ is the equivalent stress amplitude to σ_a that accounts for a maximum stress of σ_y, the yield strength. The -3 sigma curve with mean stress effects is shown in Figure 4-2 and is compared to the ASME Code Design Fatigue Curve for Inconel 600 with the maximum effect of mean stress. The curve utilized in this evaluation is clearly well below the code curve reflecting the effect of an AVT environment on fatigue and [ ]^{a,c} for accounting for mean stress that applies to materials in a corrosive environment.

Two other mean stress models were investigated for the appropriateness of their use in providing a reasonable agreement with the expected range of initiating stress amplitudes. These were the [ ]^{a,c} shown in Figure 4-3. With a [ ],^{a,c} the [

]^{a,c}

The assessment of the benefit of a reduction in stability ratio begins with the relationship between stability ratio and deflection. For a specific tube geometry, the displacement change is directly proportional to change in stress so that stress has the same relationship with stability ratio,

$$\left[\qquad\right]^{a,c}$$

The slope in this equation can range from [ ]^{a,c} on a log scale depending on the amplitude of displacement. Knowing the stress resulting from a change in stability ratio from SR_1 to SR_2, the cycles to failure at the stress amplitude were obtained from the fatigue curve. A fatigue usage per year was then determined assuming continuous cycling at the natural frequency of the tube. The initial stress was determined to be in the range of 4.0 to 10.0 ksi by the fractography analysis.

It was further developed that the maximum initiating stress amplitude was not more than 9.5 ksi. This was based on [

]^{a,c}

[

].[a,c] The corresponding stress level is 5.6 ksi.

The maximum stress, 9.5 ksi, would be reduced to [ ][a,c] ksi with a 10% reduction in stability ratio and would have a future fatigue usage of [ ][a,c] per year at 75% availability, Figure 4-4. The minimum stress, 5.6 ksi, would be reduced to [ ][a,c] ksi with a 5% reduction in stability ratio and would have future fatigue usage of [ ][a,c] per year, Figure 4-5. In addition, if a tube were already cracked, the crack could be as large as [ ][a,c] inch in length and through-wall and would not propagate if the stress amplitudes are reduced to $\leq$ 4.0 ksi.

Subsequent to the return to power evaluation for North Anna Unit 1, the time history of operation was evaluated on a normalized basis to the last cycle. [

],[a,c]
cumulative fatigue usage may then be computed to get a magnitude of alternating stress for the last cycle that results in a cumulative usage of 1.0 for the nine-year duty cycle. The result of the iterative analysis is that the probable stress associated with this fatigue curve during the last cycle of operation was approximately [ ][a,c] ksi for R9C51, North Anna Unit 1, Steam Generator C, and that the major portion of the fatigue usage came in the second, third and fourth cycles. The first cycle was conservatively omitted, since denting is assumed, for purposes of this analysis, to have occurred during that first cycle. Based on this evaluation, the tube fatigue probably occurred over most of the operating history of North Anna Unit 1.

A similar calculation can be performed for the time history of operation assuming that [

].[a,c] On this
basis, the effect of a 10% reduction in stability ratio is to reduce the stress amplitude to 4.0 ksi and results in a future fatigue usage of [ ].[a,c]

Other combinations of alternating stress and mean stress were evaluated with -3 sigma and -2 sigma fatigue curves to demonstrate the conservatism of the 10% reduction in stability ratio. Table 4-1 presents the results of the cases analyzed clearly demonstrating that the 10% reduction in stability ratio combined with a -3 sigma fatigue curve and with maximum mean stress effects is conservative. Any higher fatigue curve whether through mean stress, mean stress model, or probability, results in greater benefit for the same reduction in stability ratio. Further, for any of these higher curves, a smaller reduction in stability ratio than 10% would result in the same benefit. In addition, there is a large benefit in terms of fatigue usage for relatively small changes in the fatigue curve.

4.2 LOCAL FLOW PEAKING CONSIDERATIONS

Local flow peaking is a factor on stability ratio that incorporates the effects of local flow velocity, density and void fraction due to non-uniform AVB insertion depths. The flow peaking factor is applied directly to the stability ratio obtained from thermal-hydraulic analysis that does not account for these local geometry

effects. Being a direct factor on stability ratio, a small percentage increase can result in a significant change in the prediction of tube response.

Since the evaluation of Watts Bar Unit 2 tubing is relative to R9C51, North Anna Unit 1, the flow peaking factors are also applied as relative ratios, i.e., a ratio of Watts Bar Unit 2 tubing to R9C51 at North Anna Unit 1. The flow peaking relative instability is obtained by testing in the air test rig described in Section 5.4, where the peaking factor is defined as the critical velocity for R9C51 AVB pattern compared to critical velocity for a uniform AVB pattern. As explained in Section 8.0, the minimum value of [ ]^{a,b,c} is appropriate for R9C51 of North Anna 1. The peaking factor for a tube in Watts Bar Unit 2 tubing is therefore divided by [ ]^{a,b,c} and the resulting relative flow peaking is multiplied times the relative stability ratio based on ATHOS results. If the peaking factor is 1.0, the relative flow peaking is [ ]^{a,b,c}.

As a further demonstration of the conservatism of [ ]^{a,b,c} as the minimum flow peaking factor for R9C51, the stress amplitude of 7.0 ksi obtained from iterating on cumulative fatigue usage (and selected as the nominal value from fractography analysis) was used to back calculate the apparent stability ratio and then the apparent flow peaking factor. Allowing for a range of slopes of the instability curve from 10 to 30, the stability ratio is in the range of 1.1 to 1.4 and the flow peaking factor is in the range of 1.8 to 2.2. This range of flow peaking agrees with the range of flow peaking factors measured in the air tests and is considered to be the best estimate of the range of the R9C51 flow peaking factor.

The range of stability ratios, 1.1 to 1.4, is based on a value of 0.63 obtained with ATHOS results without flow peaking and with nominal damping that is a function of modal effective void fraction (MEVF). The nominal damping reflects the nominal reduction in damping that occurs with denting at the tube support plate. Therefore, a minimum damping scenario that is independent of void fraction is not considered to be credible and is not addressed in the evaluation that follows.

4.3 STRESS RATIO CONSIDERATIONS

In Section 4.1, a 10% reduction in stability ratio was established to reduce the stress amplitude on the Row 9 Column 51 tube of North Anna Unit 1 to a level that would not have ruptured, 4.0 ksi. To apply this same criteria to another tube in the same or another steam generator, the differences in [

].[a,c]

[a,c

]

[ ]a,c

By establishing their equivalent effect on the stress amplitude that produced the tube rupture at North Anna 1, several other effects may be accounted for. These include a lower mean stress (such as for non-dented tubes), different frequency tubes from the [ ]a,c,e hertz frequency of R9C51, North Anna 1, and shorter design basis service.

In the case of lower mean stress, the stress amplitude that would have caused the failure of R9C51, North Anna 1, would have been higher. [

].a,c

A lower or higher frequency tube would not reach a usage of 1.0 in the same length of time as the R9C51 tube due to the different frequency of cycling. The usage accumulated is proportional to the frequency and, therefore, the allowable number of cycles to reach a usage of 1.0 is inversely proportional to frequency. The equivalent number of cycles to give the usage of 1.0 for a different frequency tube [

].a,c

For a different time basis for fatigue usage evaluation, [

].a,c,e

Knowing the magnitude of the stress ratio allows: 1) the determination of tubes that do not meet a value of ≤ 1, and 2) the calculation of maximum stress in the acceptable tubes,

[ ]a,c

Having this maximum stress permits the evaluation of the maximum fatigue usage for Watts Bar Unit 2 based on the time history expressed by normalized stability ratios for the duty cycle (see Section 7.4).

Table 4-1 Fatigue Usage per Year Resulting From Stability Ratio Reduction

Sr. % Reduction	Stress Basis(1)	Fatigue Curve(2)	Mean Stress Model	Usage Per Year
5.	9 yrs to fail [ ]a,c			a,c
5.	9 yrs to fail [ ]a,c			
5.	9 yrs to fail [ ]a,c			
10.	max. stress amplitude(4) [ ]a,c			
10.	max. stress amplitude(4) [ ]a,c			
10.	max. stress amplitude(4) [ ]a,c			
10.	max. stress amplitude(4) [ ]a,c			
10.	max. stress based on duty cycle(5) [ ]a,c			

Notes:

(1) This gives the basis for selection of the initiating stress amplitude and its value in ksi.

(2) S_m is the maximum stress applied with $S_m = S_{mean} + S_a$.

(3) [ ].a,c

(4) Cycles to failure implied by this combination of stress and fatigue properties are notably less than implied by the operating history. Consequently this combination is a conservative, bounding estimate.

(5) Cycles to failure implied by the operating history require [ ]a,c fatigue curve at the maximum stress of [ ].a,c

[a,b,c

]a,b,c

Figure 4-1 Vibration Displacement vs. Stability Ratio

Figure 4-2 Fatigue Strength of Inconel 600 in AVT Water at 600°F

Figure 4-3 Fatigue Curve for Inconel 600 in AVT Water Comparison of Mean Stress Correction Models

[ ]a,c

Figure 4-4 Modified Fatigue with 10% Reduction in Stability Ratio for Maximum Stress Condition


a,c

Figure 4-5 Modified Fatigue with 5% Reduction in Stability Ratio for Minimum Stress Condition

5 SUPPORTING TEST DATA

This section provides a mathematical description of the fluid elastic mechanism that was determined to be the most likely causative mechanism for the North Anna tube rupture, as discussed in Section 3.3, to highlight the physical conditions and corresponding parameters directly related to the event and associated preventative measures. The basis for establishing the appropriate values and implications associated with these parameters are provided. Where appropriate, test results are presented.

5.1 STABILITY RATIO PARAMETERS

Fluid elastic stability ratios are obtained by evaluations for specific configurations, in terms of active tube supports, of a specific tube. These stability ratios represent a measure of the potential for tube vibration due to instability during service. Fluid elastic stability evaluations are performed with a computer program, which provides for the generation of a finite element model of the tube and tube support system. The finite element model provides the vehicle to define the mass and stiffness matrices for the tube and its support system. This information is used to determine the modal frequencies (eigenvalues) and mode shapes (eigenvectors) for the linearly supported tube being considered.

The methodology is comprised of the evaluation of the following equations:

Fluid elastic stability ratio = SR = U_{en}/U_c for mode n,

where U_c (critical velocity) and U_{en} (effective velocity) are determined by:

$$U_c = \beta f_n D \sqrt{\frac{m_0 \delta_n}{\rho_0 D^2}} \qquad [1]$$

and;

$$U_{en}^2 = \frac{\sum_{j=1}^{N} \left(\frac{\rho_j}{\rho_0}\right) U_j^2 \phi_{jn}^2 z_j}{\sum_{j=1}^{N} \left(\frac{m_j}{m_0}\right) \phi_{jn}^2 z_j} \qquad [2]$$

where,

D	=	tube outside diameter, inches
U_{en}	=	effective velocity for mode n, inches/sec
N	=	number of nodal points of the finite element model
m_j, U_j, ρ_j	=	mass per unit length, cross flow velocity and fluid density at node j, respectively
ρ_o, m_o	=	reference density and a reference mass per unit length, respectively (any representative values)
δ_n	=	logarithmic decrement (damping)
Φ_{jn}	=	normalized displacement at node j in the nth mode of vibration

z_j = average of distances between node j to j-1, and j to j+1
β = an experimentally correlated stability constant

Substitution of Equations [1] and [2] into the expression, which defines stability ratio, and cancellation of like terms, leads to an expression in fundamental terms (without the arbitrary reference mass and density parameters). From this resulting expression, it is seen that the stability ratio is directly related to the flow field in terms of the secondary fluid velocity times square-root-density distribution (over the tube mode shape), and inversely related to the square root of the mass distribution, square root of modal damping, tube modal frequency, and the stability constant (beta).

The uncertainty in each of these parameters is addressed in a conceptual manner in Figure 5-1. The remainder of this section (Section 5.0) provides a discussion, and, where appropriate, the experimental bases to quantitatively establish the uncertainty associated with each of these parameters. In addition, Section 5.3 provides the experimental basis to demonstrate that tubes with [

].[a,c] This implies that those tubes [ ][a,c] would not have to be modified because their instability response amplitude (and stress) would be small. The very high degree of sensitivity of tube response (displacements and stresses) to changes in the velocity multiplied by the square-root-density distribution is addressed in Section 4.0. This is important in determining the degree of change that can be attained through modifications.

Frequency

It has been demonstrated by investigators that analytically determined frequencies are quite close to their physical counterparts obtained from measurements on real structures. Thus, the uncertainty in frequencies has been shown to be quite small. This is particularly appropriate in the case of dented (fixed boundary condition) tubes. Therefore, uncertainty levels introduced by the frequency parameter are expected to be insignificant (see also "Average Flow Field" subsection below).

Instability Constant (Beta)

The beta (stability constant) values used for stability ratio and critical velocity evaluations (see above equations) are based on an extensive database comprised of both Westinghouse and other experimental results. In addition, previous field experiences are considered. Values have been measured for full length U-bend tubes in prototypical steam/water environments. In addition, measurements in U-bend air models have been made with both no AVB and variable AVB supports (Figure 5-3).

To help establish the uncertainties associated with ATHOS flow velocity and density distribution predictions on stability analyses, the Model Boiler (MB-3) tests performed at Mitsubishi Heavy Industries (MHI) in Japan were modeled using ATHOS. A beta value consistent with the ATHOS predicted flow conditions and the MB-3 measured critical velocity was determined. These analyses supported a beta value of [ ].[a,b,c]

A summary of the test bases and qualifications of the beta values used for these assessments is provided by Figure 5-2. The lowest measured beta for tubes without AVBs was a value of [ ].[a,b,c] This value is

used for the beta parameter in all stability ratio evaluations addressed in this Report (see also "Average Flow Field" subsection below).

Mass Distribution

The mass distribution parameter is based on known information on the tube and primary and secondary fluid physical properties. The total mass per unit length is comprised of that due to the tube, the internal (primary) fluid, and the external (secondary) fluid (hydrodynamic mass). Data in Reference 5-2 suggests that at operating void fractions [

]^{a,c}

Tube Damping

Test data are available to define tube damping for clamped (fixed) tube supports, appropriate to dented tube conditions, in steam/water flow conditions. Prototypic U-bend testing has been performed under conditions leading to pinned supports. The data of Axisa in Figure 5-4 provides the principal data for clamped tube conditions in steam/water. This data was obtained for cross flow over straight tubes. Uncertainties are not defined for the data from these tests. Detailed tube damping data used in support of the stability ratio evaluations addressed in this report are provided in Section 5.2, below.

Flow Field - Velocity Times Square-Root-Density Distribution

Average and U-bend-local flow field uncertainties are addressed independently in the following.

Average Flow Field

Uncertainties in the average flow field parameters, obtained from ATHOS analyses, coupled with stability constant and frequency, are essentially the same for units with dented or non-dented top support plates. If the errors associated with these uncertainties were large, similar instabilities would be expected in the non-dented units with resulting wear at either the top support plate or inner row AVBs. Significant tube wear has not been observed in inner row tubes in operating steam generators without denting. Thus, an uncertainty estimate of about [ ]^{a,c} for the combined effects of average flow field, stability constant and frequency appears to be reasonable. To further minimize the impact of these uncertainties, the Watts Bar Unit 2 tubes are evaluated on a relative basis, so that constant error factors are essentially eliminated. Thus, the uncertainties associated with the average velocity times square-root-density (combined) parameter are not expected to be significant.

U-bend Local Flow Field

Non-uniform AVB insertion depths have been shown to have effects on stability ratios. Flow peaking, brought about by the "channeling" effects of non-uniform AVBs, leads to a local perturbation in the velocity times square-root-density parameter at the apex of the tube where it will have the largest effect (because the apex is where the largest vibration displacements occur). Detailed local flow field data used in support of the stability ratio evaluations addressed in this report are provided in Section 5.2, below.

Overall Uncertainties Assessment

Based on the above discussions, and the data provided in the following sections, it is concluded that local flow peaking is likely to have contributed significantly to the instability and associated increased vibration amplitude for the failed North Anna tube. Ratios of stresses and stability ratios relative to the North Anna tube, R9C51, are utilized in this report to minimize uncertainties in the evaluations associated with instability constants, local flow field effects and tube damping.

5.2 TUBE DAMPING DATA

The damping ratio depends on several aspects of the physical system. Two primary determinants of damping are the support conditions and the flow field. It has been shown that tube support conditions (pinned versus clamped) affect the damping ratio significantly. Further, it is affected by the flow conditions, i.e., single-phase or two-phase flow. These effects are discussed below in more detail.

Reference (5-1) indicates that the damping ratio in the two-phase flow is a sum of contributions from structural, viscous, flow-dependent, and two-phase damping. The structural damping will be equal to the measured damping in air. However, in two-phase flow, the damping ratio increases significantly and is dependent on the void fraction or quality. It can be shown that the damping contribution from viscous effects is very small.

Damping ratios for tubes in air and in air-water flows have been measured and reported by various authors. However, the results from air-water flow are poor representations of the actual conditions in a steam generator (steam-water flow at high pressure). Therefore, where available, results from prototypic steam-water flow conditions should be used. Fortunately, test data on tube vibration under steam-water flow has been developed for both pinned and clamped tube support conditions.

Two sources of data are particularly noteworthy and are used here. The first is a large body of unpublished data from high-pressure steam-water tests conducted by Mitsubishi Heavy Industries (MHI). These data were gathered under pinned tube support conditions. The second is comprised of the results from tests sponsored by the Electric Power Research Institute (EPRI) and reported in References (5-2) and (5-3).

The damping ratio results from the above tests are plotted in Figure 5-4 as a function of void fraction. It is important to note that the void fraction is determined on the basis of [ ]^{a,c} (Reference (5-4)). The upper curve in the figure is for pinned support conditions. This curve represents a fit to a large number of data points not shown in the figure. The points on the curve are only plotting aids, rather than specific test results.

The lower curve pertains to the clamped support condition, obtained from Reference (5-3). Void fraction has been recalculated on the basis of slip flow. It may be noted that there is a significant difference in the damping ratios under the pinned and the clamped support conditions. Damping is much larger for pinned supports at all void fractions. Denting of the tubes at the top support plate effectively clamps the tubes at that location. Therefore, the clamped tube support curve is used in the current evaluation to include the effect of denting at the top tube support plate.

The Reference 5-3 data as reported show a damping value of 0.5% at 100% void fraction. The 100% void fraction condition has no two-phase damping and is considered to be affected principally by mechanical or structural damping. Westinghouse tests of clamped tube vibration in air have shown that the mechanical damping is only [ ]^{a,c} rather than the 0.5% reported in Reference (5-3). Therefore the lower curve in Figure 5-4 is the Reference (5-3) data with all damping values reduced by [ ].^{a,c}

5.3 TUBE VIBRATION AMPLITUDES WITH SINGLE-SIDED AVB SUPPORT

A series of wind tunnel tests were conducted to investigate the effects of tube/AVB eccentricity on the vibration amplitudes caused by fluid elastic vibration.

[

].^{a,c} Prior test results obtained during the past year using this apparatus have demonstrated that the fluid elastic vibration characteristics observed in the tests performed with the cantilever tube apparatus are in good agreement with corresponding characteristics observed in wind tunnel and steam flow tests using U-bend tube arrays. Summary of these prior results is given in Table 5-1.

An overall view of the apparatus is shown in Figure 5-5. Figure 5-6 is a top view of the apparatus. [

].^{a,c}

As shown in Figure 5-7, the tube vibration amplitude below a critical velocity is caused by [

].^{a,c} Figure 5-7 shows the manner in which the zero-to-peak vibration

amplitude, expressed as a ratio normalized to [ ],[a,c] varies when one gap remains at [ ].[a,c] For increasing velocities, up to that corresponding to a stability ratio of [ ].[a,c] Figure 5-8 shows typical vibration amplitude and tube/AVB impact force signals corresponding to those obtained from the tests which provided the results shown in Figure 5-7. As expected, impacting is only observed in the [ ].[a,c]

It is concluded from the above test results that, [ ].[a,c]

5.4 TESTS TO DETERMINE THE EFFECTS ON FLUID-ELASTIC INSTABILITY OF COLUMNWISE VARIATIONS IN AVB INSERTION DEPTHS

This section summarizes a series of wind tunnel tests that were conducted to investigate the effects of variations in AVB configurations on the initiation of fluid-elastic vibration. Each configuration is defined as a specific set of insertion depths for the individual AVBs in the vicinity of an unsupported U-bend tube.

The tests were conducted in the wind tunnel using a modified version of the cantilever tube apparatus described in Section 5.3. Figure 5-9 shows the conceptual design of the apparatus. The straight cantilever tube, [ ].[a,c]

[ ].[a,c] Figure 5-11 shows the AVBs, when the side panel of the test section is removed. Also shown is the top flow screen which is [

].[a,c] The AVB configurations tested are shown in Fig. 5-12. Configuration 1a corresponds to tube R9C51, the failed tube at North Anna. Configuration 2a corresponds to one of the cases in which the AVBs are inserted to a uniform depth and no local velocity peaking effects are expected.

As shown in Figure 5-9, [ ].[a,c]

All the tubes except the instrumented tubes (corresponding to Row 10) are [ ].[a,c] As discussed in Section 5.3, prior testing indicates that this situation provides a valid model. The instrumented tube [ ][a,c] as shown in Figure 5.10. Its [ ][a,c] direction vibrational motion is measured using a non-contacting transducer.

[ ].[a,c] The instrumented tube corresponds to a Row 10 tube as shown in Figure 5-9. However, depending on the particular AVB configuration, it can reasonably represent a tube in Rows 8 through 11. The AVB profile in the straight tube model is the average of Rows 8 and 11. The difference in profile is quite small for these bounding rows.

[ ][a,c] using a hot-film anemometer located as shown in Figure 5-9.

Figure 5-13 shows the root mean square (RMS) vibration amplitude, as determined from PSD (power spectral density) measurements made using a fast fourier transform (FFT) spectrum analyzer, versus flow velocity for Configuration 1a. Configuration 1a corresponds to the final, evaluated positions of AVBs near tube R9C51 in North Anna (See Figures 8-6 and 8-7). Data for three repeat tests are shown and the critical velocity is identified. The typical rapid increase in vibration amplitude when the critical velocity for fluid elastic vibration is exceeded is evident.

The main conclusions from the tests are:

1. Tube vibration below the critical velocity is relatively small, typical of turbulence-induced vibration, and increases rapidly when the critical velocity for the initiation of fluid elastic vibration is exceeded.

2. Configuration 1b (which was initially thought to represent AVB positions near R9C51 in North Anna until re-evaluation indicated Configuration 1a has the lowest critical velocity of all the configurations tested.

3. Configuration 1b is repeatable and the configuration was rerun periodically to verify the consistency of the test apparatus.

The initial test results obtained in support of the Watts Bar Unit 2 evaluation are summarized in Table 5-2. The test data are presented as velocity peaking ratios, the ratio of critical velocity for North Anna tube R9C51 Configuration 1a, to that for each Watts Bar Unit 2 AVB configuration evaluated.

5.5 REFERENCES

[a,b,c

]

Table 5-1 Wind Tunnel Tests On Cantilever Tube Model

OBJECTIVE:	Investigate the effects of tube/AVB fit-up on flow-induced tube vibration.
APPARATUS:	Array of cantilevered tubes with end supports [ ].[a,c]
MEASUREMENTS	Tube vibration amplitude and tube/AVB impact forces or preload forces.
RESULTS	

a,b,c

Table 5-2 Watts Bar Unit 2 Fluid-Elastic Instability Velocity Peaking Ratios for Column-Wise Variation in AVB Insertion Depths

[

] a,b,c

a,c

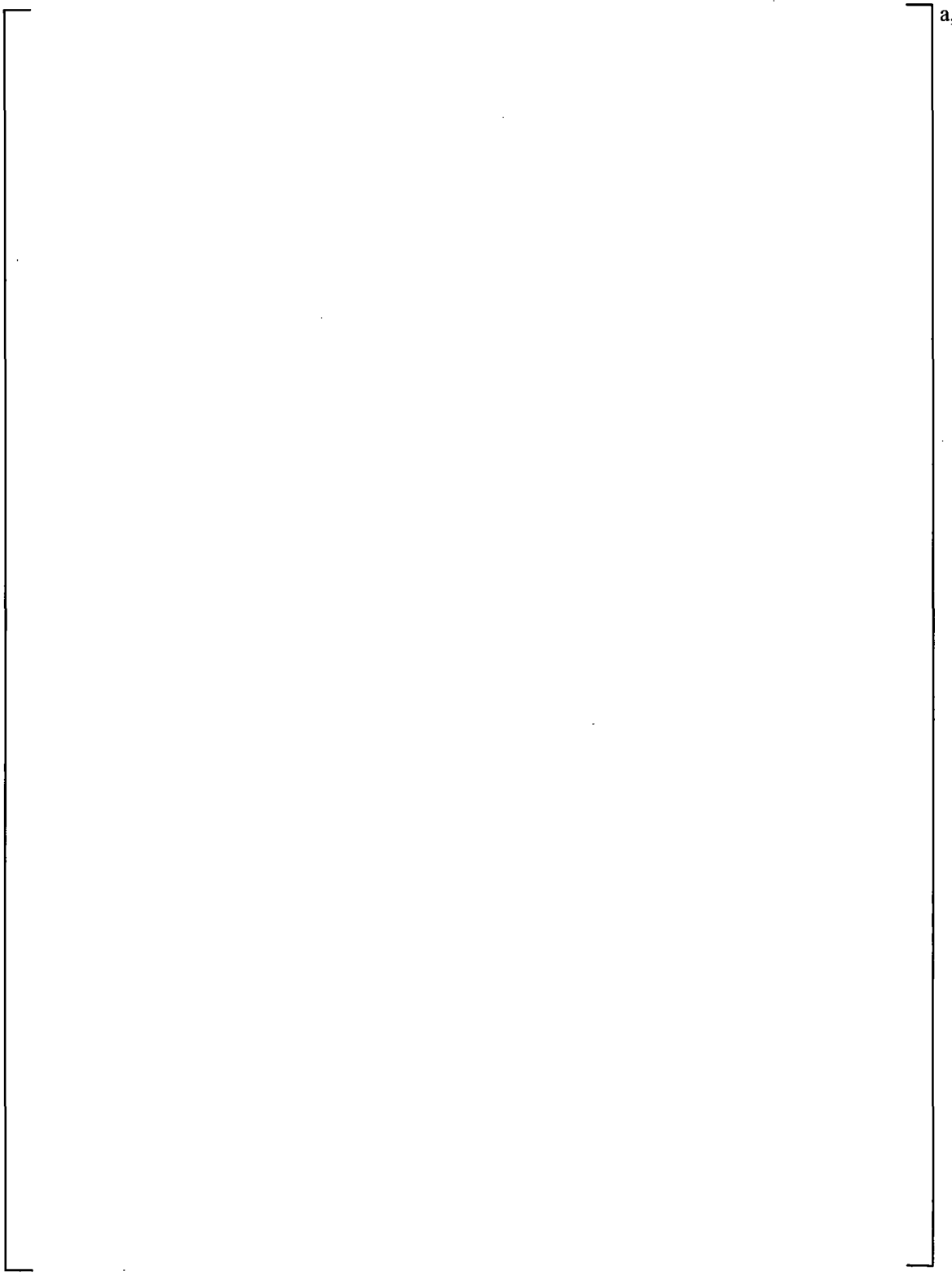

Figure 5-1 Fluid-Elastic Instability Uncertainty Assessment


a,c,e

Figure 5-2 Instability Constant – β

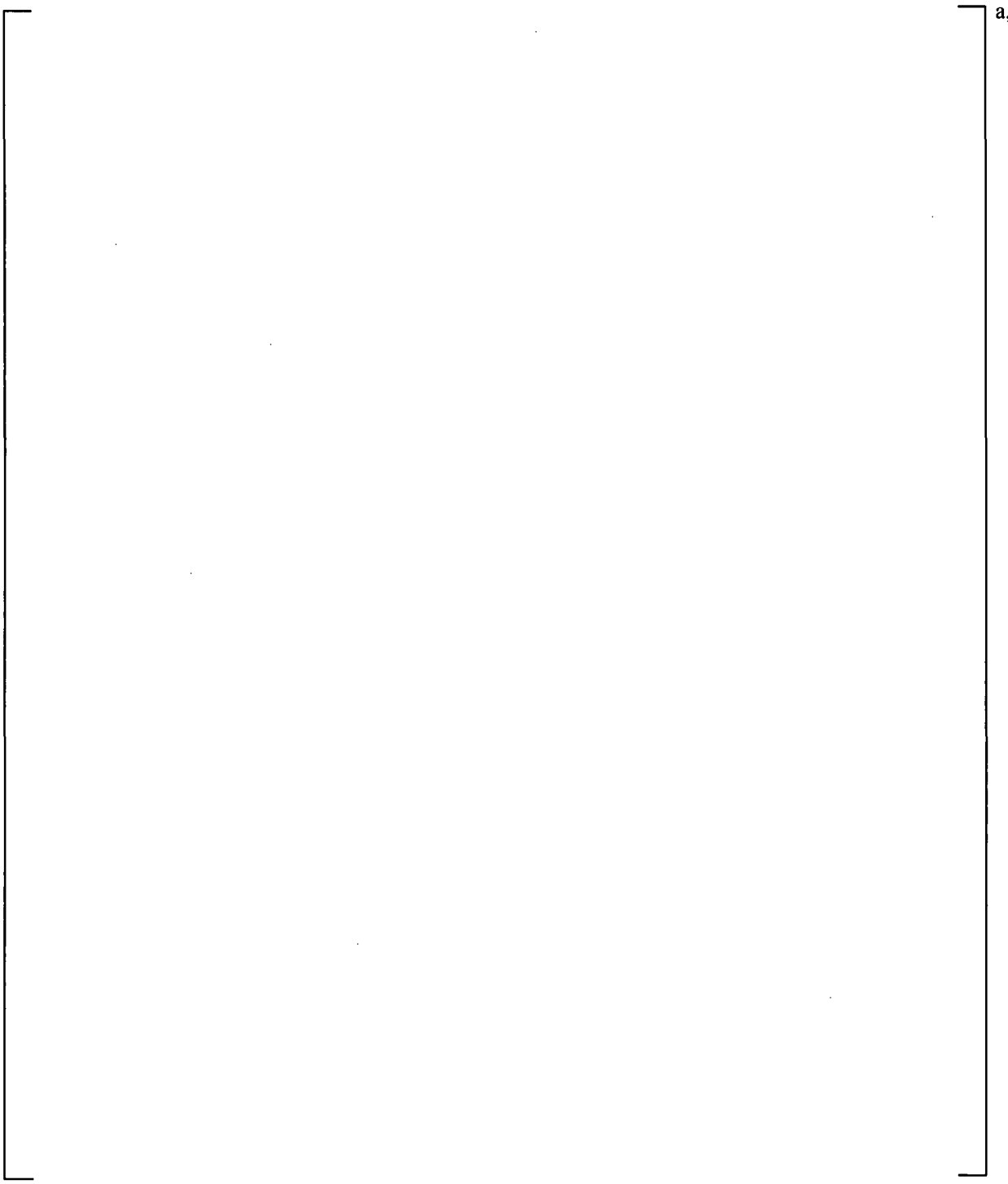
a,c,e

Figure 5-3 Instability Constants, β, Obtained for Curved Tubes from Wind Tunnel Tests on the 0.214 Scale U-bend Model

a,c,e

Figure 5-4 Damping versus Slip Void Fraction

a,b,c

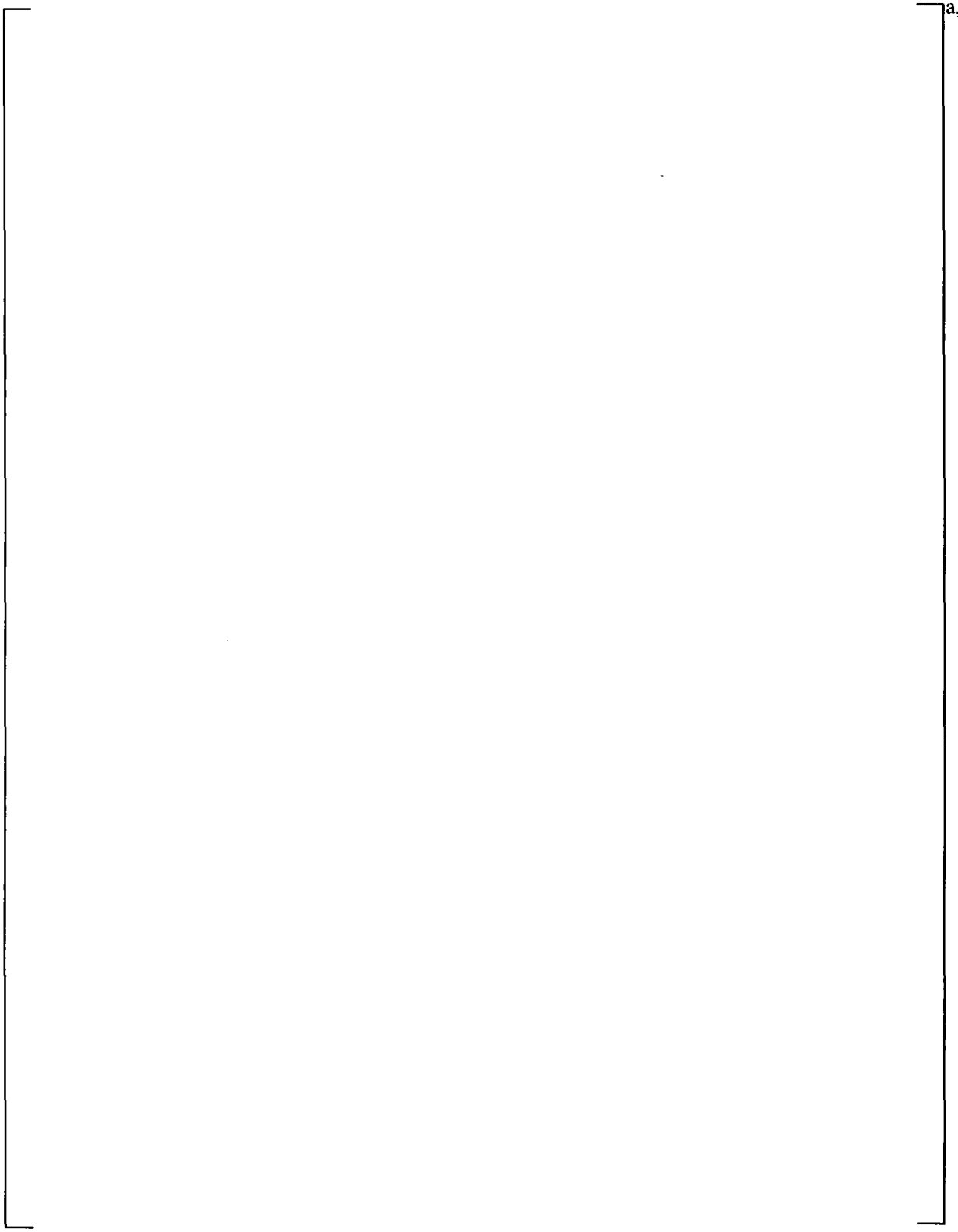

Figure 5-5 Overall View of Cantilever Tube Wind Tunnel Model


a,b,c

Figure 5-6 Top View of Cantilever Tube Wind Tunnel Model

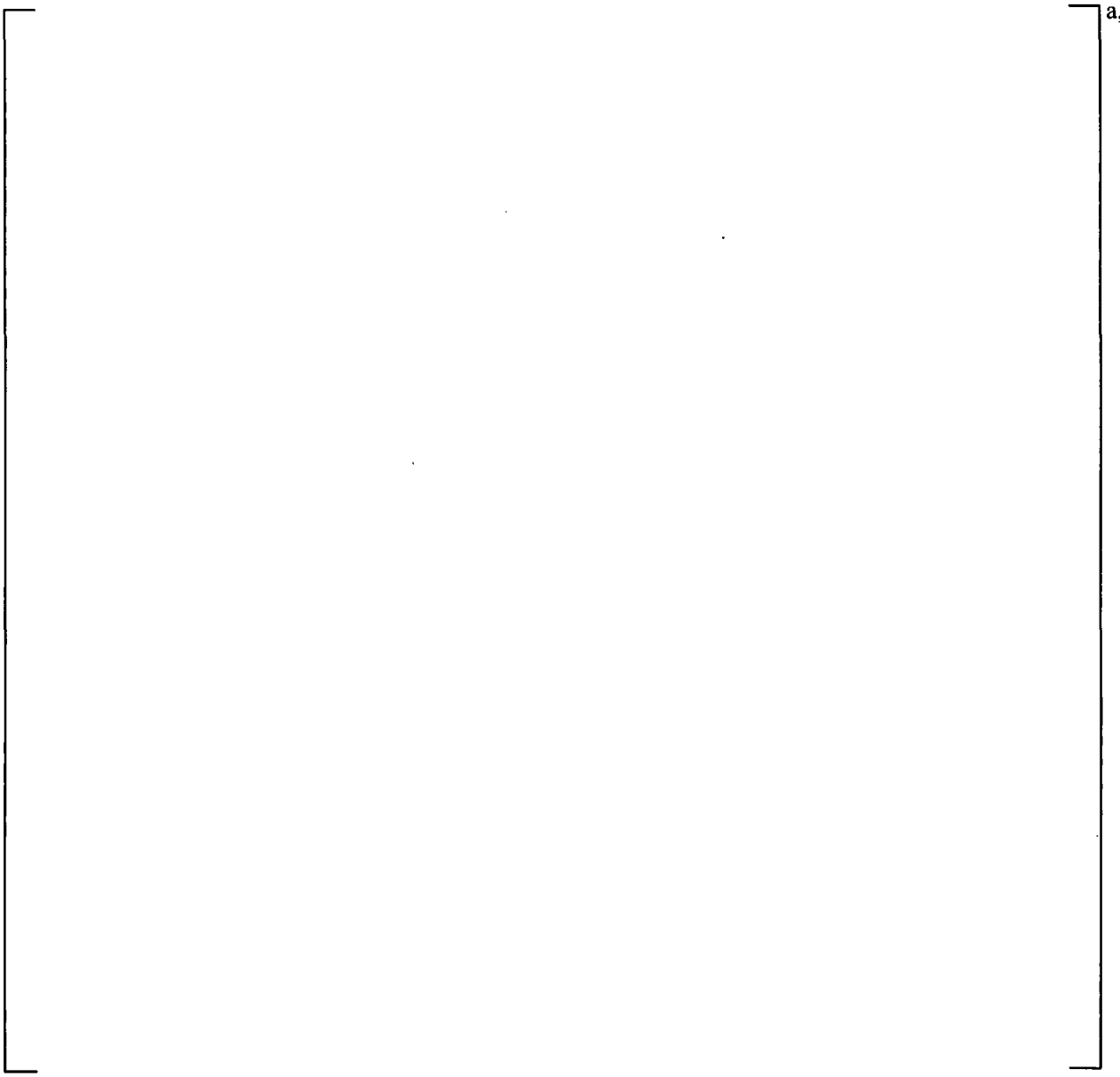

Figure 5-7 Fluid-Elastic Vibration Amplitude with Non-uniform Gaps

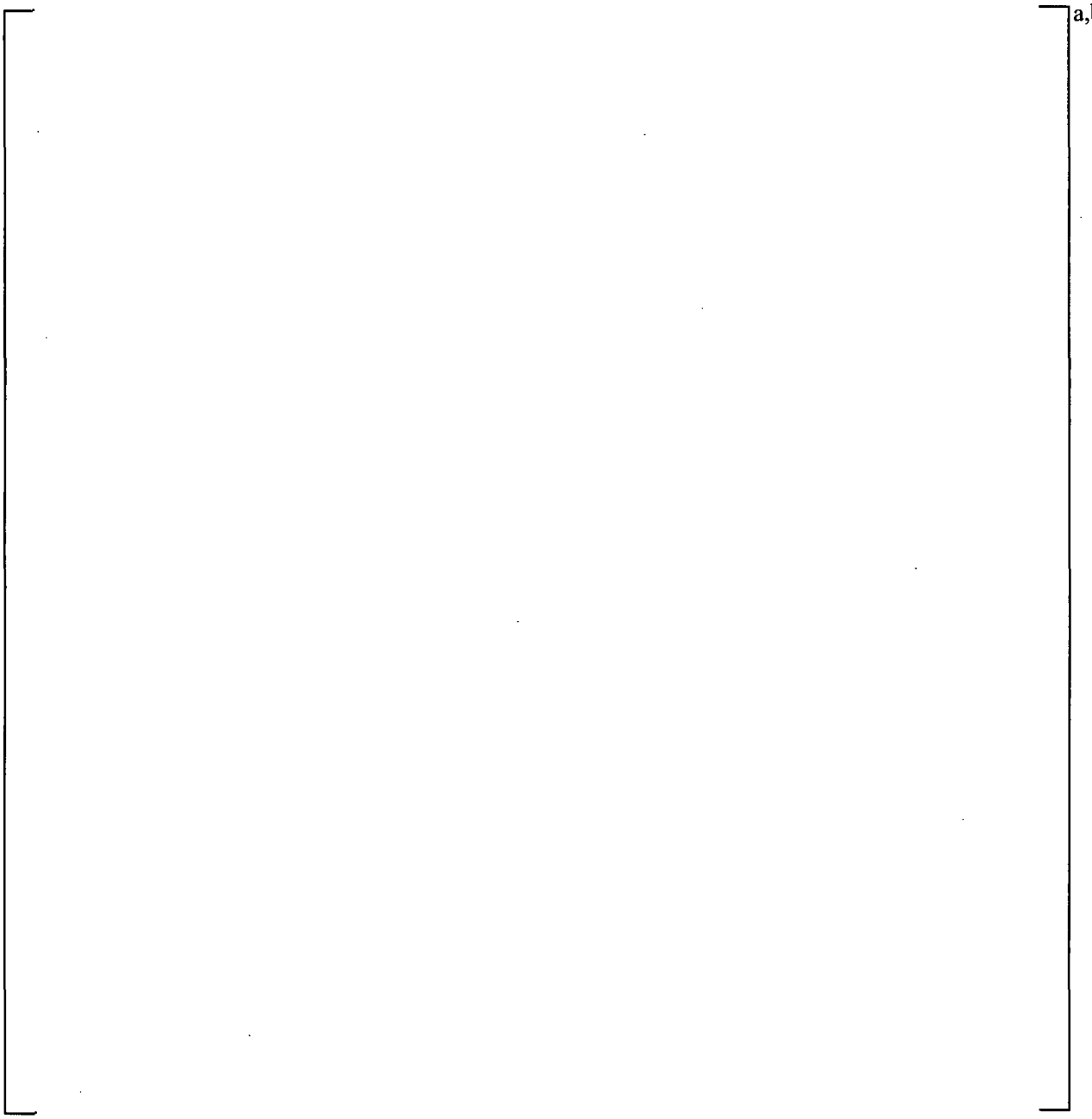
a,b,c

Figure 5-8 Typical Vibration Amplitude and Tube/AVB Impact Force Signals for Fluid-Elastic Vibration with Unequal Tube/AVB Gaps

Figure 5-9 Conceptual Design of the Apparatus for Determining the Effects of Fluid Elastic Instability of Column-Wise Variations in AVB Insertion Depths

Figure 5-10 Overall View of Wind Tunnel Test Apparatus

a,b,c

Figure 5-11 Side View of Wind Tunnel Apparatus with Cover Plates Removed to Show Simulated AVBs and Top Flow Screen

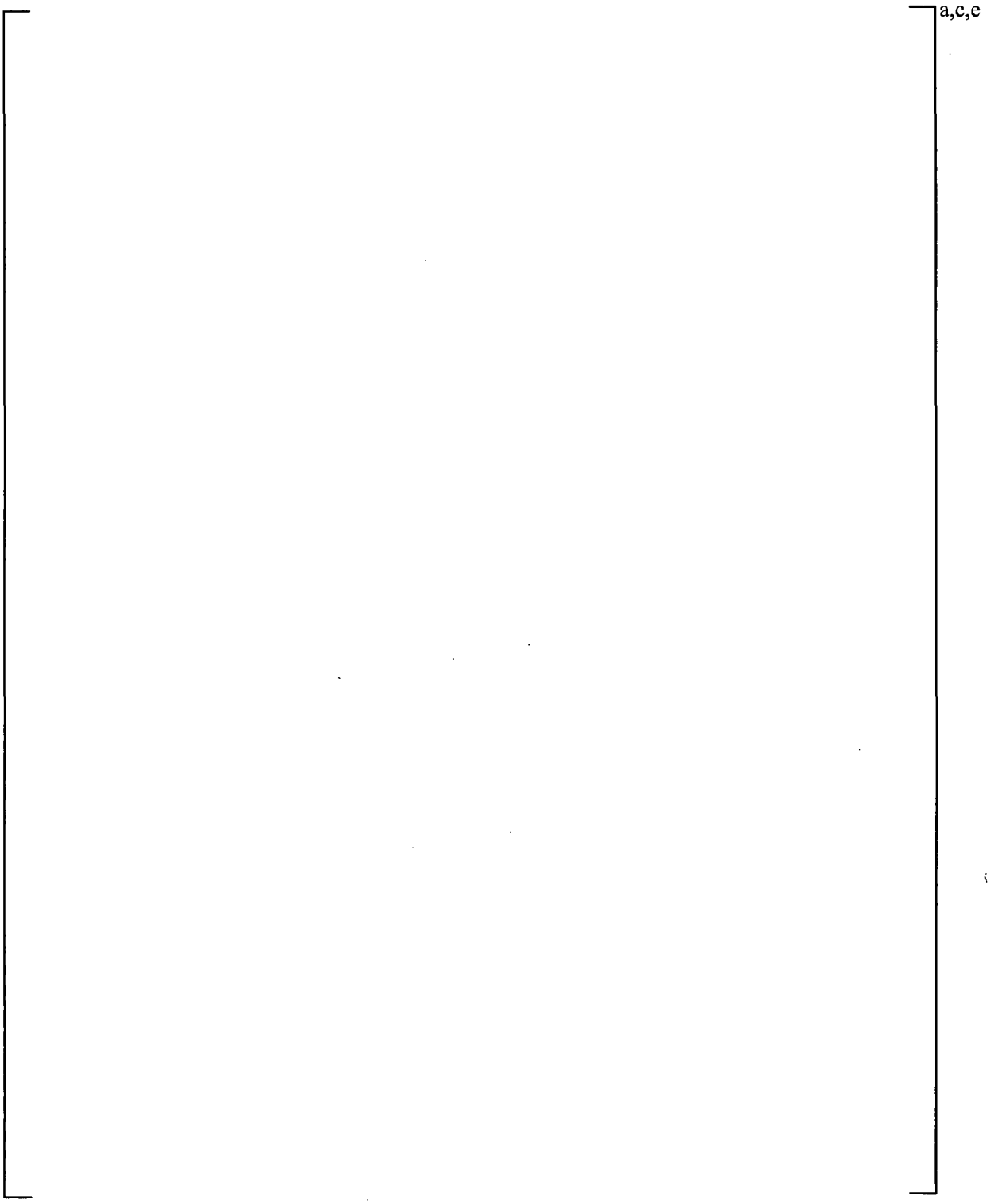

Figure 5-12 AVB Configurations Tested Applicable to Watts Bar Unit 2

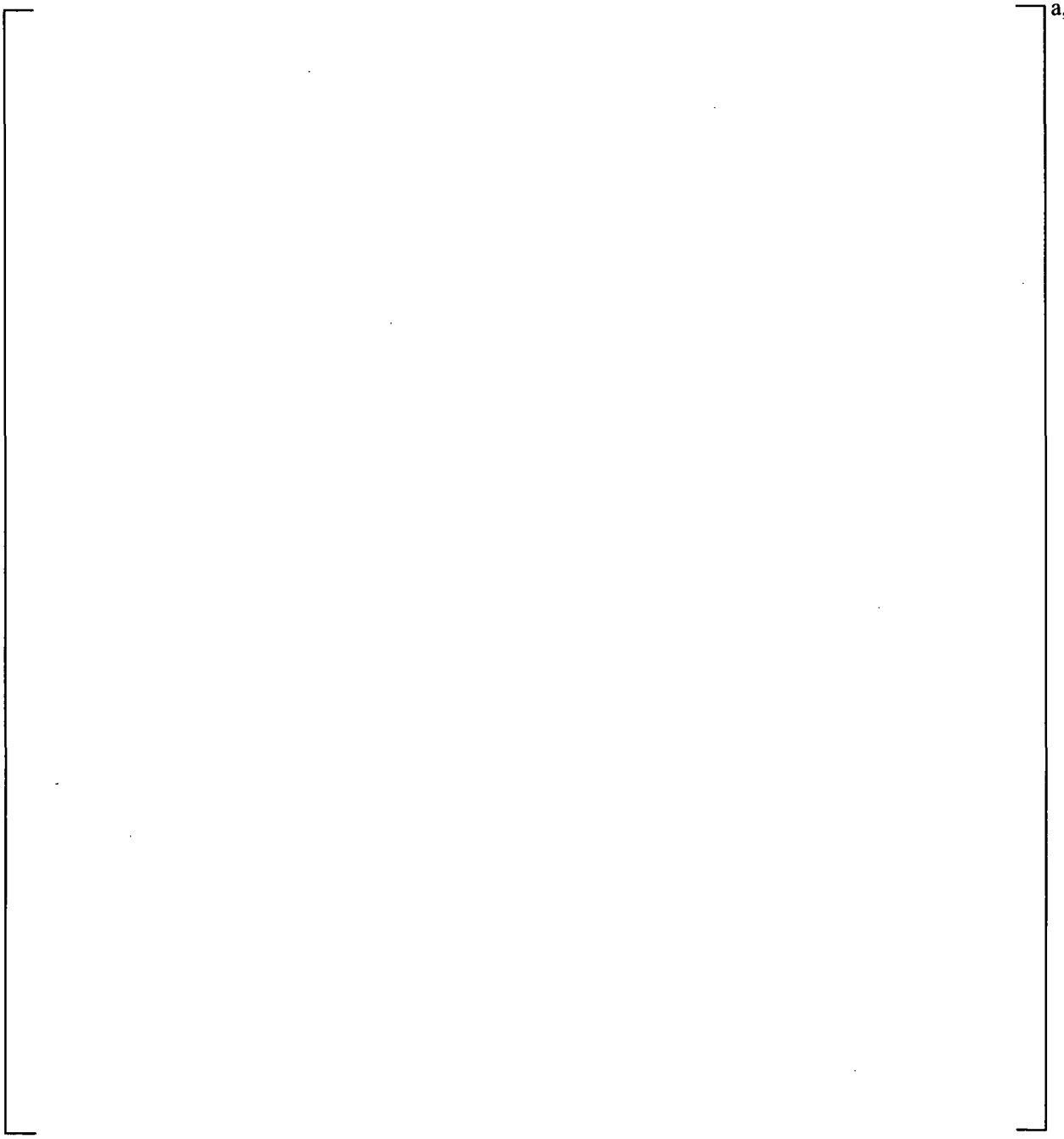
a,c,e

Figure 5-13 Typical Variation of RMS Vibration Amplitude with Flow Velocity for Configuration 1a in Figure 5-12

6 EDDY CURRENT TEST DATA AND AVB POSITIONS

Westinghouse performed a review of ECT data acquired during the February 2010 pre-service inspection of the four Westinghouse Model D3 SGs at Watts Bar Unit 2. Approximately 800 ECT traces, one trace for each tube in Rows 8 through 14, from each SG were analyzed for the presence of signals indicating AVBs. The necessary information from the ECT data are: 1) the total measured U-bend length of the tube from the top TSP on the hot leg side to the top TSP on the cold leg side and 2) the distances from the top TSP to the AVB intersection points with the tubes. The depiction of the AVB positions is documented using AVB insertion depth maps. The AVB maps enable the determination of unsupported tubes and provide an indication of potential local flow peaking.

6.1 WATTS BAR UNIT 2 AVB ASSEMBLY DESIGN

[

].[a,c,e]

[

].[a,c,e] Review of the ECT data for Watts Bar Unit 2 shows that the AVB insertion depth is reasonably uniform across the bundle with some exceptions. Generally, the AVBs are inserted deeper than the design insertion. Deeper insertion of the AVBs is in the conservative direction if no significant local insertion variations occur to cause flow peaking factors (see Section 8) since the lower numbered tube rows are less subject to flow-induced vibration.

6.2 EDDY CURRENT TEST DATA FOR AVB POSITIONS

The AVB insertion depths were determined on the basis of interpretation of the ECT data. To locate the AVBs, the ECT data traces were searched for the characteristic peaks seen in the signals which indicate the intersection of an AVB (or a tube support plate) with the tube. Since the interpretation of the ECT data is not unique with regard to determining the AVB position, due to the inability of ECT testing to differentiate on which side of a tube a "visible" AVB is located, other information was used to assist in establishing the location of the AVBs as follows:

[ ]a,c

[ ] a,c

When two or more ECT signals are identified in the tube, the signals are interpreted as [

].[a,c]

The direct observation data (the number of AVB intersections or tangencies indicated by the ECT probe) are the principal basis for determining the AVB positions and thus, tube support. Where the direct observations are ambiguous or there is a conflict between observations and projections, the more conservative method is used to determine the AVB positions. Since 'direct observation' gives a binary type (yes - no) answer, the projection method is used to 'interpolate' AVB insertion depths between rows

Except for occasional extraordinary conditions, the AVB projections shown on the AVB maps are always based [

]^{a,c} The following ambiguities can result:

[ ] a,c

In these cases, the data for surrounding tubes are analyzed, and factored into the results that are presented. These conditions can result from noise, deposit signals, and as-built AVB geometry variations. Since the Watts Bar Unit 2 SGs have not been operated, noise from deposits was not observed in the ECT data. [

].[a,c]

6.3 TUBE DENTING AT TOP TUBE SUPPORT PLATE

The condition of the tube/TSP interface at the top TSP affects the end condition and damping of the tubes, thus having a significant effect on the potential for tube vibration. The effect of denting on the fatigue usage of the tube is conservatively maximized by assuming the maximum effect of mean stress in the tube fatigue usage evaluation, and by incorporating reduced damping in the tube vibration evaluation.

The ECT data for Watts Bar Unit 2 were not evaluated for denting at the top tube support plate. For the vibration analysis of the tubes, the assumption will be made that all of the top TSP crevices are dented, leading to a conservative structural condition for the tubes (See Section 9-3).

6.4 AVB MAP INTERPRETATIONS

6.4.1 Tube Support

The following criteria have been developed for determining tube support based on the interpretation of the ECT data and application of the AVB position projection method:

- A tube is considered to be supported if the inside edge of the AVB radius is determined, or projected, to be at, or below, the centerline of the tube. This is conservative since the full thickness (0.296 inch) of the AVB would be below this position. Therefore for a Row 10 tube to be supported the projection would have to be ≤10. A projected AVB position that exceeds the row number of an adjacent tube is considered not to provide support to that tube, even though the AVB position would have to exceed the tube position by about 30% of the pitch for the tube to be unsupported.

- A tube is considered supported if only [

]^{a,c}

6.4.2 Summary of Support Conditions

The positions of the AVBs were determined based on: a) observations of AVB signals in the tubes, and b) calculation of the AVB positions based on the design geometry of the tubes and the AVBs. All tubes which are mapped showing an AVB inserted to a depth even with the tube centerline are considered to be supported.

Steam Generator 1

The AVB insertion depth map for SG 1 is provided as Figure 6-1. The number of unsupported tubes in each of Rows 8 through 14 for SG 1 is summarized on Table 6-1.

Steam Generator 2

The AVB insertion depth map for SG 2 is provided as Figure 6-2. The number of unsupported tubes in each of Rows 8 through 14 for SG 2 is shown in Table 6-2.

Steam Generator 3

The AVB insertion depth map for SG 3 is provided as Figure 6-3. The number of unsupported tubes in each of Rows 8 through 14 for SG 3 is shown in Table 6-3.

Steam Generator 4

The AVB insertion depth map for SG 4 is provided as Figure 6-4. The number of unsupported tubes in each of Rows 8 through 14 for SG 4 is shown in Table 6-4.

Table 6-1 Watts Bar Unit 2 SG 1 Quantity of Unsupported Tubes	
Row	**Number**
8	43 unsupported tubes. The unsupported tubes are located in Columns 2 through 20, 88 and 91 through 113.
9	29 unsupported tubes. The unsupported tubes are located in Columns 2 through 12 and 96 through 113.
10	18 unsupported tubes. The unsupported tubes are located in Columns 2 through 8 and 103 through 113.
11	2 unsupported tubes. The unsupported tubes are located in Columns 104 and 113.
12	No unsupported tubes.
13	No unsupported tubes.
14	No unsupported tubes.

Table 6-2 Watts Bar Unit 2 SG 2 Quantity of Unsupported Tubes	
Row	**Number**
8	All tubes are unsupported tubes.
9	57 unsupported tubes. The unsupported tubes are located in Columns 7 through 16, 19 through 23, 54, 58, 60, 68, 70 through 81 and 88 through 113.
10	19 unsupported tubes. The unsupported tubes are located in Columns 11 and 95 through 112.
11	5 unsupported tubes. The unsupported tubes are located in Columns 104 through 108.
12	No unsupported tubes.
13	No unsupported tubes.
14	No unsupported tubes.

Table 6-3 Watts Bar Unit 2 SG 3 Quantity of Unsupported Tubes

Row	Number
8	94 unsupported tubes. The unsupported tubes are located in columns 2 through 11, 18, 19, 21, 23, 27, 29, 31 through 85, 87 and 92 through 113.
9	17 unsupported tubes. The unsupported tubes are located in columns 2 through 8 and 104 through 113.
10	8 unsupported tubes. The unsupported tubes are located in columns 3 through 5 and 109 through 113.
11	2 unsupported tubes. The unsupported tubes are located in columns 112 and 113.
12	No unsupported tubes.
13	No unsupported tubes.
14	No unsupported tubes.

Table 6-4 Watts Bar Unit 2 SG 4 Quantity of Unsupported Tubes

Row	Number
8	98 unsupported tubes. The unsupported tubes are located in columns 2 through 8, 15 through 26, 32 through 95 and 99 through 113.
9	18 unsupported tubes. The unsupported tubes are located in columns 2 through 7, 18, 19, 103 through 111 and 113.
10	11 unsupported tubes. The unsupported tubes are located in columns 2, 3 and 103 through 111.
11	7 unsupported tubes. The unsupported tubes are located in columns 104 through 110.
12	4 unsupported tubes. The unsupported tubes are located in columns 106 through 109. No ECT inspection data exists for Column 113. Record revealed that this tube had a welded plug installed at the manufacturer.
13	No unsupported tubes.
14	No unsupported tubes.

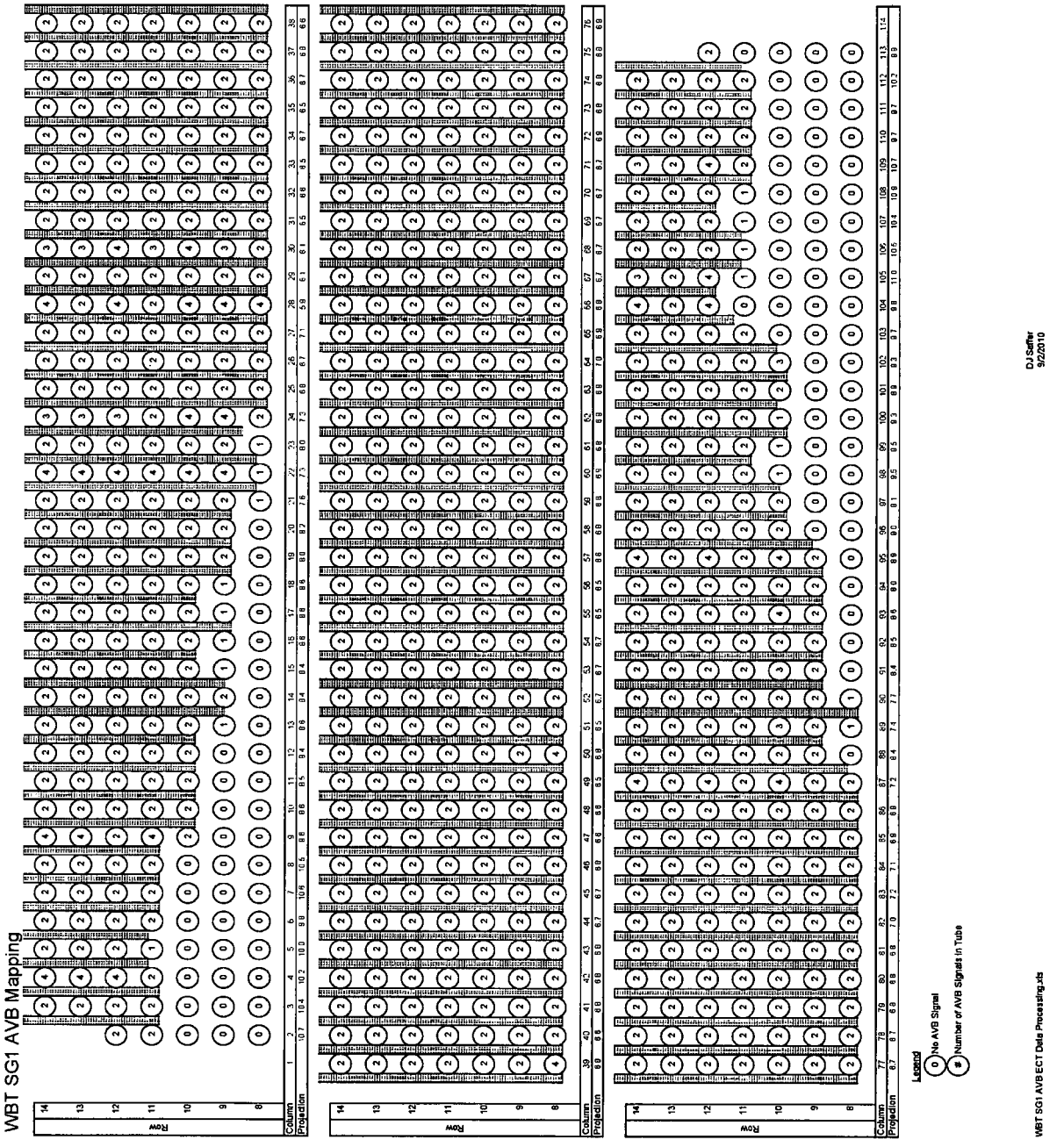

Figure 6-1 Watts Bar Unit 2 SG 1 AVB Insertion Map

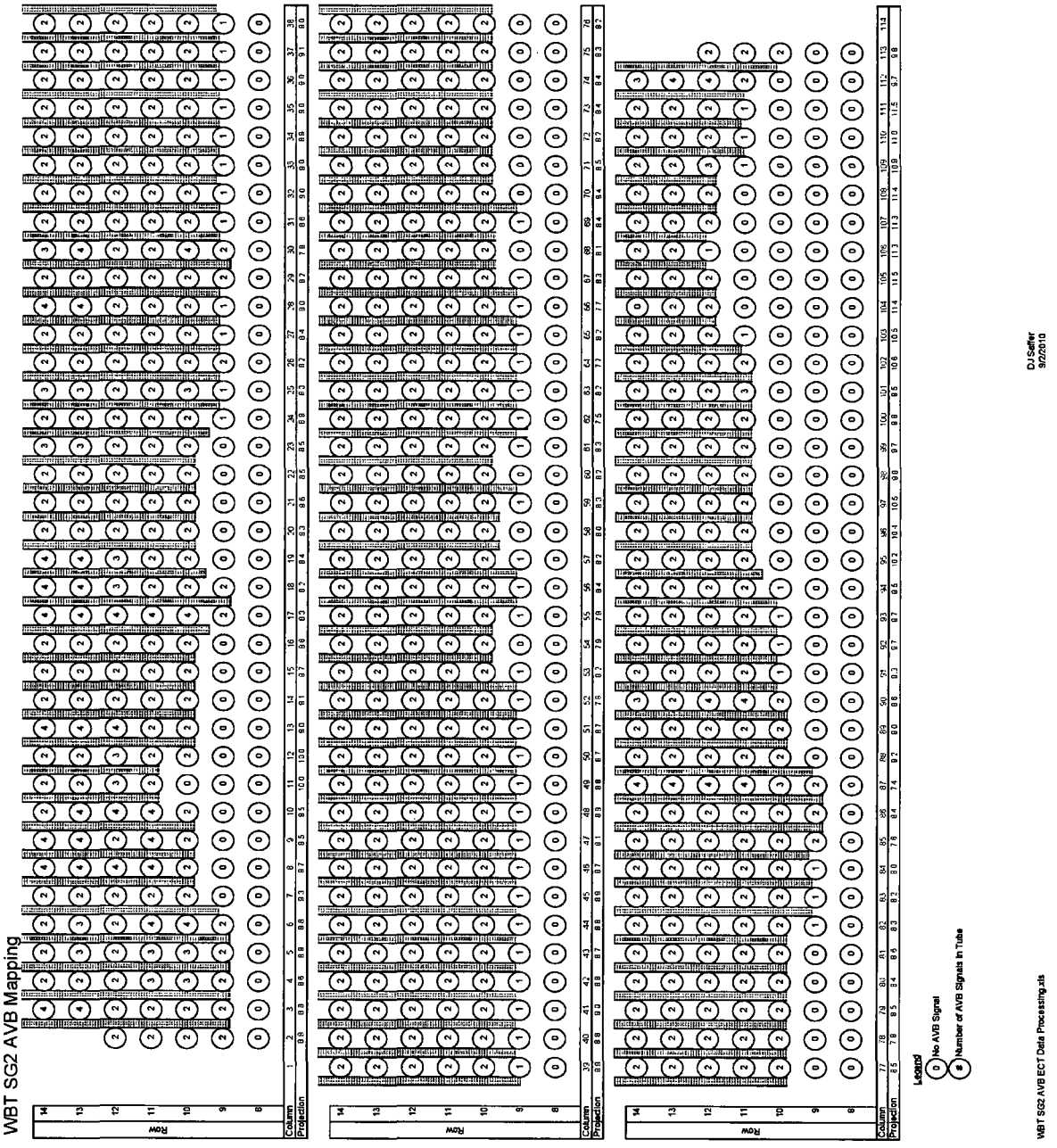

Figure 6-2 Watts Bar Unit 2 SG 2 AVB Insertion Map

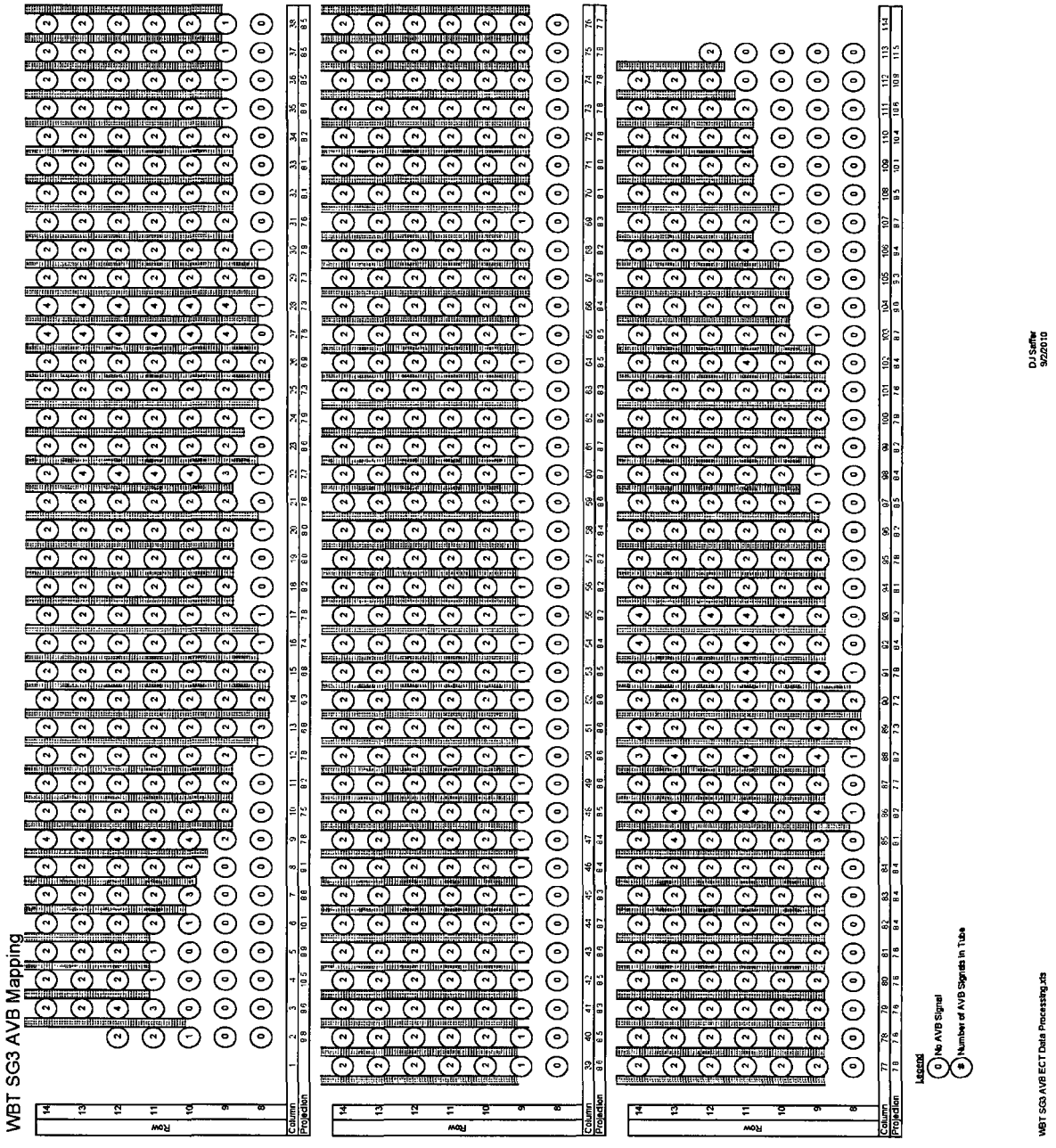

Figure 6-3 Watts Bar Unit 2 SG 3 AVB Insertion Map

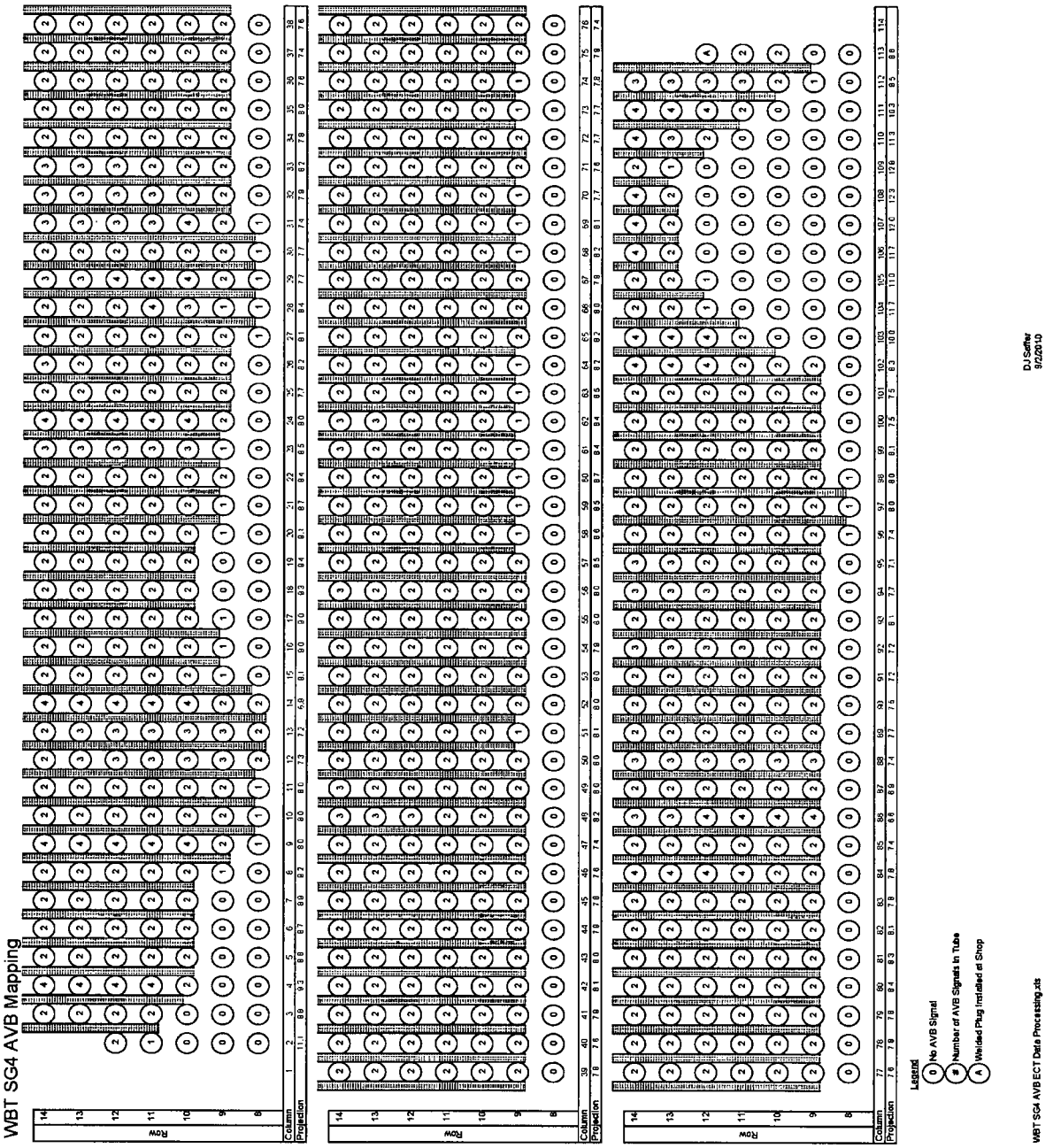

Figure 6-4 Watts Bar Unit 2 SG 4 AVB Insertion Map

7 THERMAL AND HYDRAULIC ANALYSIS

This section presents the results of a thermal-hydraulic analysis of the flow field on the secondary side of the Watts Bar Unit 2 steam generator using the three-dimensional (3-D) ATHOS computer code, Reference 7-1. The major results of the analysis are the water/steam velocity components, density, void fraction, and the primary and secondary fluid and tube wall temperatures. The distributions of the tube gap velocity and density along a given tube were obtained by reducing the ATHOS results. The bundle parameter distributions used in the Watts Bar Unit 2 analysis are based on the ATHOS results for another Model D3 steam generator having nearly the same operating conditions. The effect of the small difference in operating conditions between the two units was accounted for by applying an adjustments factor of the computed stability ratios.

In the following subsections, the operating condition data for Watts Bar Unit 2 is presented with a comparison with the corresponding conditions on which the reference Model D3 tube bundle study was based. As part of this comparison, a one-dimensional relative stability ratio calculation technique is described. The adjustment of the reference stability ratios is based on this technique.

7.1 ATHOS ANALYSIS MODEL

The calculation of relative stability ratios involves comparing the stability ratio calculated for one or more tubes in a given plant to the ratio calculated for the ruptured Row 9 Column 51 (R9C51) tube in the North Anna Series 51 steam generator. It makes use of the ATHOS computed flow profiles for both tube bundles. Since the presence of AVBs in the U-bend region of the tube bundle could influence the overall flow field and/or the local flow parameters for a particular tube of interest, some discussion of the treatment of AVBs is necessary before presenting a description of the ATHOS model.

The ATHOS family of codes did not include the capability to model the presence of the AVBs in the U-bend region at the time of the original reference Model D3 analysis. However, Westinghouse had modified the code to include the capability to model the AVBs via flow cell boundary resistance factors. Practical lower limits of cell size in the ATHOS code, however, prevent a fine grid representation of the AVB V-bar shape which, in turn, limits the accuracy of the AVB representation. ATHOS calculations have been performed with and without AVBs in the model. [

].[a,c]

The reference Model D3 analysis is based on a Cartesian coordinate system for the array of flow cells instead of the typical, and more widely used, cylindrical coordinate system. With a Cartesian coordinate system, the tube array and any AVBs are arranged in a square pitched configuration which is in line with the coordinate axes. This alignment provides an improved representation of the tube bundle.

The ATHOS Cartesian coordinate system model for the Model D3 steam generator consists of 18,720 flow cells having 39 divisions in the x-axis (perpendicular to the tube lane) direction, 16 divisions in the y-axis (along the tube lane) direction, and 39 divisions in the z-axis (axial) direction. In the ATHOS analysis, the steam generator is considered to be symmetrical about the x-axis of the tube bundle. The model therefore, consists of one-half of the hot leg and one-half of the cold leg sides of the steam generator. Figures 7-1 and 7-2 show the plane and the elevation views of the model. These two figures show the layout of the flow cells and identify locations for some of the geometric features.

As shown in Figure 7-1, with the Cartesian coordinate system, the circular wrapper boundary is represented by a step-wise wall as indicated by the heavy lines. All of the flow cells outside the simulated wrapper boundary above the first axial slab were blocked off by specifying extremely high flow resistances on the faces of the appropriate cells. Tube lane flow slots in the tube support plates are also modeled.

Figure 7-2 shows the elevation view of the model on the vertical plane of symmetry of the steam generator. The feedwater nozzle is located at axial indices IZ = 11 and 12. Ten axial layers of cells were included in the U-bend near the top tube support plate (IZ =27 to IZ = 36) to more closely model the flow conditions in the area of interest.

Figure 7-3 reproduces the plane view of the model but with the tube layout arrangement superimposed. This figure illustrates the locations of the tubes in the various flow cells. The grid lines in the Cartesian model are in line with the tube array, providing for all of the tubes to be within the boundary of the flow cells. The fineness of the cell mesh is evident; the largest cells contain only 25 tubes while some of the smallest cells include only three tubes. Note, in particular, that additional detail was added near the bundle periphery (IY = 12 to IY = 16, see Figure 7-1) to more closely model the inner radius tubes.

7.2 ATHOS RESULTS

The results from the ATHOS analysis consist of the thermal-hydraulic flow parameters necessary to describe the 3-D flow field on the secondary side of the steam generator (velocity, density, and void fraction) plus the distributions of the primary fluid and mean tube wall temperatures. The secondary side mixtures velocity is composed of three components (V_x. V_y, and V_z) which ATHOS computes on the surfaces of the flow cell. Since the local gap velocity surrounding a tube is required in the vibration analysis, a post-processor is used which:

1. Interpolates among the velocity components for the cells located nearest to the tube of interest.

2. Accounts for the minimum flow area between tubes to calculate the tube-to-tube gap velocity.

The post-processor performs the necessary interpolations to determine both in-plane and out-of-plane gap velocities at specific intervals along the length of a tube. It also interpolates on the ATHOS cell-centered density and void fraction to determine the required local parameters along the tube length. The output of the post-processing is a data file which contains these parameter distributions for all the tubes in the generator and which provides a portion of the input data required for tube vibration analysis.

Figure 7-4 shows a vector plot of the flow pattern on the vertical plane of symmetry of the steam generator (the vectors are located at the center of the flow cells shown in Figure 7-2). The zig-zag flow pattern through the split flow pre-heater is clearly shown in the figure. On the hot leg side, the vertical flow upward through most of the tube bundle is also clearly shown. The vertical velocity (V_z) component entering the U-bend region on the hot leg side is about twice that of the cold leg side as seen in Figure 7-5 (at model vertical layer index IZ = 27).

The lateral velocity components, $VR = (V_x^2 + V_y^2)^{.5}$, on the same horizontal plane (IZ = 27) are shown in Figure 7-6. Viewing Figures 7-5 and 7-6, it is seen that at the entrance to the U-bend region the vertical velocity component is about twice that of the lateral velocity resultant on the hot leg side, but is about three times of that on the cold leg side.

Figure 7-7 shows the plot of the void fraction contours on the vertical plane of symmetry of the steam generator. In the pre-heater, the void fraction is essentially zero. By comparison, the hot leg side void fraction develops rapidly from the lower bundle region. In the U-bend region the void fraction is about 0.9 to 0.95 on the hot side, decreasing to about 0.60 at the bundle periphery on the cold leg side.

Figures 7-8, 7-9, and 7-10 show a sample of the individual tube gap velocity and density distributions along three tubes at Row 10. In each figure the gap velocity and density along the length of the tube are plotted from the hot leg tubesheet end on the left of the figure to the cold leg end on the right. The mixture gap velocity and density distribution are required as part of the input for tube vibration analysis to determine the tube stability ratios. This data was generated by the ATHOS post-processor for each tube in the model and stored in a data file. The data file was then utilized in the subsequent stability ratio calculations.

Figure 7-11 shows the plot of the average in-plane gap velocity normal to the tube and density profiles as a function of the column number along Row 10. The average values were taken as the numerical average of the parameter over the entire 180° span of a U-bend at a given column location. The average velocity values are between 7.3 and 8.4 ft/sec. The velocity variations seen in the figure at Columns 22, 38, and 50 are related to the effects of the flow slots along the tube lane of the top support plate.

7.3 RELATIVE STABILITY RATIO ANALYSIS

Full power steam generator operating condition data for Watts Bar Unit 2 is presented in Table 7-1. Full power steam generator operating condition data for Watts Bar Unit 2, including a measurement uncertainty recapture (MUR) uprate, is presented in Table 7-2. Each operating condition considers 0% and 10% tube plugging while the primary inlet temperature is maintained at its nominal value. This level of plugging reduced the nominal design pressure in each instance.

With the above data, calculations were completed using the Westinghouse SG performance computer Code, GENF, to verify the plant data and to establish a complete list of operating conditions for an ATHOS analysis. The GENF code determines the primary side temperature and steam flow rate required to obtain the specified steam pressure at the given power rating. Besides confirming these parameters, the code calculates the circulation ratio which is of primary importance to the stability ratio analysis since it, together with the steam flow, establishes the total bundle flow rate and average loading on the tubes. It also provides an overall indication of the voids within the tube bundle since the bundle exit quality is inversely proportional to the circulation ratio (X_{exit} = 1/circulation ratio). The calculated circulation ratio is also listed in Tables 7-1 and 7-2. In addition, the operating conditions on which the reference Model D3 ATHOS study was based are listed in Table 7-3.

With respect to their effect on tube stability ratios, three of the operating parameters are of primary importance: steam flow, steam pressure, and the circulation ratio. Note that primary side temperatures have only a very minor influence on stability ratios. As mentioned previously, the steam flow rate and circulation influence the total bundle flow rate and tube-to-tube gap velocity in the U-bend. The steam pressure also influences the gap velocity via the void fraction and density, however, its major impact is on the tube dampening. High U-bend flow along with low steam pressure results in a higher loading on the tubes with reduced dampening. Both of these factors lead to higher, more limiting stability ratios. As indicated in Table 7-1, the normal operating conditions for Watts Bar Unit 2 are very similar to those of the reference Model D3 steam generator. Only small differences exist in the steam flow rate, pressure, and circulation ratio. The MUR uprate power conditions listed in Table 7-2 are representative of MUR uprate power conditions that would occur for the Watts Bar Unit 2 Model D3 steam generators.

The fluid elastic stability ratio is defined as the ratio of the effective fluid velocity acting on a given tube to the critical velocity at which large amplitude fluid elastic vibration initiates:

$$SR = \frac{U_e}{U_c} \tag{7-1}$$

Where;

SR = Fluid elastic stability ratio

U_e = Effective velocity

U_c = Critical velocity at onset of instability

In this ratio, the effective velocity depends on the distribution of flow velocity and fluid density, and on the mode shape of vibration. The critical velocity is based on experimental data and has been shown to be dependent upon the tube natural frequency, damping, the tube geometry, the tube pattern, and the fluid density, along with the appropriate correlation coefficients.

The detailed calculation of the stability ratio using velocity and density distributions requires three-dimensional thermal-hydraulic and tube vibration calculations that are lengthy. Therefore, a simplified, one-dimensional version of this ratio has been used to provide a relative assessment technique for determining the effect of changes in operating conditions on the stability ratio. The relative stability ratio is defined by the following equation:

$$\left[\quad\right]^{a,c} \tag{7-2}$$

In this equation "*WBT*" refers to Watts Bar Unit 2 operating conditions and "*REF*" to the reference Model D3 conditions used for the ATHOS analysis. Note that *SR* for the *REF* plant had been calculated by using 3-D velocity and density distributions as calculated by the ATHOS computer code for the whole tube bundle. The *WBT* plant would have had similar 3-D velocity and density distributions within the whole tube bundle. Therefore, Equation (7-2) would be adequate to describe fluid elastic behavior for the WBT plant. Four components make up this ratio: a loading term based on the dynamic pressure (ρV^2), a tube incremental mass (m) term, the natural frequency of the tube (f_n), and a damping ratio (δ) term. It should be noted that the ratio is relative, in that each component is expressed as a ratio of the value for a given operating condition to that of a reference operating point.

[

].[a,c] The particular damping correlation which is used for all normalized stability ratio calculations is based on a dented condition at the top tube support plate (a clamped condition, as discussed in Section 5.2). The clamped condition is also assumed in calculating the tube natural frequency.

As shown in the comparison in Table 7-4, the effect of the small difference in operating conditions between normal operating conditions at Watts Bar Unit 2 and the reference Model D3 conditions only produces a 3% increase in the relative stability ratio and a maximum of 8% increase for MUR uprate power conditions with 10% tube plugging. The change in steam pressure between the operating conditions is the primary factor leading to the increase between conditions. The existing stability ratios for the reference Model D3 steam generator will be adjusted upward by at least 3% and at most 8% to generate a set of 3-D stability ratios for Watts Bar Unit 2.

Justification for use of a one-dimensional (1-D) relative stability ratio adjustment factor is [

].[a,c]

7.4 STEAM GENERATOR OPERATING CONDITIONS AND 1-D RELATIVE STABILITY RATIO

This subsection develops relative stability ratios for Watts Bar Unit 2 at conditions which bound normal operating conditions and anticipated MUR uprate power operating conditions. Stability ratios will be calculated in relation to the North Anna (NA) operating conditions according to a verified algorithm for both the WBT and REF plants as follows:

[ ] a,c

7.4.1 Stability Ratio Cases Examined

Relative stability ratios were calculated for the following sets of conditions.

1. The Reference ATHOS conditions.
2. Watts Bar Unit 2 plant conditions at 100% normal power and 0% plugging.
3. Watts Bar Unit 2 plant conditions at 100% normal power and 10% plugging.
4. Watts Bar Unit 2 plant conditions at 100% MUR uprate power conditions and 0% plugging.
5. Watts Bar Unit 2 plant conditions at 100% MUR uprate power conditions and 10% plugging.

7.4.2 Input Assumptions

The four operating conditions for Watts Bar Unit 2 are presented in Table 7-1 and Table 7-2. Table 7-1 presents the normal operating parameters for Watts Bar Unit 2. Table 7-2 presents the operating parameters for Watts Bar Unit 2 considering the measurement uncertainty recapture NSSS Power uprate. one-dimensional (1-D) relative stability ratios were developed for the four possible operating conditions at Watts Bar Unit 2 to address any future changes.

The reference conditions presented in Table 7-3 were used in the ATHOS analysis.

7.4.3 Relative Stability Ratio Results

Table 7-4 lists the operating parameters for input to the relative stability ratio calculation along with relative stability ratios calculated for these conditions.

7.4.4 Future Operating Conditions

For future operation, it is assumed that the plant power level will start at the original 3427 MWt NSSS power level. Over time, steam pressure, the other principal parameter affecting the relative stability ratio, can decrease as a result of plugging, fouling, or primary temperature reductions. The steam generator operating characteristics and relative stability ratios were also calculated at a reduced steam pressure to account for these occurrences during future operation. The reduced steam pressure conditions were obtained by assuming 10% plugging with fouling and primary temperature held at the current levels. Water level is assumed to be at the normal value.

Also included are the relative stability ratios for a 3475 MWt NSSS power uprate. This condition is assumed to occur in the future, after the plant has been operating at the original 3427 MWt NSSS power level. As with the original 3427 MWt NSSS power level, steam pressure can decrease as a result of plugging, fouling, or primary temperature reductions. Again, the steam generator operating characteristics and relative stability ratios were calculated at a reduced steam pressure to account for these occurrences during future operation. The reduced steam pressure conditions were obtained by assuming 10% plugging with the fouling and primary temperatures held at current levels (relative to the 3475 MWt NSSS power uprate). Water level is assumed to be at the normal value.

Once a limiting relative stability ratio for a fatigue usage of 1 is calculated (Section 9) for the most susceptible tubes, the stability ratio calculated for future operation can be used to determine whether the tubes can continue in service for the remainder of plant operation or will require preventative action.

7.4.5 References

7.1 L. W. Keeton, A. K. Singhal, et. al., "ATHOS3: A Computer Program for Thermal-Hydraulic Analysis of Steam Generators," Vol. 1, 2, and 3, EPRI NP-4604-CCM, July 1986.

Table 7-1 Normal Operating Parameters for Watts Bar Unit 2

a,c

Table 7-2 Operating Parameters with MUR Uprate for Watts Bar Unit 2

a,c

Table 7-3 Operating Parameters for the ATHOS Analysis*

Thermal Design Parameters	Reference Value

a,c

Table 7-4 Watts Bar Unit 2 Relative Stability Ratios

Plant Condition	Steam Flow Rate , (lb/hr)	Circulation Ratio	Steam Pressure, (psia)	Stability Ratio	
				Relative to North Anna Units 1/2	Relative to ATHOS Reference

a,c

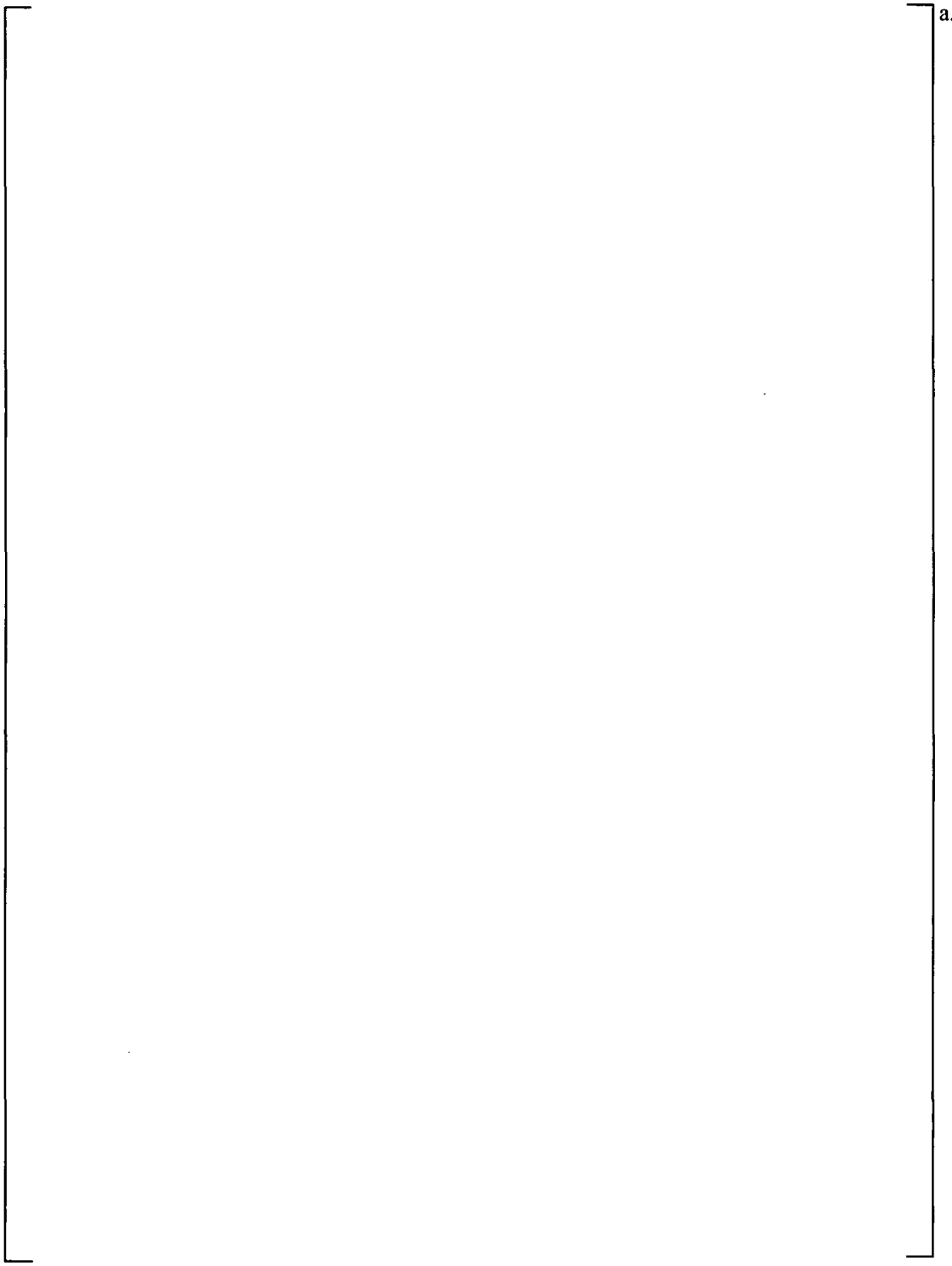

Figure 7-1 Plane View of ATHOS Cartesian Model for Model D3 Steam Generator

[a,c

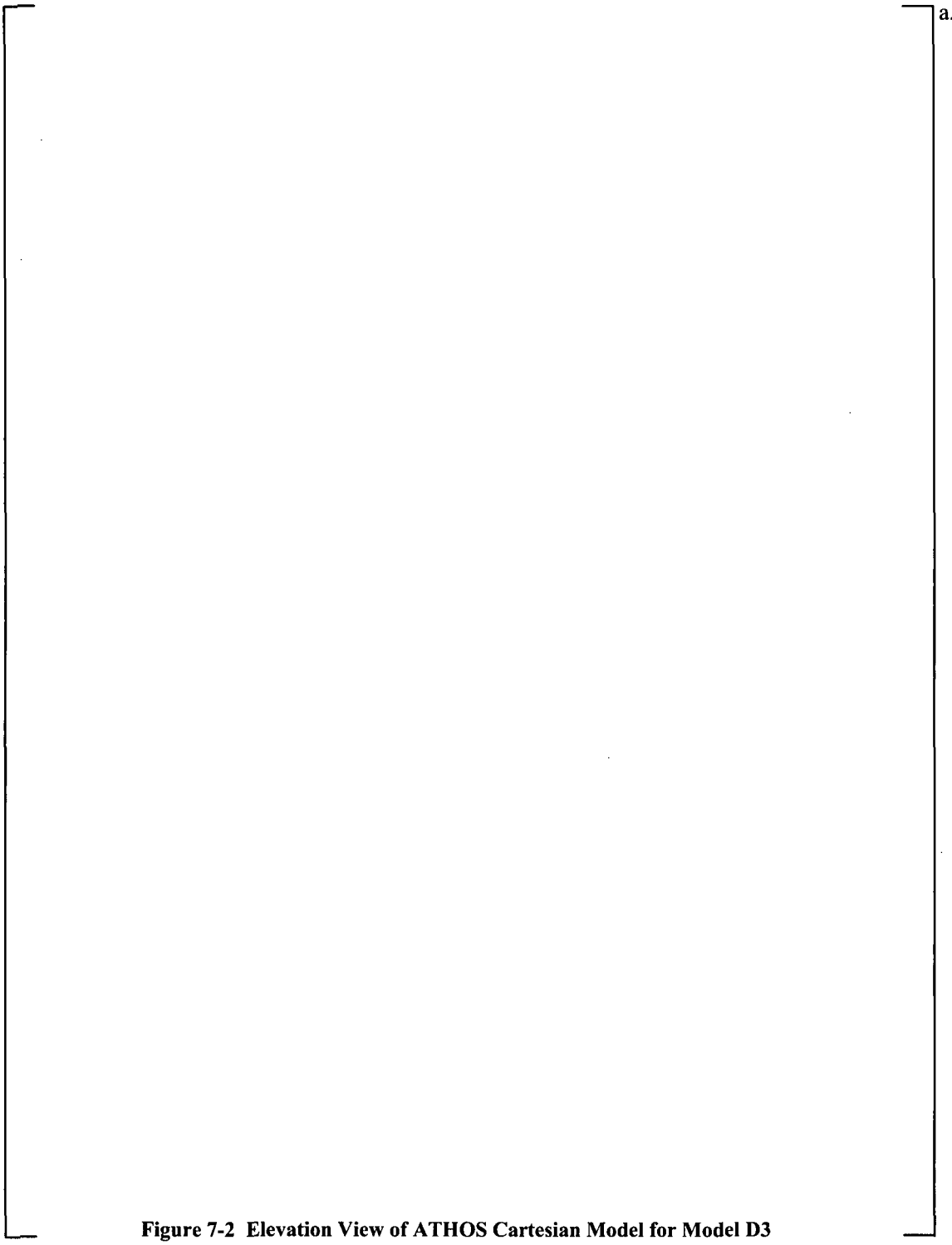

]

Figure 7-2 Elevation View of ATHOS Cartesian Model for Model D3

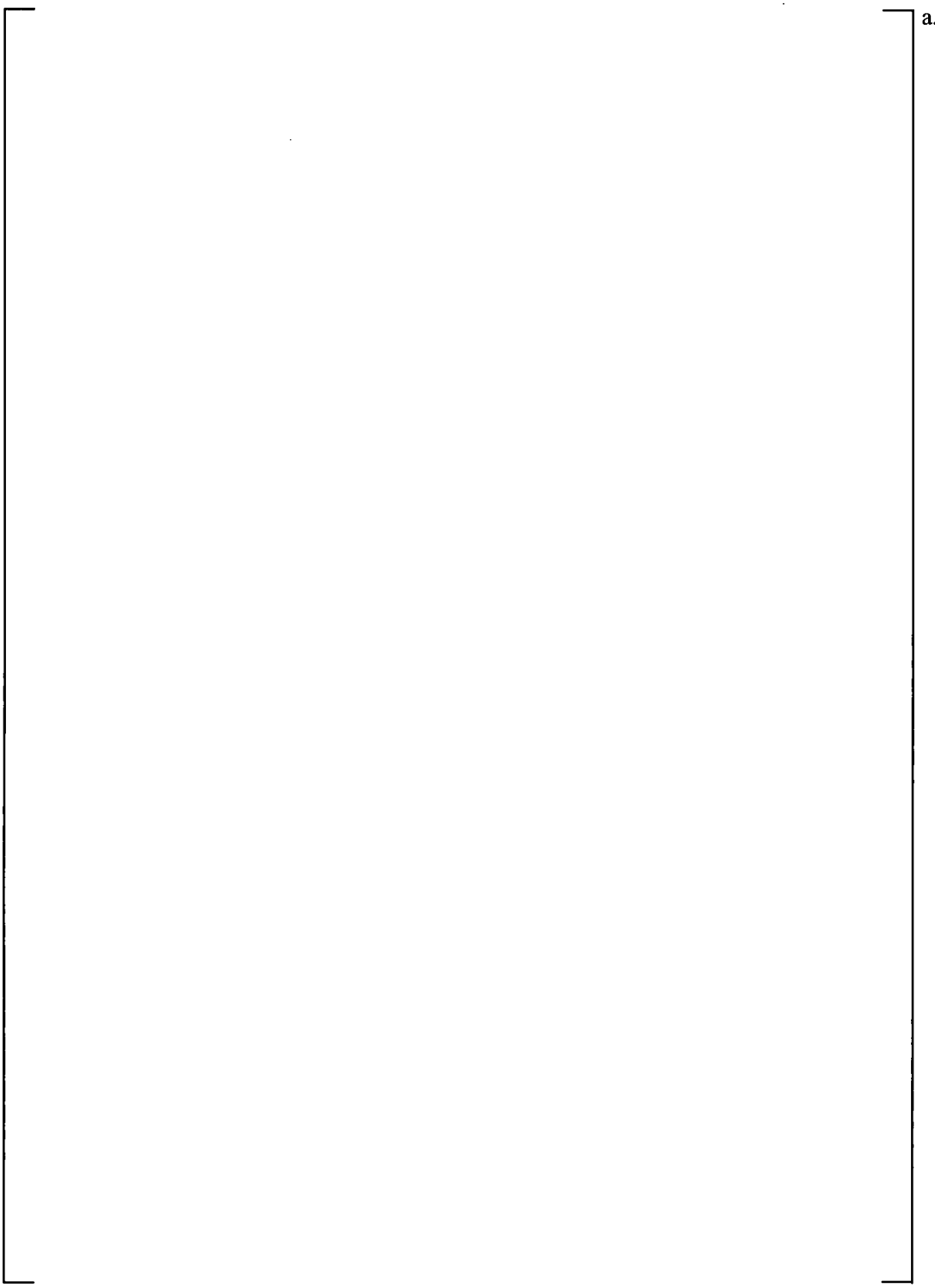

Figure 7-3 Plane View of ATHOS Cartesian Model for Model D3 Indicating Tube Layout

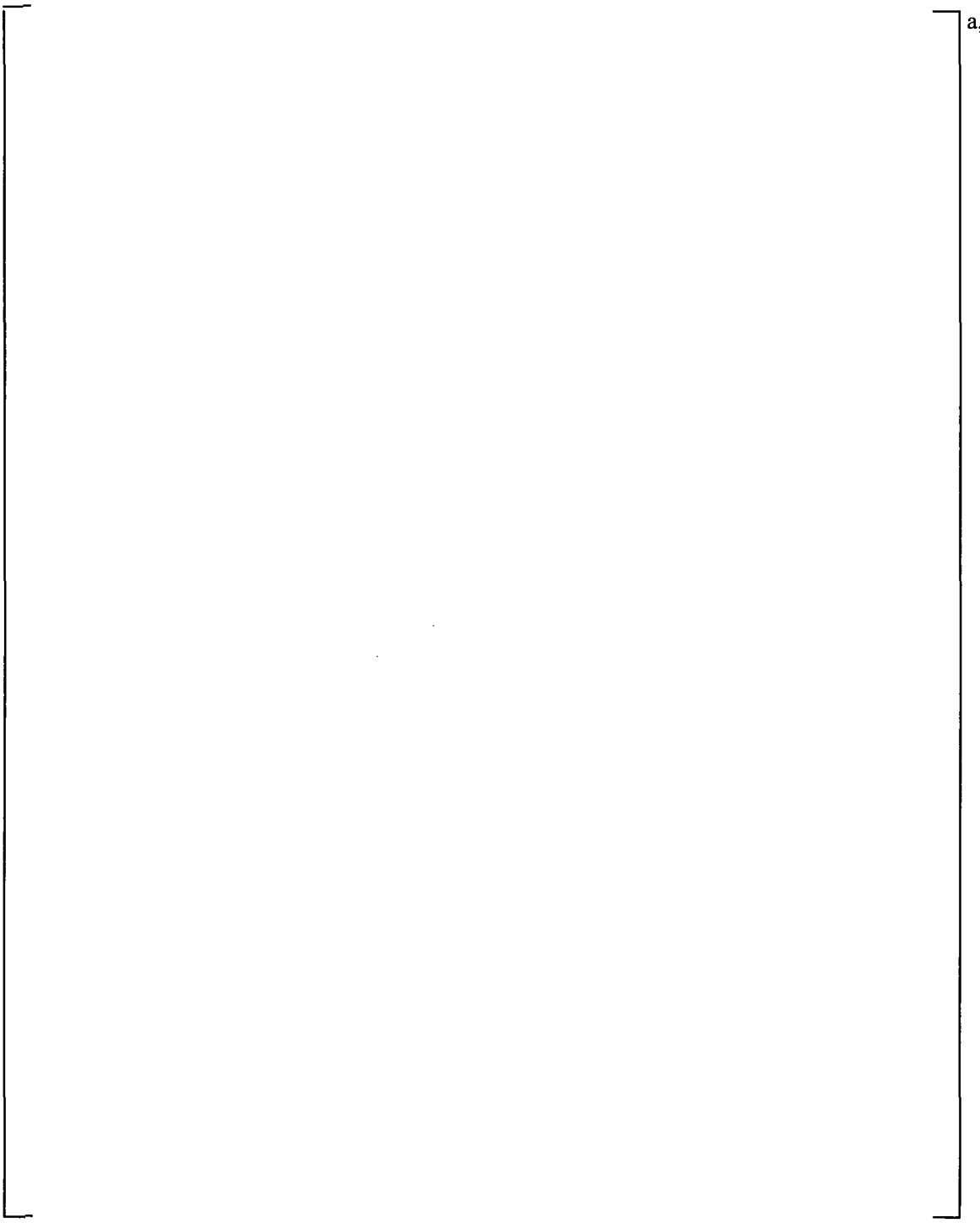

Figure 7-4 Flow Pattern on Vertical Plane of Symmetry

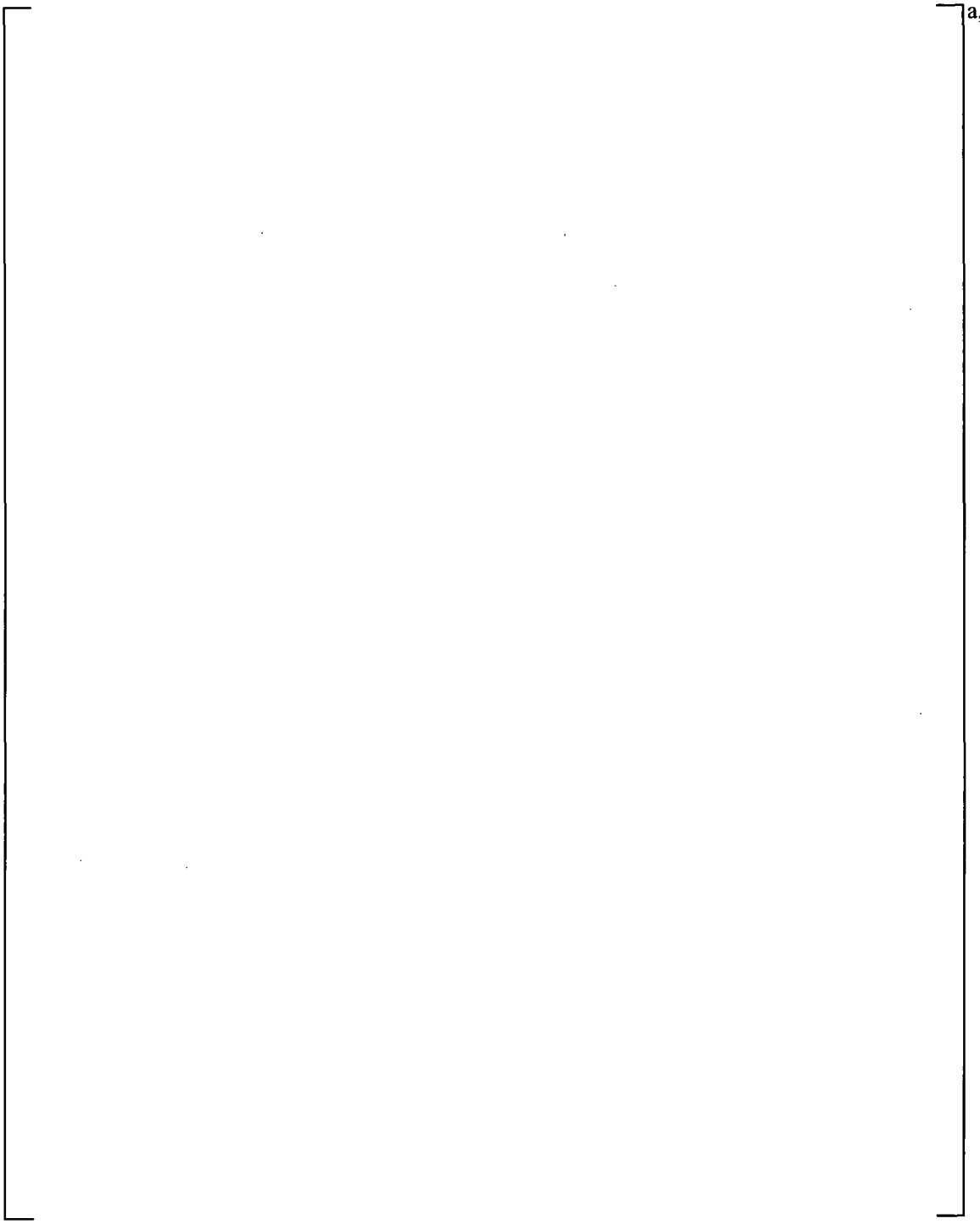

Figure 7-5 Vertical Velocity Contours on a Horizontal Plane at the Entrance to the U-bend Region

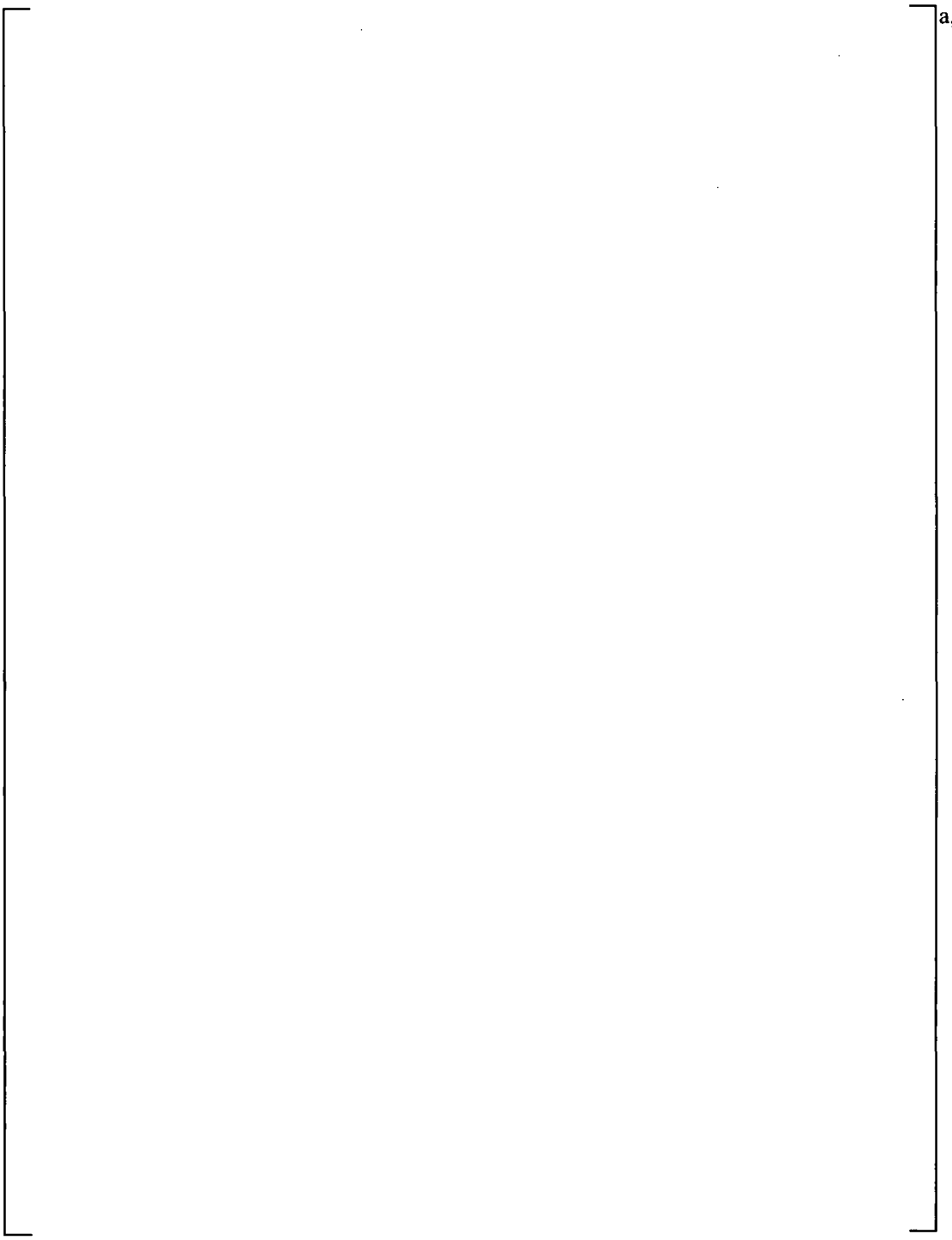

Figure 7-6 Lateral Flow Pattern on a Horizontal Plane at the Entrance to the U-bend Region

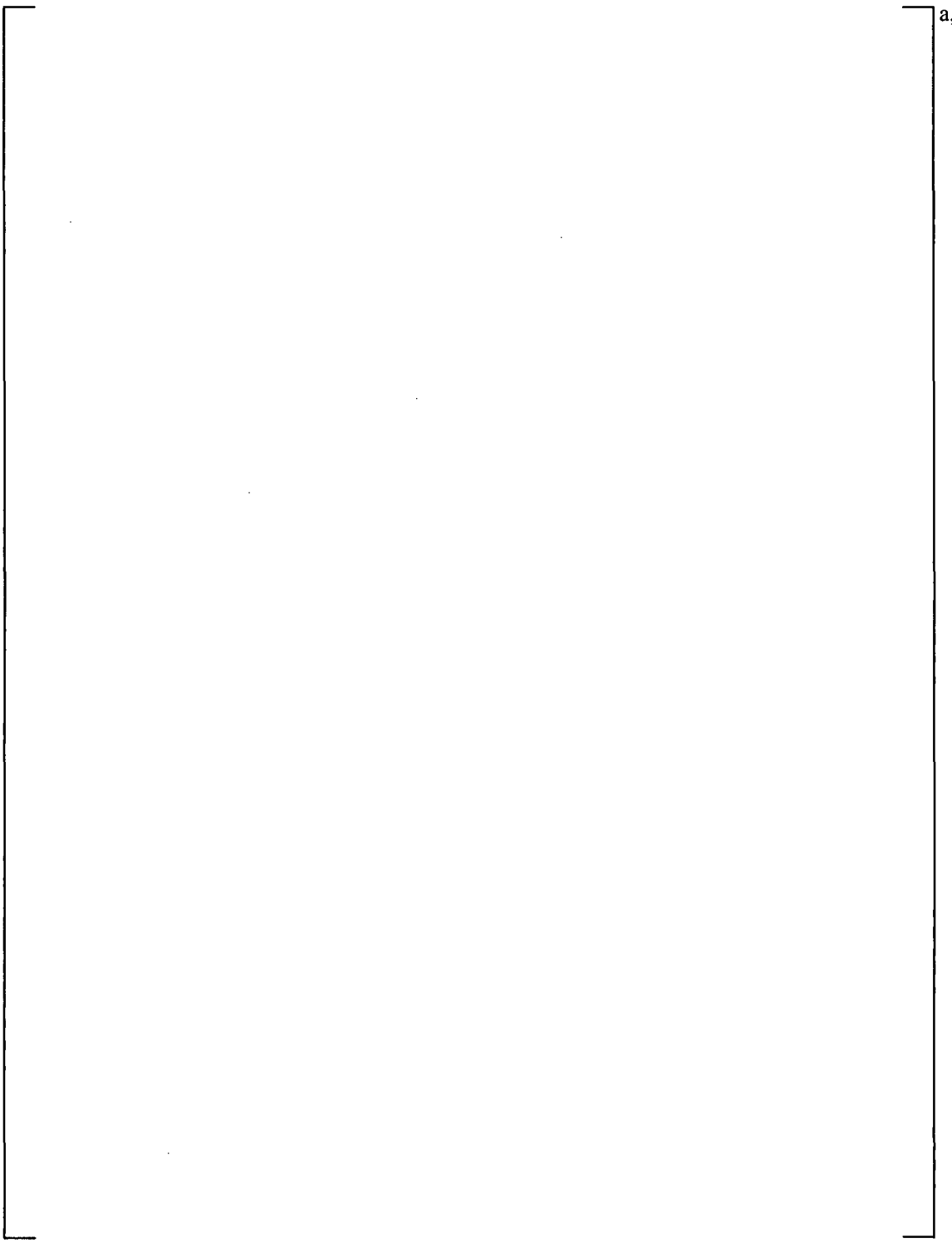

Figure 7-7 Void Fraction Contours on Vertical Plane of Symmetry

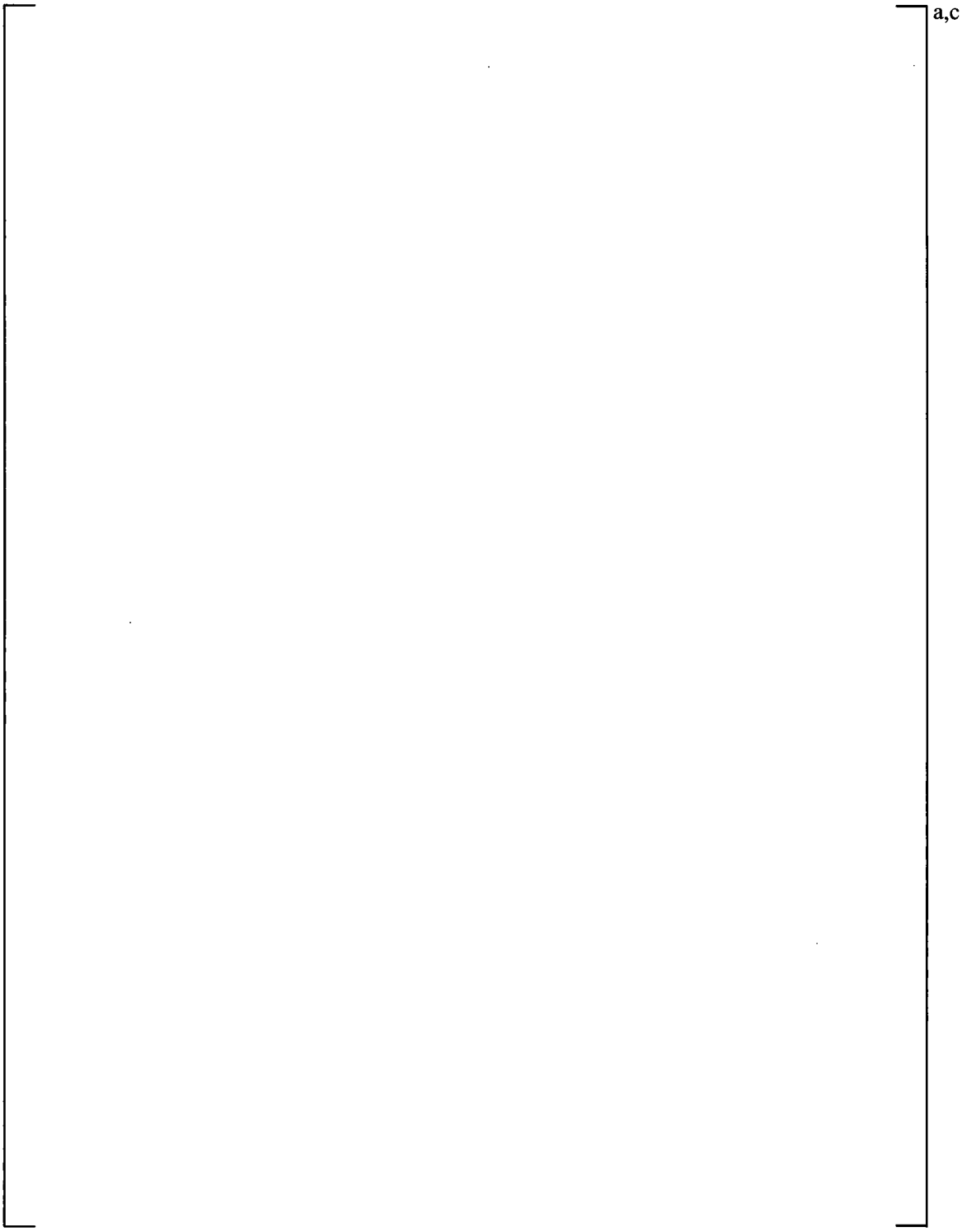

Figure 7-8 Tube Gap Velocity and Density Distributions for Tube Row 10/Column 5

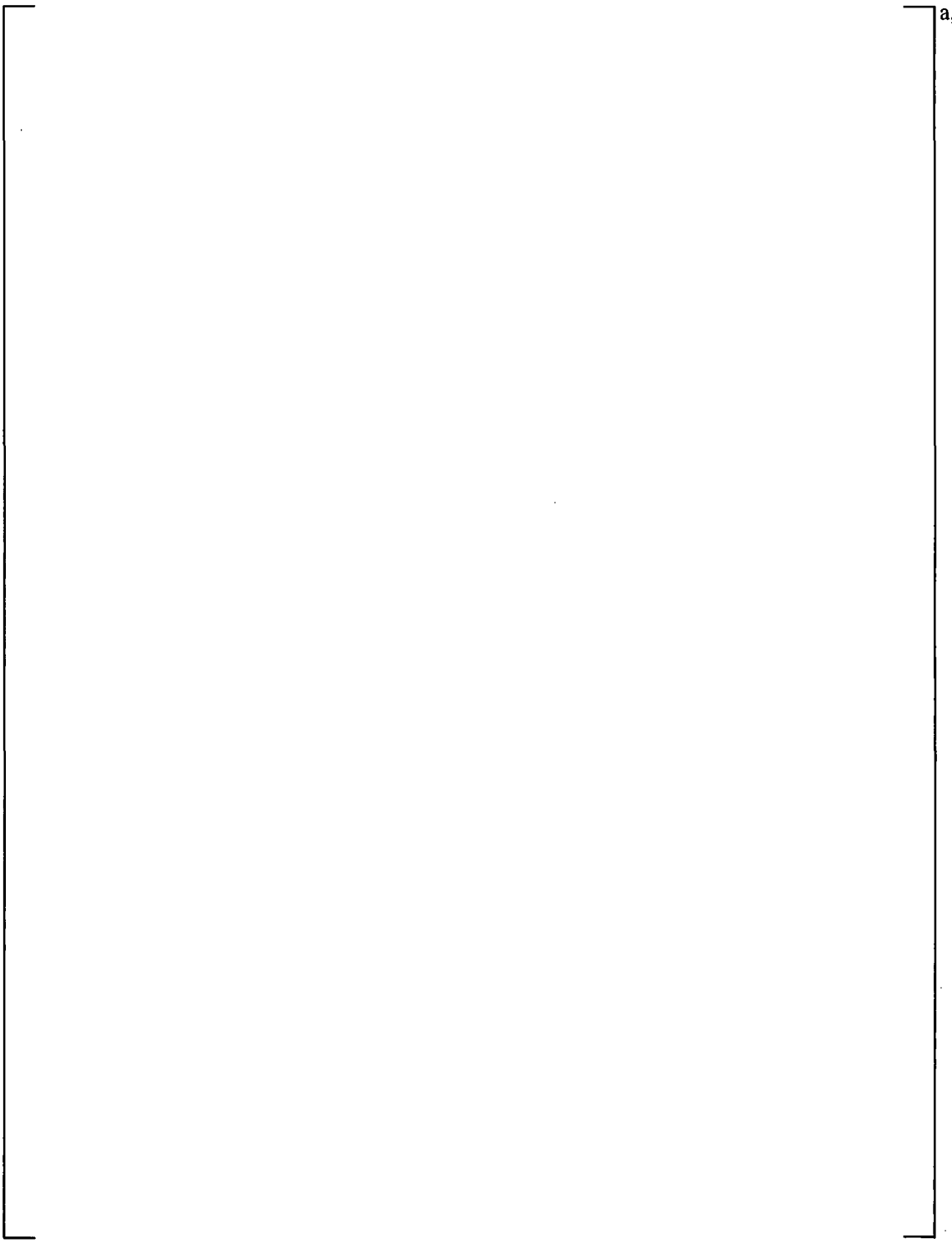

Figure 7-9 Tube Gap Velocity and Density Distributions for Tube Row 10/Column 20

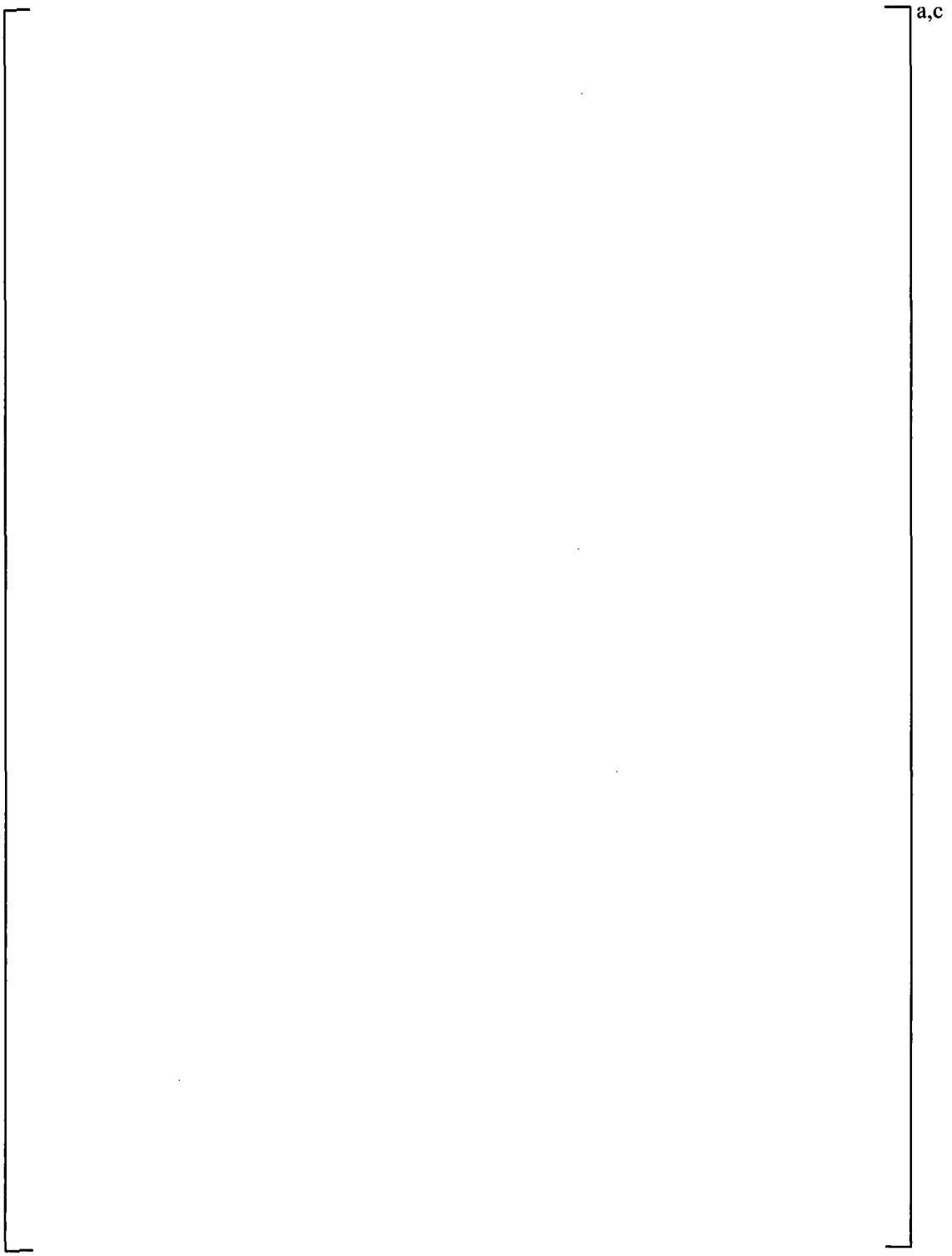

Figure 7-10 Tube Gap Velocity and Density Distribution for Tube Row 10/Column 40

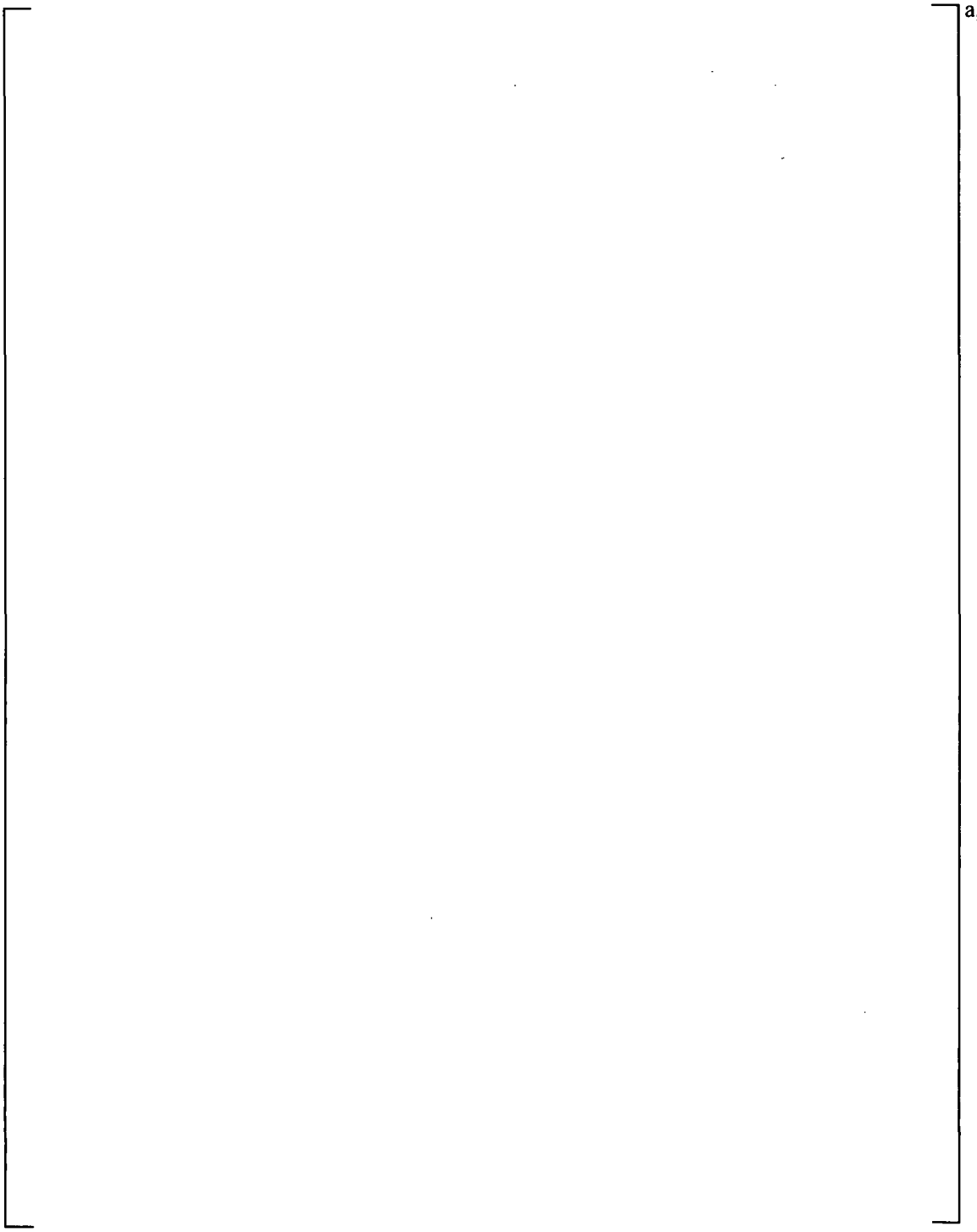

Figure 7-11 Average Velocity and Density Distributions in the Plane of the U-bends Normal to Row 10

8 FLOW PEAKING EVALUATION

This section describes the overall peaking factor evaluation to define the test-based peaking factors for use in the tube fatigue evaluation. The evaluation of the eddy current data to define the AVB configuration for North Anna 1 Tube Row 9 Column 51 (R9C51) is described. This configuration is critical to the tube fatigue assessments as the peaking factors for all other tubes are utilized relative to the R9C51 peaking factor. Uncertainties associated with applying the air model test results to the tube fatigue assessments are also included in this section. Included in the uncertainty evaluation are the following contributions:

- Extrapolation of air test results to two-phase steam-water
- Cantilever tube simulation of U-bend tubes
- Test measurements and repeatability
- AVB insertion depth uncertainty

8.1 NORTH ANNA UNIT 1 CONFIGURATION

8.1.1 Background

The AVB configuration of the ruptured tube in North Anna, R9C51, is the reference case for the tube fatigue evaluations for other plants. In accordance with the NRC Bulletin 88-02, the acceptability of unsupported tubes in steam generators at other plants is based on tube-specific analysis relative to the North Anna R9C51 tube, including the relative flow peaking factors. Thus, the support conditions of the R9C51 tube are fundamental to the analyses of other tubes. Because of the importance of the North Anna tube, the support conditions of this tube, which were originally based on "AVB Visible" interpretations of the eddy current test (ECT) data (Figure 8-1), were re-evaluated using the projection technique developed since the North Anna event. The projection technique is particularly valuable for establishing AVB positions when deposits on the tubes tend to mask AVB signals such as found for the North Anna 1 tubes. The results of this evaluation are summarized below.

8.1.2 Description of the Method

The basic method utilized was the projection technique in which the AVB position is determined based on measured AVB locations in larger row tubes in the same column. In this study, the projection technique was utilized in the "blind" mode, (AVBs called strictly based on the data) as well as the reverse mode (data examined on the basis of predicted AVB positions). The objective of this application was, with the greatest confidence possible, to establish the positions of the AVBs in an 8 column range around the R9C51 tube in North Anna 1, Steam Generator C.

8.1.3 Data Interpretation

The ECT traces for the U-bends in Rows 8-12 (in one case, 13) were examined for Columns 48-55. The original AVB visible calls are shown in Figure 8-1. The data was examined by an eddy current analyst

experienced in reading these traces, and by a design engineer knowledgeable in the geometry of the Model 51 U-bend region.

The intent of this review was to determine if the presence or absence of AVBs as shown in Figure 8-1 could be confirmed using the AVB projection technique. Preliminary projected AVB positions were based on geometric data provided for a few of the tubes near R9C51. The features which were sought were evidence of data "spikes" where AVBs were predicted, offset indications (multiple spikes) where offset AVBs were predicted, single indications where single AVB intersections were predicted, etc. The data evaluation method used was a critical examination of the data, which was biased toward the presence of AVBs unless a confident call of "no AVB" could be made, and then checking the consistency of the data among the tubes in a column and against the theoretical data for the predicted AVB positions. [

].[a,c]

[

].[a,c]

[

].[a,c]

Figure 8-4 is the "AVB visible" map for Columns 48 through 55, based on the critical review of the data. It should be noted that the original data interpretations and the review interpretations are consistent.

8.1.4 Projections

The [ ]^{a,c} ECT traces were utilized for projecting the position of the AVBs according to the standard format of the projection method.

The results of the projections are presented in Figure 8-5, which shows a matrix of projections for tube Rows 8 through 13 in Columns 48 through 55. For many of the tubes, more than one and as many as three, projection values are shown. Multiple projections are expected for a tube if the AVBs on either side of the tube are not at the same elevation, or if the upper and lower AVB support that tube. As many as four different projections are possible if it is assumed that the tube is supported by the upper and lower AVBs, and both upper and lower bars are staggered in elevation as shown in Figure 8-2.

The logic in arranging the projection data is based on the following two rules:

Rule 1. The projections of the same AVB based on different tubes in the same column [ ]^{a,c}

[

]^{a,c}

[

]^{a,c}

Rule 2. Two adjacent tubes in the same row [ ]^{a,c} Consequently, the difference in the [ ]^{a,c}

[

]^{a,c}

The arrangement of the AVBs as shown in Figure 8-5 satisfies the rules above and is consistent with the rupture of R9C51. The resulting AVB arrangements, based on the projection matrix of Figure 8-5 is shown in Figure 8-6.

8.1.5 Conclusions

The general AVB arrangement surrounding the ruptured tube in North Anna Unit 1, Steam Generator C, which was the basis for the analysis, is confirmed by a detailed critical review of the ECT data. Differences exist in the AVB pattern between tube Columns 48-49, in which the AVBs appear to be less inserted than previously indicated. The pattern of Figure 8-6 is the best fit to the rules which were adopted for determining the position of the AVBs, as well as consistent with the explanation of the tube failure.

The basis of the review was a projection technique which utilizes data from tubes one or more rows removed from the actual inserted position of the AVB to determine the position of the AVB. The intent of the review was to establish the positions of the AVBs by confirming or eliminating features of AVB alignments such as side to side offsets, etc., of the AVBs adjacent to the tubes. Overall, the conclusions regarding the positions of the AVBs around R9C51 in North Anna Unit 1, Steam Generator C are based on consistency among all the available data.

8.2 TEST MEASUREMENT UNCERTAINTIES

The descriptions of the peaking factor tests and apparatus were provided in Section 5.4. All practical measures were taken to reduce uncertainties. Nevertheless, some still remain and should be properly accounted for. The important parameter measured during testing that has a significant impact on peaking factor is the air velocity. The air velocity at test section inlet was measured using a [ ].[a,c] Based on considerable experience with the use of such instruments, it is known that the magnitude of uncertainty is very small. A [ ][a,c] measurement uncertainty is used in this analysis based on past experience.

8.3 TEST REPEATABILITY

During the peaking factor testing of the AVB configuration, each test was performed at least two times to confirm repeatability. It has been demonstrated that the tests are quite repeatable with the results often falling within 2 or 3% of one another for the repeat tests. An upper bound value of 5% was used in the current uncertainty analysis.

8.4 CANTILEVER VERSUS U-TUBE

A first order estimate can be made of the validity of modeling a U-bend tube by a cantilever tube in tests to determine the effects of the AVB insertion depth on the initiation of fluid elastic vibration. The following assumptions are used:

[ ]a,c

[a,c

For the purposes of this estimate, the geometry of the cantilever measuring tube in the air test model is compared with the geometry of a prototypical Row 10 tube. [

].[a,c]

The comparison between a U-bend tube and the model tube involve the consideration of an effective velocity associated with the flow perturbation caused by the AVBs. [

].[a,c] Using these values, the ratio of the effective velocity for the cantilever measuring tube to that for the U-bend tube is about [ ][a,c] for the case treated.

A similar evaluation can be made for a Row 10 tube that lies in the projection or shadow of an AVB that is inserted to a depth required to support a Row 9 tube. [

][a,c]

[
].[a,c] The net result is that the ratio of the effective velocity for the cantilever tube to that for the U-bend tube is about [ ].[a,c]

These results indicate that, for the particular assumptions used, the cantilever tube model appears to be a reasonable representation of the U-bend with respect to determining relative peaking factors for different AVB configurations. This evaluation also shows that, on the average, the magnitude of the systematic uncertainty associated with the use of the cantilever tube to simulate the U-bend is about [ ].[a,c]

8.5 AIR VERSUS STEAM-WATER MIXTURE

The local peaking factors from the air tests can be applied to the steam generator steam/water conditions either as a direct factor on the mixture velocity and thus a direct factor on a stability ratio, or as a factor on the steam velocity only with associated impacts on density, void fraction and damping. This method leads to a reduction in tube damping which enhances the peaking factor compared to the direct air test value. For estimating an absolute stability ratio, this application of the peaking factor is a best estimate approach. However, for the evaluation of tubes relative to stability ratio criteria, it is more conservative to minimize the peaking factor for the North Anna Unit 1 tube R9C51 through direct application of the air test peaking factor. This conservative approach is therefore used for evaluating tube acceptability.

Under uniform AVB insertion (or aligned AVB insertion), there are no local open channels for flow to escape preferentially. Therefore, air flow is approximately the same as steam/water flow relative to velocity perturbations. Under non-uniform AVB insertion the steam/water flow may differ from air, as the steam and water may separate from each other when an obstruction, such as an AVB, appears downstream. The water would continue along the same channel while steam readily seeks a low resistance passage and thus turns into adjacent open channels. Two-phase tests indicate a tendency for steam to preferentially follow the low pressure drop path compared to the water phase. Based on the above discussion, the peaking factors, F_i, are considered to more appropriately apply to the steam phase. Thus, it follows that mixture mass velocity for the tube subject to flow perturbation can be written as follows:

$$\left[\qquad\qquad\right]^{a,c} \qquad (8\text{-}1)$$

where D_g is the vapor density, D_f the water density, F_a the velocity peaking factor determined from air tests, j_g^* the nominal superficial vapor velocity, and j_f^* the superficial water velocity. Steam quality can then be determined as follows:

$$\left[\qquad\qquad\right]^{a,c} \qquad (8\text{-}2)$$

The Lellouche-Zolotar correlation (algebraic slip model), as used in the ATHOS code, is applied to determine void fraction. Subsequently, mixture density, velocity and damping coefficients for the tube which is not supported and subject to flow perturbation is evaluated. Therefore, similar to the air velocity peaking factor, local scaling factors of mixture density and velocity and damping coefficient can be readily determined. Finally, a local stability peaking factor for fluid elastic vibration can be calculated as follows:

[ ]a,c (8-3)

where F_s is the stability peaking factor, F_d the density scaling factor, F_v the velocity scaling factor, and F_{dp} the damping coefficient scaling factor. If we use the air velocity peaking factor without translating to steam/water conditions, then:

[ ]a,c (8-4)

As shown in Table 8-1 stability peaking factors for the steam/water mixture are slightly higher than air velocity peaking factors. The difference between the steam/water and air peaking factors increases as the air peaking factor increases.

For application to tube fatigue evaluations, the ratio of the peaking factor for a specific tube to that for North Anna R9C51 is the quantity of interest. Larger values for this ratio are conservative for the tube fatigue assessment. The North Anna R9C51 peaking factor is one of the highest peaking factors. As discussed in Section 8.7, a peaking factor of nearly [ ]^{a,c} is determined for the R9C51 tube. The differences between [

].^{a,c} Typical values are shown in Table 8-2. These results show that the direct application of the air test data yields the higher relative peaking factor compared to R9C51. To obtain conservatism in the peaking factor evaluation, [

].^{a,c}

Comparing the values in the first and last columns of Table 8-1, it may be noted that the stability peaking factor for steam water is [ ]^{a,c} higher than the air velocity peaking factor. On the average, the uncertainty associated with the conservative use of air velocity peaking factor is [ ].^{a,c}

The conclusion that the peaking factor for steam/water flow would be higher due to the dependency of the damping ratio on void fraction was supported by an alternate study. In this study, a section of steam generator tubes were simulated using the ATHOS code under prototypic flow conditions. The objective of this study was to examine the magnitude of the changes in void fraction and thus stability ratio as a consequence of non-uniform AVB insertion patterns. The current version of ATHOS has modeling limitations that prevent accurate modeling of local geometry effects. In addition, it is believed that an analysis using a two-fluid modeling procedure is mandatory to a calculation of the peaking factors for a steam generator to account for the preferential steam flow along the low resistance path. Consequently,

the intent of this analysis is only to help bound the uncertainty on void fraction effects from extrapolating the air tests to steam-water.

First the analysis was conducted with uniformly inserted AVBs in the ATHOS model. The ATHOS results were processed by the FLOVIB code to determine stability ratios for the specific tubes of interest. The calculation was repeated using a non-uniform AVB insertion pattern in the model. The results show that the void fraction distribution changes as a result of flow perturbation. Further, the impact on the stability ratio resulting from the changes in void fraction profiles was about [ ].[a,c] This alternate calculation provides independent corroboration of the prior discussion regarding the stability peaking factors under steam-water conditions versus in air.

8.6 AVB INSERTION DEPTH UNCERTAINTY

The most significant uncertainty for the low peaking configurations is not in the test results, but in the determination of actual AVB insertion patterns adjacent to specific tubes. The methodology used for obtaining the AVB insertion patterns from eddy current data can ascertain the AVB location only approximately. The effect on the peaking factor resulting from this uncertainty is addressed using test results of AVB configurations that varied from one another by up to [ ].[a,c]

Based on maps of AVB insertion depth of various plants, several configurations have been tested for determining fluid elastic instability flow rate by an air cantilever model. Stability peaking factors were then determined from the ratio of critical flow rate for a uniform AVB insertion configuration to a specific configuration. Figure 8-7 summarizes the AVB configurations tested.

The position of the AVB insertion depth is determined from Eddy Current Test (ECT) data. The positioning of the AVB from ECT data reading is subject to uncertainty; its accuracy is probably about [ ].[a,c] A change of an AVB insertion depth in a given configuration leads to a different configuration, and thus a different peaking factor. A review of the tested AVB type has been made and results summarized in Table 8-3. As can be seen, a decrease in depth of an appropriate AVB tends to decrease the peaking factor, for instance, a [ ].[a,c] Such a trend can be explained; a decrease in a specific AVB depth will open up more channels for incoming fluid to distribute and thus less flow perturbation. However, this applies only to those changes without inducing the reinforcement of flow perturbation from upstream to downstream.

On the average, the uncertainty in peaking factor resulting from small variations in AVB insertion (of the order of 1/2 tube pitch) is found to be [ ].[a,c]

8.7 OVERALL PEAKING FACTOR WITH UNCERTAINTY

As discussed in the previous subsections, there are several aspects to be considered in applying the laboratory test data to steam generator conditions. These considerations were reviewed one at a time in those subsections. This section will integrate the pieces into one set of stability peaking factors.

Looking forward to how these peaking factors are used in the analysis (Section 9), the relative stability ratio calculated for a given tube without the consideration of flow peaking is corrected using the ratio of the peaking factor of the specific tube to that of the North Anna R9C51 tube (Configuration 1a).

It is to be noted that the test results would be applied as ratios of a specific tube peaking factor to the R9C51 peaking factor. This will reduce the influence of some uncertainties since the systematic uncertainties would affect both the numerator and the denominator in the ratio of peaking factors. The major difference will be in those configurations whose peaking factors are significantly lower than that of R9C51. The approach employed here is intended to provide that conservative peaking factors are employed for such apparently low peaking configurations.

The uniform AVB configuration (2a) is selected as a reference configuration, and the peaking factors of all configurations tested are recomputed on the basis of this reference. As discussed below, some of the test uncertainties are applied to the reference case to account for its significantly low peaking relative to the R9C51 configuration.

The uncertainties in the test results and their extrapolation are those due to test measurements, test repeatability, cantilever tubes in the test versus U-tubes in the steam generator, and air tests versus steam-water mixture. These were discussed in more detail in the previous subsections. The magnitudes of these uncertainties are listed in Table 8-4.

Of these uncertainties, those due to measurement and repeatability of tests are random errors and can occur in any test. Therefore, these are treated together. The total random uncertainties are calculated by [ ].[a,c] The RSS value of these is [ ].[a,c] Since these can occur in any test, these are to be applied to all tests. One way of doing this is to apply it to the R9C51 value, that being in the denominator of the final peaking factor ratio. Thus the peaking factor for configuration 1a (R9C51) is reduced by this amount to yield a value of [ ][a,c] instead of the [ ][a,c] appearing in Table 5-2.

The next three uncertainties in Table 8-4 are systematic uncertainties. It could be argued that these appear in the peaking factors of both the specific tube under consideration and the R9C51 tube and are therefore counter balanced. However, the relative magnitude of these may be different, particularly for configurations with much lower peaking than R9C51. Therefore it was judged that the [ ].[a,c] Similarly, as noted above, the effect on the peaking factor due to the uncertainty in the field AVB configuration is also included in this reference case. Thus, [ ].[a,c] The peaking factor of the reference Configuration 2a (Table 8-5) is raised by this amount to a value of [ ].[a,c]

The change in peaking factors of Configurations 1a and 2a resulting from the application of uncertainties as described above are shown in Column 3 of Table 8-5. The peaking factors of all configurations are recomputed on the basis of this reference Configuration (2a). These values are displayed in Column 4 of Table 8-5.

Some of the uncertainties were applied to the reference Configuration (2a) in order to apply them to all low peaking configurations conservatively. Thus, no configuration should have a lower peaking factor than this reference configuration. Therefore, when a peaking factor value less than [ ][a,c] is calculated for any configuration, (in Column 4 of Table 8-5), it should be altered to [ ].[a,c] Further, for some of the configurations that are conceptually similar, the more limiting (higher) value is used. For example, a

peaking factor of [ ]^{a,c} is used for Configurations 5a and 5b based on their similarity to Configuration 5c.

The final stability ratio peaking factors calculated on this basis (with Configuration 2a as the reference) are shown in Table 8-6.

The overall conclusions from the peaking factor assessment are:

1. As noted in Table 8-4, five elements have been included in the uncertainty evaluation for the peaking factors. The uncertainty estimates were developed from both test and analysis results as described in Sections 8.2 to 8.6. The largest single uncertainty of [ ]^{a,c} is attributable to uncertainties of up to [ ]^{a,c} on determination of AVB insertion depths from field eddy current data. This relatively large uncertainty is applicable only to low peaking conditions where the AVB uncertainties can contribute to small peaking factors. The definition of "no flow peaking" was increased to encompass the small peaking effects from AVB insertion uncertainties. For the AVB patterns leading to significant peaking factors, AVBs were positioned within uncertainties to maximize the peaking factor. For these configurations, variations of AVB insertion within these uncertainties are expected to reduce the peaking factor compared to the final values of Table 8-6 and Figure 8-7.

2. Including uncertainties directed toward conservatively decreasing the peaking factor for the North Anna tube R9C51, the final R9C51 peaking factor is [ ]^{a,c} relative to a no flow peaking condition such as with uniform AVB insertion depths.

8.8 PEAKING FACTORS FOR SPECIFIC TUBES

Peaking factors for Watts Bar Unit 2 were determined using the methodology described above. Table 8-7 summarizes the results of peaking factors. The AVB positions on each insertion pattern of Figure 8-7 should be carefully noted. Where the AVBs are shown [

].^{a,c}

In applying the methodology to Watts Bar Unit 2, maps of the AVB insertion depths shown in Figures 6-1 through 6-4 were first reviewed. The second step was to identify locations having significant AVB insertion configurations. The resulting AVB insertion configuration for the tube is then compared with the existing bank of unique AVB configurations that have a corresponding velocity peaking factor determined from tests. Finally, the velocity peaking factor for the tube with its AVB insertion configuration was conservatively estimated using the data bank.

Determination of peaking factors for identified tubes is described in detail below. Sections 8.8.1 to 8.8.4 are divided into small tables for ease in following the description.

8.8.1 Steam Generator 1

The following table gives the peaking factors for the tubes with unique configurations of AVB insertion depths. Each configuration is shown in Figure 8-7.

Steam Generator	Column Number	Row Number	Type of AVB Insertion	Peaking Factor	Peaking Ratio

a,c

The R11C104 tube (type [ ]^{a,c} was selected as a bounding configuration and a peaking factor of [ ]^{a,c} resulted. Tube R8C88 can be conservatively bounded by Type [ ]^{a,c} and thus a peaking factor of [ ]^{a,c} was obtained.

8.8.2 Steam Generator 2

The following table gives the peaking factors for the tubes with unique configurations of AVB insertion depths. Each configuration is shown in Figure 8-7.

Steam Generator	Column Number	Row Number	Type of AVB Insertion	Peaking Factor	Peaking Ratio

a,c

Tubes R10C11, R9C54, and R9C68 were chosen as the bounding configuration (Type [ ]^{a,c} and a peaking factor of [ ]^{a,c} resulted. Tubes R9C20 and R9C22 can be conservatively bounded by Type [ ]^{a,c} and thus have a peaking factor of [ ].^{a,c} Tube R9C58 was conservatively determined to by Type [ ]^{a,c} with a flow peaking of [ ].^{a,c}

8.8.3 Steam Generator 3

The following table gives the peaking factors for the tubes with unique configurations of AVB insertion depths. Each configuration is shown in Figure 8-7.

[

Steam Generator	Column Number	Row	Type of AVB Insertion	Peaking Factor	Peaking Ratio

]a,c

Tube R8C87 was approximated to be Type [ ]^{a,c} with a flow peaking factor of [ ].^{a,c} Tube R8C87 was determined to be the bounding configuration for Steam Generator 3. Tube R9C8 was conservatively determined to be Type [ ]^{a,c} which provides a peaking factor of [ ].^{a,c}

8.8.4 Steam Generator 4

The following table gives the peaking factors for the tubes with unique configurations of AVB insertion depths. Each configuration is shown in Figure 8-7.

[

Steam Generator	Column Number	Row Number	Type of AVB Insertion	Peaking Factor	Peaking Ratio

]a,c

8.8.5 Summary

According to the above evaluation for all four steam generators, Table 8-7 summarizes the peaking factors for all tubes with large peaking factors at Watts Bar Unit 2. In finalizing this table, the highest peaking factor for each tube was used when there is more than one type of AVB insertion configurations selected. Therefore, peaking factors as tabulated in Table 8-7 are conservative for the fatigue evaluation.

Table 8-1 Stability Peaking Factor Due to Local Velocity Perturbation Scaling Factors for Steam/Water

Air Velocity Peaking Factor, F_a	Void Fraction Scaling, F_v	Density Scaling, F_d	Velocity Scaling, F_v	Damping Scaling, F_{dp}	Stability Peaking Factor, F_s

a,c

NOTE: 1. Stability peaking factor for steam/water mixture is calculated as follows:

[ ] a,c

2. Damping scaling factor is calculated using MEVF of [ ]^{a,c} for R9C51 tube.

Table 8-2 Comparison of Air and Steam-Water Peaking Factor Ratios

Air Peaking Factor	Air Peaking Ratio	Steam Peaking Factor	Steam Peaking Ratio

a,c

Table 8-3 Effect of Local Variation of AVB Insertion

Type A	Type B	A to B AVB Variation	Peaking Factor A	Peaking Factor B	Ratio (B/A)

a,c

Table 8-4 Uncertainties in Test Data and Extrapolation

	Source of Uncertainty	Type	Magnitude, %
1	Velocity measurement	Random	a,c
2	Test repeatability	Random	
3	Cantilever versus U-tube	Systematic	
4	Air versus steam-water mixture	Systematic	
5	Field AVB configuration	*	

*This is not an uncertainty associated with the test data. It results from the inaccuracy in determining the true AVB position in the field using eddy current data.

Table 8-5 Extrapolation of Test Results to Steam Generator Conditions

Configuration	Test Data	Data with Uncertainties	Peaking Factor Referenced to Configuration 2a

a,c

Table 8-6 Final Peaking Factors

Configuration	Peaking Factor

a,c

Table 8-7 Stability Velocity Peaking Factors for Specific Tubes Watts Bar Unit 2

a,c

Steam Generator	Column	Row	Type of AVB Insertion	Peaking Factor	Peaking Ratio

Notes:

(1) Test data not available for original AVB design insertion configuration, test data for modified AVB design used.

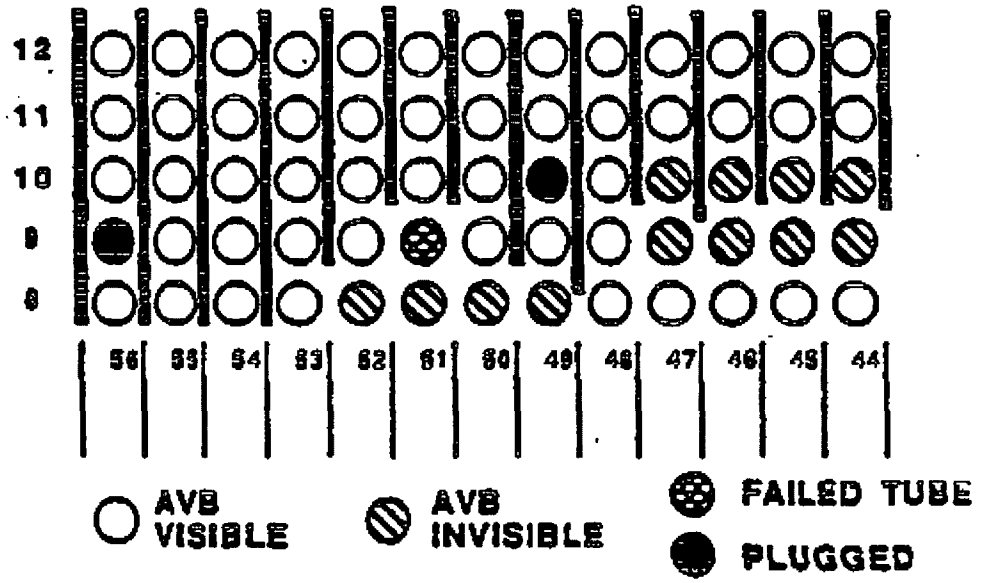

Figure 8-1 Original North Anna AVB Configuration (Configuration 1b)

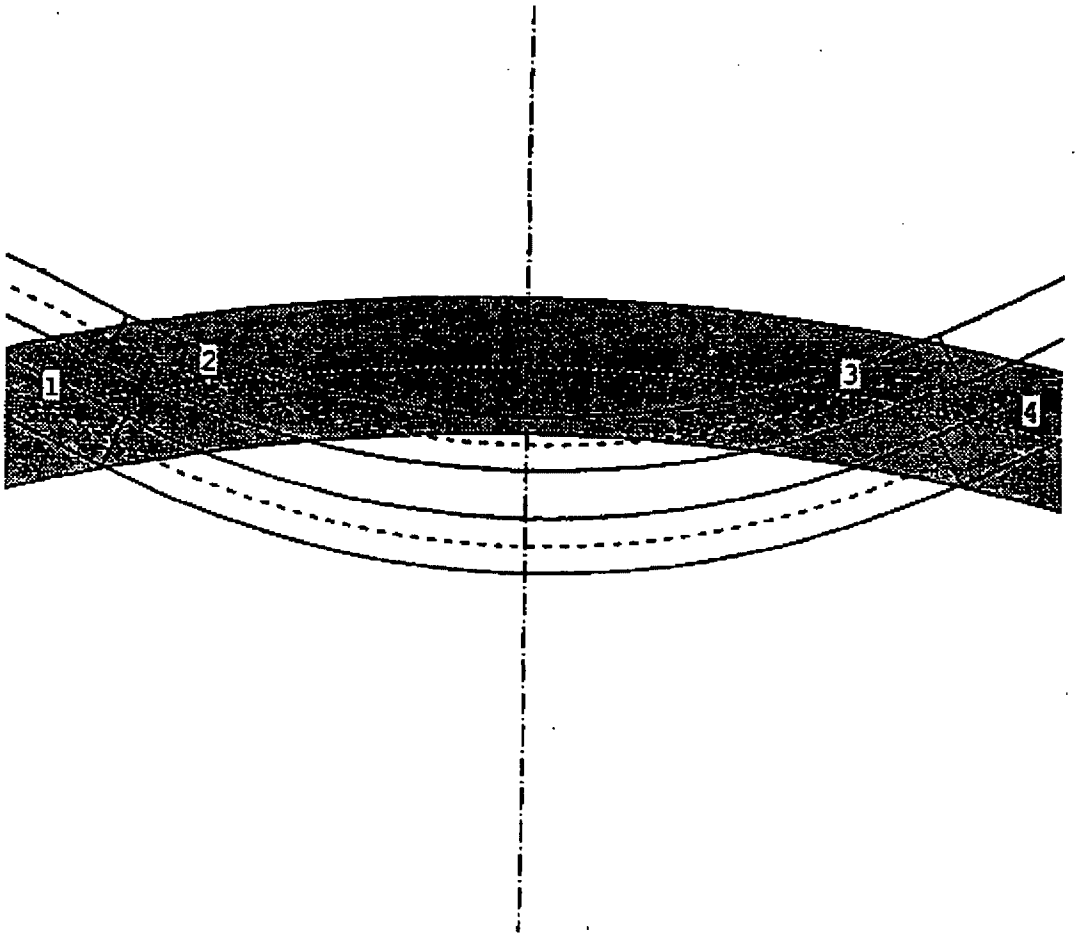

Figure 8-2 Schematic of Staggered AVBs

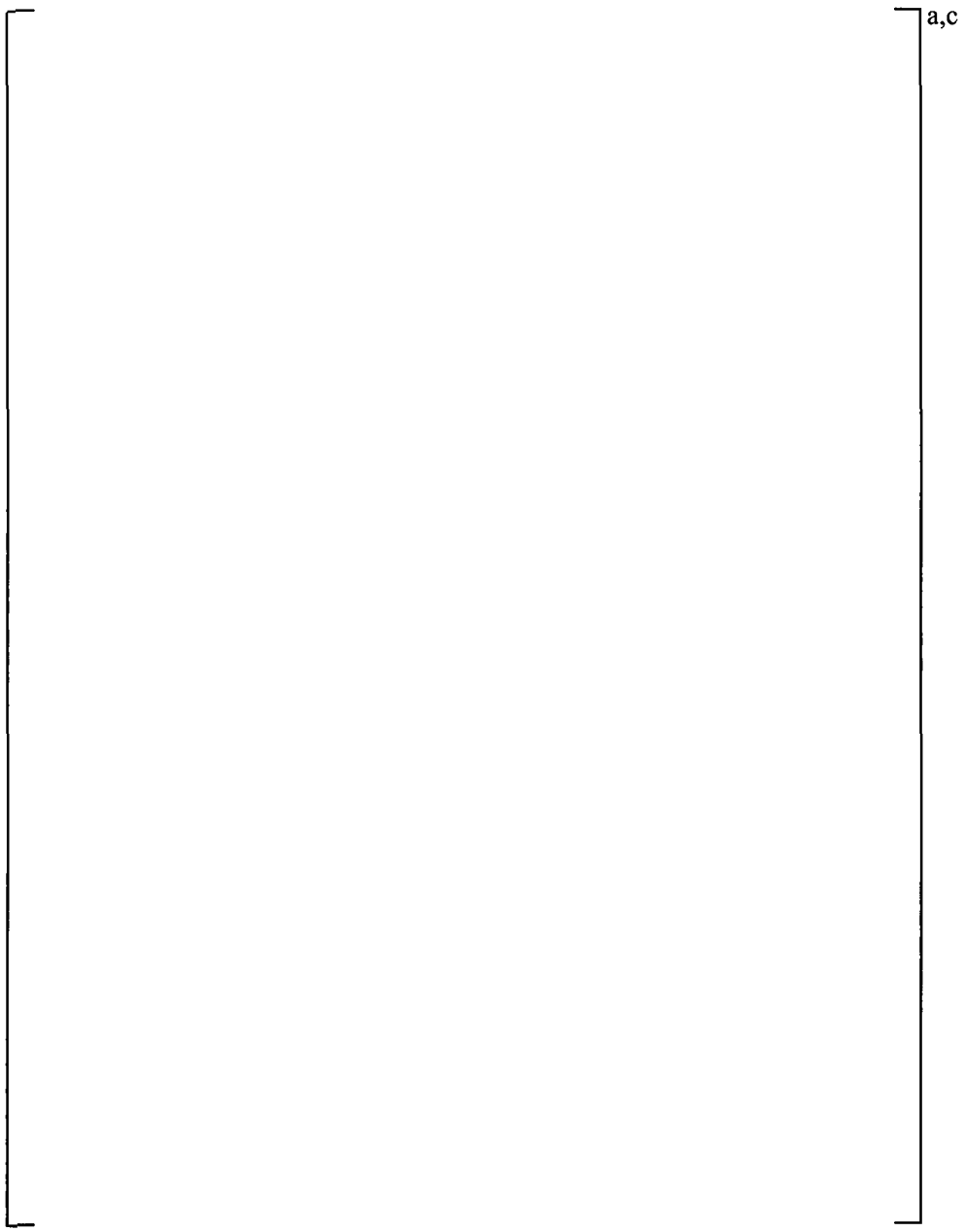

Figure 8-3 AVB "Pair" in ECT Trace

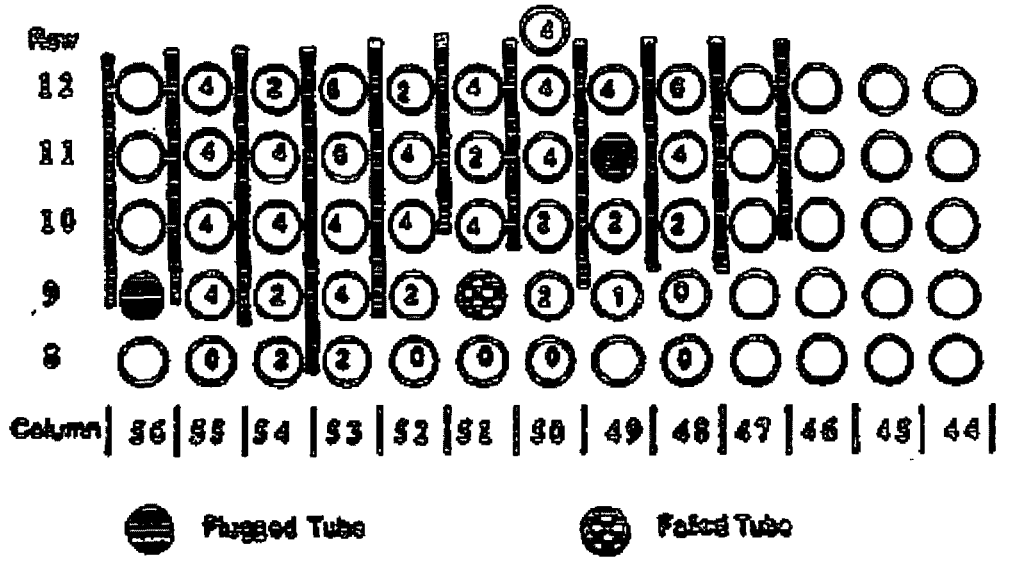

Number of circles in Column Range 48-56 represent readable AVB intersection signals, based on critical review of the ECT traces. Open circle in this range means no data is available.

Figure 8-4 North Anna 1, Steam Generator C, AVB Positions Critical Review "AVB Visible" Cells

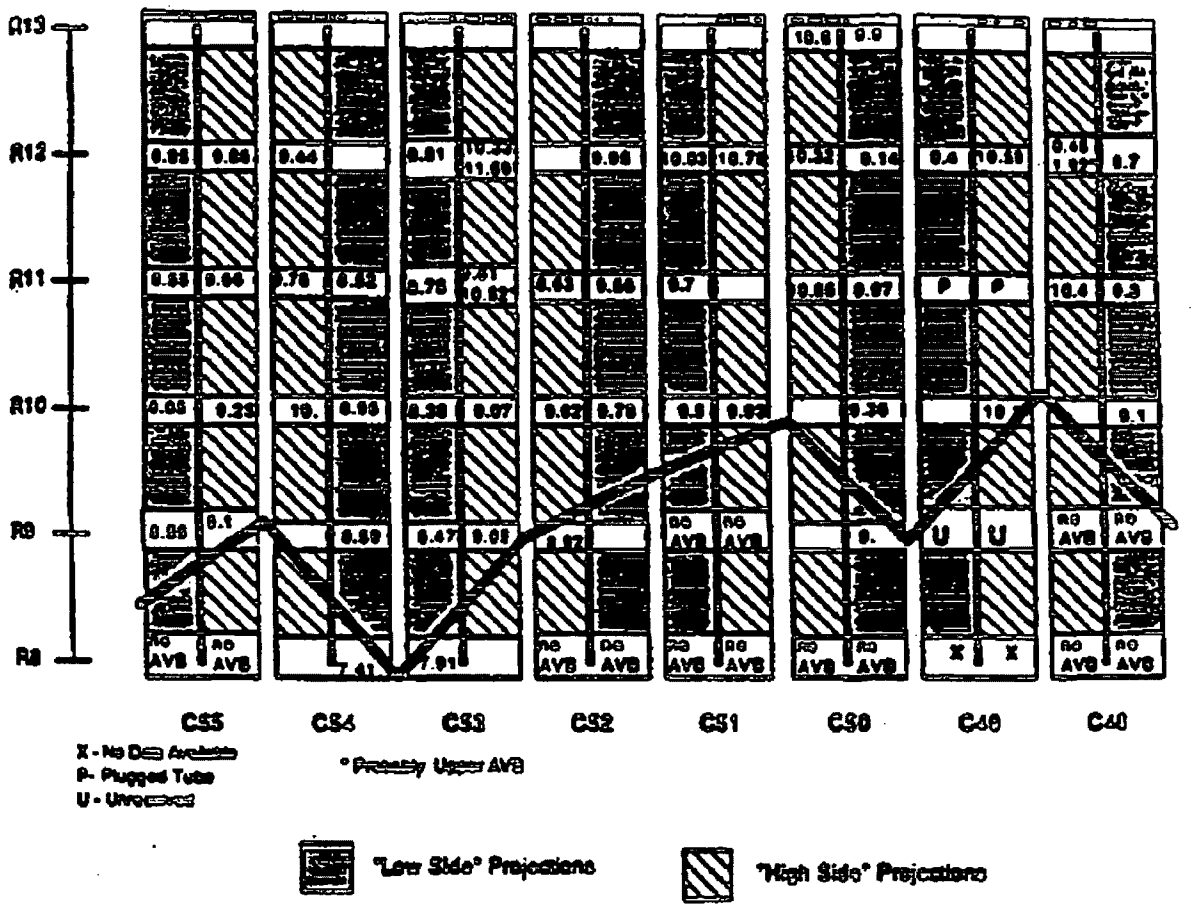

Figure 8-5 North Anna 1, Steam Generator C, R9C51 AVB [ ]^{a,c} Matrix

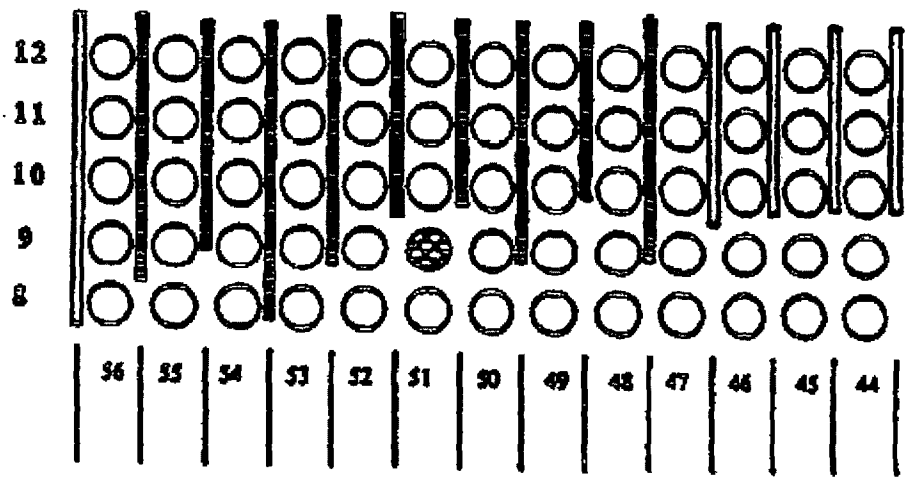

Figure 8-6 North Anna R9C51 Final [ ]^{a,c} Positions (Configuration 1a)

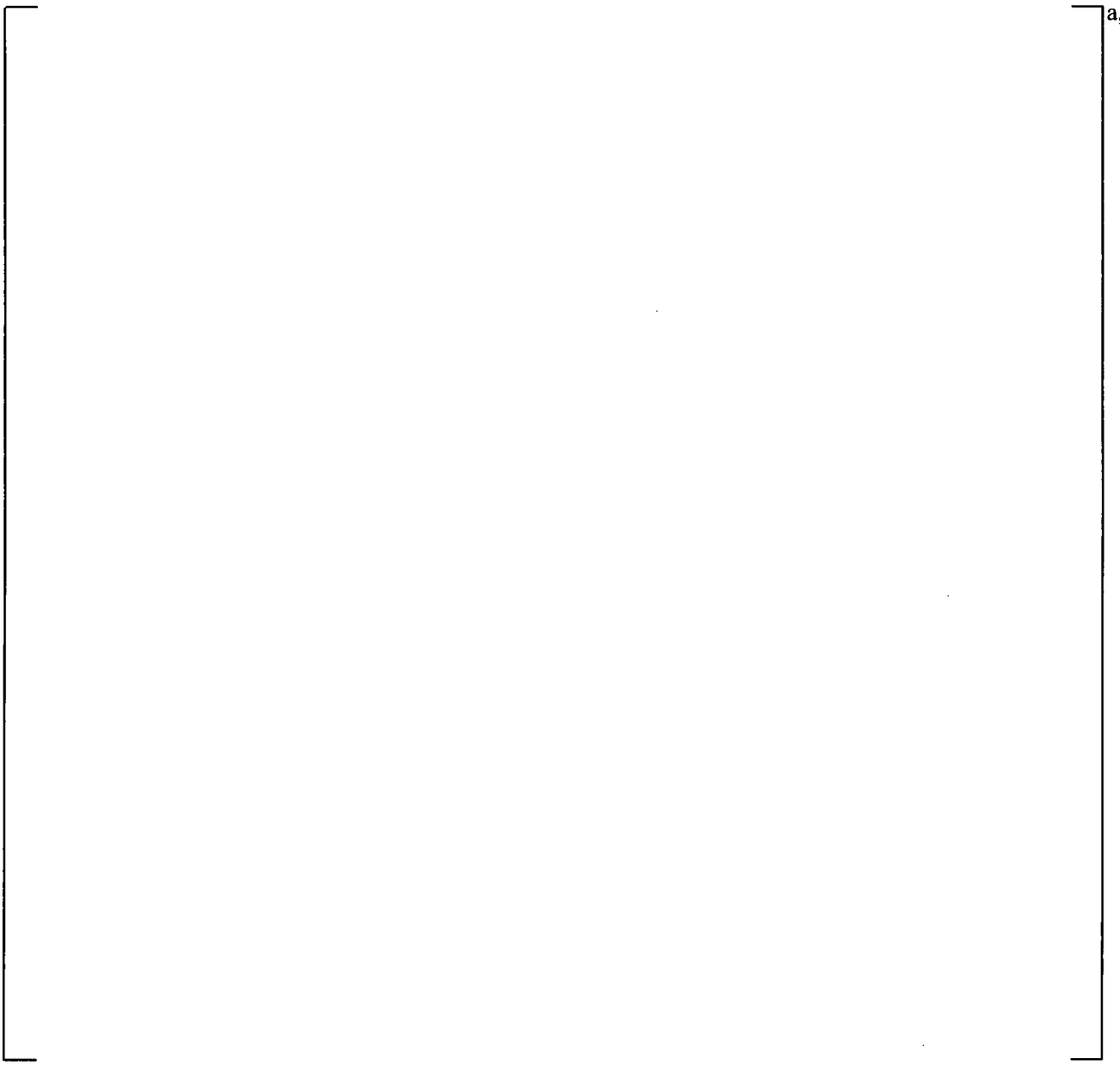

Figure 8-7 AVB Insertion Configurations and Final Peaking Factors for Watts Bar Unit 2

9 STRUCTURAL AND TUBE VIBRATION ASSESSMENTS

9.1 TUBE MEAN STRESS

This section summarizes the analysis to determine stresses in a dented, but undeformed, tube at 100% power. Loads are imposed on the tube corresponding to steady-state pressure, differential thermal expansion between the tube and the support plate, and a thru-wall thermal gradient. The analysis assumes the tube to be [ ]^{a,c} at cold shutdown.

The temperature and pressure parameters used for mean stress calculations at 100% power in the vicinity of the top support plate are provided in Table 9-1. These temperatures and pressures correspond to the MUR uprate power level with 10% tube plugging and are the limiting conditions. The tube temperature corresponds to the average of the primary side water temperature and the plate temperature. The resulting tube/plate radial interference is [ ].^{a,c}

Stresses due to differential pressure and interference loads are calculated using finite element analysis with the model shown in Figure 9-1. The model prescribes [

]^{a,c}

Two reference cases were run using the finite element model, the first for a primary-to-secondary side pressure gradient of 1000 psi, and the second for a [ ]^{a,c} inch radial interference between the tube and plate. The pressure case incorporates the axial load on the tube by applying a pressure loading along the top face of the model. Plots showing the stress distributions on the tube outer surface are provided for the two reference cases in Figures 9-2 and 9-3. Thermal bending stresses due to the through-wall thermal gradient are calculated to be [ ]^{a,c} ksi using conventional analysis techniques. The combined stress distribution along the tube length, shown in Figure 9-4, was obtained by combining the thermal bending stresses and the reference solutions with appropriate multipliers based on 100% power operating parameters.

Table 9-2 shows the calculation combined stress. The stresses from the finite element model for the 1000 psi Internal Pressure condition and the 1.0 Mil Interference at TSP condition are from Reference 9-1.

[

]^{a,c}

If a tube is dented with deformation, the mean stress is limited by tube yielding. For the case of dented tubes with deformation, the maximum effect of mean stress was incorporated by using $s_{max} = s_y$ in determining stability ratios and fatigue usage.

9.2 STABILITY RATIO DISTRIBUTION BASED UPON ATHOS

An assessment of the potential for tubes to experience fluid elastic instability in the U-bend region has been performed for each of the tubes in rows eight through twelve. This analysis utilizes FASTVIB, a Westinghouse proprietary finite element based computer code, and PLOTVIB, a post processor to FASTVIB. These codes predict the individual responses of an entire row of steam generator tubing exposed to a location dependent fluid velocity and density profile. The program calculates tube natural frequencies and mode shapes using a linear finite element model of the tube. The fluid elastic stability ratio U_e/U_c (the ratio of the effective velocity to the critical velocity) and the vibration amplitudes caused by turbulence are calculated for a given velocity/density/void fraction profile and tube support condition. The velocity, density and void fraction distributions are determined using the ATHOS computer code as described in Section 7. The WECAN-generated mass and stiffness matrices used to represent the tube are also input to the code. (WECAN is also a Westinghouse computer code.) Additional input to FASTVIB/PLOTVIB consists of tube support conditions, fluid elastic stability constant, turbulence constants, and location dependent flow peaking factors.

This process was performed for the reference McGuire steam generator tubes and also for the North Anna Row 9 Column 51 tube (R9C51), using similarly appropriate ATHOS models. Watts Bar Unit 2 stability ratios were determined from the McGuire stability ratios by multiplying by a factor (the 1D RSR factor). The 1D RSR factor accounts for differences in U-bend flow conditions between Watts Bar Unit 2 and McGuire and is equal to 1.08 for the limiting case (MUR uprate with 10% tube plugging). Ratios of the Watts Bar Unit 2 results to those for North Anna Unit 1 R9C51 were generated to produce a quantity that could be used to provide an initial assessment of the Watts Bar Unit 2 tubes relative to the ruptured tube at North Anna Unit 1.

Figure 9-5 shows the results of this process for each of the rows under investigation. The relative ratios are obtained using the following conditions for Watts Bar Unit 2 and North Anna Unit 1:

1. Tube is fixed at the top tube support plate,
2. Void fraction-dependent damping,
3. No AVB supports are active,
4. Location-dependent flow peaking factors.

It is to be noted that the stability ratios plotted in Figure 9-5 are composites of all steam generators using mirror image tubes. That is, any peaking effect for a given tube location indicated on the plot represents the maximum value of the peaking factor in all steam generators at that location.

The relative stability ratio of 0.90 is the point where a ten percent reduction in stability ratio exists relative to North Anna R9C51. (See Section 4.1 for a discussion of the stability ratio reduction criteria.) All the tubes with ratios above this line would be considered to have stability ratios larger than ninety percent of North Anna R9C51.

Figure 9-5 indicates that most tubes in Rows 8 through 12 of the Watts Bar Unit 2 steam generators when unsupported by the AVBs are below the 0.9 RSR line.

9.3 STRESS RATIO DISTRIBUTION WITH PEAKING FACTOR

An evaluation was performed to determine the ratio of the Watts Bar Unit 2 tube stress over the North Anna R9C51 tube stress. This ratio is determined using relative stability ratios discussed in the previous section, relative flow peaking factors (Table 8-7 factors multiplied by [ ]^{a,c}), tube size, and bending moment factors. Sections 4.2 and 4.3 contain additional information and describe the calculation procedure used to obtain the results presented in this section. The results presented below are based upon the following conditions:

1. Tube is fixed at the top tube support plate,
2. Damping is void fraction dependent,
3. Tubes have no AVB support,
4. 10% criteria with frequency effects,
5. Location-dependent flow peaking effects
6. Tubes are assumed to be dented with deformation (labeled with denting) or clamped at the top support plate due to crevice corrosion (labeled without denting).

A tube can be considered acceptable if the stress ratio is less than 1.0 when calculated using the procedure described in Sections 4.2 and 4.3, including the conditions listed above, and subject to confirmation of the fatigue usage acceptability. Conformance to these requirements implies that the stress acting on a given tube is expected to be insufficient to produce a fatigue event in a manner similar to the rupture that occurred in the R9C51 tube at North Anna Unit 1.

Figure 9-6 shows the results of the stress ratio calculations for each of the Watts Bar Unit 2 tubes in Rows 8 through 12 in the dented condition. As in Figure 9-5, the stress ratios in Figure 9-6 represent the composite ratios for all Watts Bar Unit 2 steam generators with the tubes in the undented condition. (Refer to Table 9-3 for salient tubes in individual steam generators). These ratios are applicable for tubes in Rows 8 through 12 that are dented at the top tube support plate. This case bounds the clamped tube condition with no tube deformation, i.e., the case corresponding to the Nuclear Regulatory Commission definition of denting with top tube support plate corrosion plus magnetite in the crevice without tube deformation. Figure 9-7 contains the results for the case where tube deformation is not present. These figures demonstrate the effects of varying the applied mean stress on the tube. Using the mean stress present in the undented results produces stress ratio values that are lower than stress ratios calculated for tubes in the dented condition.

As can be observed in Figures 9-6, Figure 9-7 and Table 9-3, most unsupported tubes fall in the acceptance region with respect to U-bend fatigue. Four tubes however, do not. These are tubes row 12 columns 106 through 109 (shown as mirror image corresponding columns 6 through 9 in Figures 9-6 and

9-7) and have stress ratios that either exceed or approach 1.0. These four tubes are recommended to be removed from service either by installing sentinel plugs or plugged with solid plugs if a cable tube damper is installed. Note that it appears the tube row 12 column 3 (and corresponding column 112) have a stress ratio equal to or greater than 1.0. However, these tubes are supported in all four steam generators. In fact, steam generator 4, row 12, columns 106 through 109 are the only row 12 tubes in any of the four steam generators that are unsupported by AVBs.

An evaluation has also been performed to determine the required relative flow peaking that will produce a stress ratio not greater than 1.0. Figure 9-8 contains the results of this process for all tubes in Rows 8 through 12. The figure was generated using the conditions outlined previously with the additional constraint that the tubes are dented. Note that this figure reads opposite of the previous figures, i.e., the top curve in the figure corresponds to Row 8 and the bottom curve corresponds to Row 12. Maximum Allowable Relative Flow Peaking is the required relative flow peaking ([ ]^{a,c} corresponds to no flow peaking) which, if used on the given tube, will produce a stress ratio (with denting) not to exceed 1.0. This curve can be used to identify the relative flow peaking required before preventive action would be recommended and, when used in conjunction with the actual flow peaking associated with each tube, to determine the margin (if any) present. This has also been performed in Table 9-3. The column with the heading "Max Allow Relative Flow Peaking" identifies the relative flow peaking factor that would be permitted, on a tube-by-tube basis, before the stress ratio criteria would be exceeded. As can be observed in the table and figure, the inner row tubes have larger values of allowable relative flow peaking when compared to the outer rows.

9.4 CUMULATIVE FATIGUE USAGE

All unsupported tubes having stress ratios $\leq$ 1.0 will have a maximum stress amplitude that is < 4.0 ksi (from 9.5 ksi), since a 10% reduction in the stability ratio for the North Anna Row 9 Column 51 tube was the criteria basis. The stability ratios for the Watts Bar Unit 2 tubing are based on the limiting operating parameters (MUR with 10% tube plugging) defined in Section 7 and with future operation on the same basis. The tubes are not expected to rupture as a result of fatigue if 1) they meet the stress ratio criteria of $\leq$1.0 and 2) their future fatigue usage will total less than 1.0.

Based on the above analyses, all of the unsupported Watts Bar Unit 2 tubes meet the relative stress ratio criteria except the Steam Generator 4 row 12 columns 106 through 109 tubes. Table 9-3 provides a summary of the combined relative stability ratios and the stress ratios for salient unsupported tubes in Rows 8 through 12.

Final acceptability of the Watts Bar Unit 2 tubing for fatigue is accomplished by demonstrating the acceptability of the tube with the highest stress ratio that is recommended to remain in service. (Which ratio must not exceed the stress ratio criteria of 1.0). For Watts Bar Unit 2 this tube is SG-4 R11C110 and has a stress ratio of [ ]^{a,c} for the analyzed cycle (operating conditions defined in Table 7-2.) Assuming this worst case tube (R11C110) will be dented in the first cycle; the total usage for the 40 year operating license would be 0.254.

9.5 CONCLUSIONS

As a result of the above, it is recommended that Steam Generator 4 Row 12 Column 106 through 109 tubes be removed from service. These tubes should either be plugged with sentinel plugs or plugged with solid plugs if a cable tube damper is installed. For all other tubes it is not necessary to recommend preventative action since the stress ratios and total cumulative fatigue usage of all the other unsupported U-bend tubes did not exceed the limiting value of 1.0. Steam generator tubes at Watts Bar Unit 2 (other than the four recommended to be removed from service above) are not expected to be susceptible to high-cycle fatigue rupture at the top tube support plate in a manner similar to the rupture that occurred at North Anna Unit 1. This conclusion applies to both the current specified operating conditions and to MUR uprate power operating conditions.

9.6 REFERENCES

9-1 Westinghouse Document WCAP-12546, Revision 0, "Watts Bar Unit 1 Evaluation for Tube Vibration Induced Fatigue," April 1990.

9-2 Westinghouse Research & Development Report 77-1D2-TUCOR-R2, "Residual Stresses in Inconel 600 Steam Generator Tubes - Part II: Straight Tubes," Westinghouse Research Laboratories, Proprietary Class 2, D. L. Harrod, October 21, 1977.

Table 9-1 100% Power Operating Parameters - Watts Bar Unit 2 Bounding Values for Mean Stress Calculations

a,c

-				

Table 9-2 Tube Mean Stress Calculation – Watts Bar Unit 2

Dist from TSP Midplane	1000 psi Internal Pressure Stress				1.0 Mil Interference at TSP Stress				100% Power Combined Loads Stress			
	Inside Surface		Outside Surface		Inside Surface		Outside Surface		Inside Surface		Outside Surface	
Inches	Axial	Hoop	Axial	Hoop	Axial	Hoop	Axial	Hoop	Axial	Hoop	Axial	Hoop

a,c

Table 9-2 Tube Mean Stress Calculation – Watts Bar Unit 2 (Continued)

a,c

Table 9-3 Watts Bar Unit 2 – Tubes with Significant Relative Stability Ratios and Stress Ratios

S/G	Row	Column	Relative Flow Peaking Ratio	RSR With Flow Peak	Stress Ratio With Denting	Stress Ratio Without Denting	Maximum Allowable Relative Flow Peaking	Remove From Service

a,c

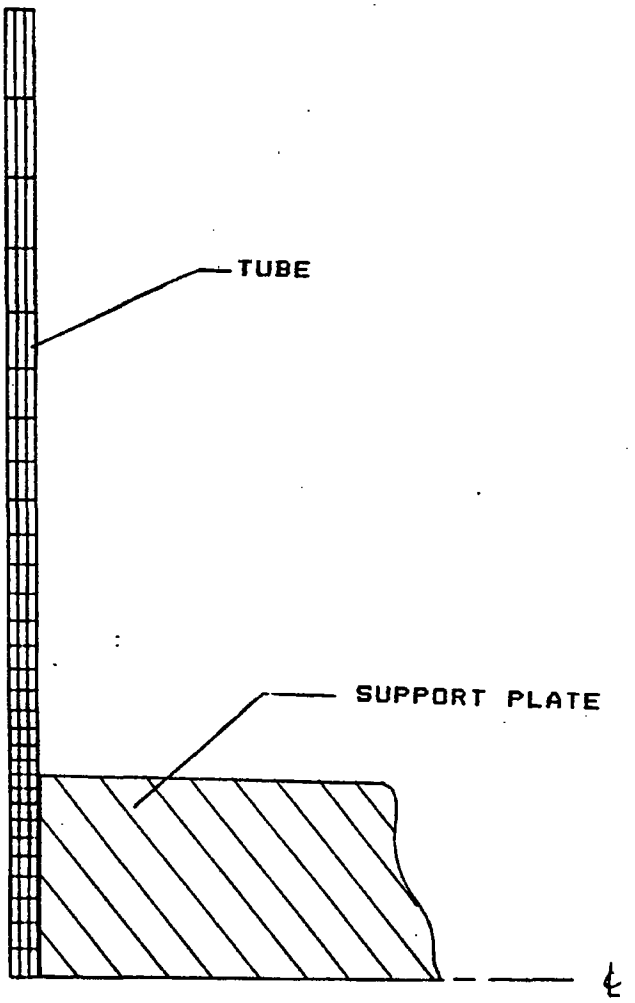

Figure 9-1 Axisymmetric Tube Finite Element Model

Figure 9-2 Dented Tube Stress Distribution - Pressure Load on TubePressure = 1000 psi - Outside Surface

Figure 9-3 Dented Tube Stress Distributions - Interference Load on Tube


a,c

Figure 9-4 Dented Tube Stress Distributions Combined Stress Results for Watts Bar Unit 2

a,c

Figure 9-5 Relative Stability Ratios Using MEVF Dependent Damping: Watts Bar Unit 2 (Composite of All Steam Generators with Umbrella Flow Peaking)

Figure 9-6 Stress Ratio vs. Column Number - Dented Condition Watts Bar Unit 2 (Composite of All Steam Generators with Umbrella Flow Peaking)

Figure 9-7 Stress Ratio vs. Column Number – Undented Condition Watts Bar Unit 2 (Composite of All Steam Generators with Umbrella Flow Peaking)


a,c

Figure 9-8 Maximum Allowable Relative Flow Peaking – Watts Bar Unit 2

Enclosure 3

WEC non-proprietary document CWA-12-3414, "Application for Withholding Information From Public Disclosure WBT-D-3807 P-Enclosure, "Watts Bar Unit 2 Evaluation for Tube Vibration Induced Fatigue," dated February 2012.

Westinghouse Electric Company
Nuclear Services
1000 Westinghouse Drive
Cranberry Township, Pennsylvania 16066
USA

U.S. Nuclear Regulatory Commission
Document Control Desk
11555 Rockville Pike
Rockville, MD 20852

Direct tel: (412) 374-4643
Direct fax: (724) 720-0754
e-mail: greshaja@westinghouse.com
Proj letter: WBT-D-3807

CAW-12-3414

February 28, 2012

APPLICATION FOR WITHHOLDING PROPRIETARY INFORMATION FROM PUBLIC DISCLOSURE

Subject: WCAP-17309-P, Revision 1, "Watts Bar Unit 2 Evaluation for Tube Vibration Induced Fatigue" (Proprietary)

The proprietary information for which withholding is being requested in the above-referenced report is further identified in Affidavit CAW-12-3414 signed by the owner of the proprietary information, Westinghouse Electric Company LLC. The affidavit, which accompanies this letter, sets forth the basis on which the information may be withheld from public disclosure by the Commission and addresses with specificity the considerations listed in paragraph (b)(4) of 10 CFR Section 2.390 of the Commission's regulations.

Accordingly, this letter authorizes the utilization of the accompanying affidavit by Tennessee Valley Authority.

Correspondence with respect to the proprietary aspects of the application for withholding or the Westinghouse affidavit should reference CAW-12-3414 and should be addressed to J. A. Gresham, Manager, Regulatory Compliance, Westinghouse Electric Company, Suite 428, 1000 Westinghouse Drive, Cranberry Township, Pennsylvania 16066.

Very truly yours,

J. A. Gresham, Manager
Regulatory Compliance

Enclosures

CAW-12-3414

AFFIDAVIT

COMMONWEALTH OF PENNSYLVANIA:

ss

COUNTY OF BUTLER:

Before me, the undersigned authority, personally appeared J. A. Gresham, who, being by me duly sworn according to law, deposes and says that he is authorized to execute this Affidavit on behalf of Westinghouse Electric Company LLC (Westinghouse), and that the averments of fact set forth in this Affidavit are true and correct to the best of his knowledge, information, and belief:

J. A. Gresham, Manager
Regulatory Compliance

Sworn to and subscribed before me
this 28th day of February 2012

Notary Public

COMMONWEALTH OF PENNSYLVANIA
Notarial Seal
Cynthia Olesky, Notary Public
Manor Boro, Westmoreland County
My Commission Expires July 16, 2014
Member, Pennsylvania Association of Notaries

(1) I am Manager, Regulatory Compliance, in Nuclear Services, Westinghouse Electric Company LLC (Westinghouse), and as such, I have been specifically delegated the function of reviewing the proprietary information sought to be withheld from public disclosure in connection with nuclear power plant licensing and rule making proceedings, and am authorized to apply for its withholding on behalf of Westinghouse.

(2) I am making this Affidavit in conformance with the provisions of 10 CFR Section 2.390 of the Commission's regulations and in conjunction with the Westinghouse Application for Withholding Proprietary Information from Public Disclosure accompanying this Affidavit.

(3) I have personal knowledge of the criteria and procedures utilized by Westinghouse in designating information as a trade secret, privileged or as confidential commercial or financial information.

(4) Pursuant to the provisions of paragraph (b)(4) of Section 2.390 of the Commission's regulations, the following is furnished for consideration by the Commission in determining whether the information sought to be withheld from public disclosure should be withheld.

(i) The information sought to be withheld from public disclosure is owned and has been held in confidence by Westinghouse.

(ii) The information is of a type customarily held in confidence by Westinghouse and not customarily disclosed to the public. Westinghouse has a rational basis for determining the types of information customarily held in confidence by it and, in that connection, utilizes a system to determine when and whether to hold certain types of information in confidence. The application of that system and the substance of that system constitutes Westinghouse policy and provides the rational basis required.

Under that system, information is held in confidence if it falls in one or more of several types, the release of which might result in the loss of an existing or potential competitive advantage, as follows:

(a) The information reveals the distinguishing aspects of a process (or component, structure, tool, method, etc.) where prevention of its use by any of

Westinghouse's competitors without license from Westinghouse constitutes a competitive economic advantage over other companies.

(b) It consists of supporting data, including test data, relative to a process (or component, structure, tool, method, etc.), the application of which data secures a competitive economic advantage, e.g., by optimization or improved marketability.

(c) Its use by a competitor would reduce his expenditure of resources or improve his competitive position in the design, manufacture, shipment, installation, assurance of quality, or licensing a similar product.

(d) It reveals cost or price information, production capacities, budget levels, or commercial strategies of Westinghouse, its customers or suppliers.

(e) It reveals aspects of past, present, or future Westinghouse or customer funded development plans and programs of potential commercial value to Westinghouse.

(f) It contains patentable ideas, for which patent protection may be desirable.

There are sound policy reasons behind the Westinghouse system which include the following:

(a) The use of such information by Westinghouse gives Westinghouse a competitive advantage over its competitors. It is, therefore, withheld from disclosure to protect the Westinghouse competitive position.

(b) It is information that is marketable in many ways. The extent to which such information is available to competitors diminishes the Westinghouse ability to sell products and services involving the use of the information.

(c) Use by our competitor would put Westinghouse at a competitive disadvantage by reducing his expenditure of resources at our expense.

(d) Each component of proprietary information pertinent to a particular competitive advantage is potentially as valuable as the total competitive advantage. If competitors acquire components of proprietary information, any one component may be the key to the entire puzzle, thereby depriving Westinghouse of a competitive advantage.

(e) Unrestricted disclosure would jeopardize the position of prominence of Westinghouse in the world market, and thereby give a market advantage to the competition of those countries.

(f) The Westinghouse capacity to invest corporate assets in research and development depends upon the success in obtaining and maintaining a competitive advantage.

(iii) The information is being transmitted to the Commission in confidence and, under the provisions of 10 CFR Section 2.390, it is to be received in confidence by the Commission.

(iv) The information sought to be protected is not available in public sources or available information has not been previously employed in the same original manner or method to the best of our knowledge and belief.

(v) The proprietary information sought to be withheld in this submittal is that which is appropriately marked in WCAP-17309-P, Revision 1, "Watts Bar Unit 2 Evaluation for Tube Vibration Induced Fatigue" (Proprietary), dated February 2012, for submittal to the Commission, being transmitted by Tennessee Valley Authority letter and Application for Withholding Proprietary Information from Public Disclosure, to the Document Control Desk.

This information is part of that which will enable Westinghouse to:

(a) Support licensing of Watts Bar Unit 2.

Further this information has substantial commercial value as follows:

(a) The information requested to be withheld reveals the distinguishing aspects of a methodology which was developed by Westinghouse.

Public disclosure of this proprietary information is likely to cause substantial harm to the competitive position of Westinghouse because it would enhance the ability of competitors to provide similar technical evaluation justifications and licensing defense services for commercial power reactors without commensurate expenses. Also, public disclosure of the information would enable others to use the information to meet NRC requirements for licensing documentation without purchasing the right to use the information.

The development of the technology described in part by the information is the result of applying the results of many years of experience in an intensive Westinghouse effort and the expenditure of a considerable sum of money.

In order for competitors of Westinghouse to duplicate this information, similar technical programs would have to be performed and a significant manpower effort, having the requisite talent and experience, would have to be expended.

Further the deponent sayeth not.

PROPRIETARY INFORMATION NOTICE

Transmitted herewith are proprietary and/or non-proprietary versions of documents furnished to the NRC in connection with requests for generic and/or plant-specific review and approval.

In order to conform to the requirements of 10 CFR 2.390 of the Commission's regulations concerning the protection of proprietary information so submitted to the NRC, the information which is proprietary in the proprietary versions is contained within brackets, and where the proprietary information has been deleted in the non-proprietary versions, only the brackets remain (the information that was contained within the brackets in the proprietary versions having been deleted). The justification for claiming the information so designated as proprietary is indicated in both versions by means of lower case letters (a) through (f) located as a superscript immediately following the brackets enclosing each item of information being identified as proprietary or in the margin opposite such information. These lower case letters refer to the types of information Westinghouse customarily holds in confidence identified in Sections (4)(ii)(a) through (4)(ii)(f) of the affidavit accompanying this transmittal pursuant to 10 CFR 2.390(b)(1).

COPYRIGHT NOTICE

Tennessee Valley Authority

Letter for Transmittal to the NRC

The following paragraphs should be included in your letter to the NRC Document Control Desk:

Enclosed are:

1. __ copies of WCAP-17309-P, Revision 1, "Watts Bar Unit 2 Evaluation for Tube Vibration Induced Fatigue" (Proprietary)

2. __ copies of WCAP-17309-NP, Revision 1, "Watts Bar Unit 2 Evaluation for Tube Vibration Induced Fatigue" (Non-Proprietary)

Also enclosed is the Westinghouse Application for Withholding Proprietary Information from Public Disclosure CAW-12-3414, accompanying Affidavit, Proprietary Information Notice, and Copyright Notice.

As Item 1 contains information proprietary to Westinghouse Electric Company LLC, it is supported by an affidavit signed by Westinghouse, the owner of the information. The affidavit sets forth the basis on which the information may be withheld from public disclosure by the Commission and addresses with specificity the considerations listed in paragraph (b)(4) of Section 2.390 of the Commission's regulations.

Accordingly, it is respectfully requested that the information which is proprietary to Westinghouse be withheld from public disclosure in accordance with 10 CFR Section 2.390 of the Commission's regulations.

Correspondence with respect to the copyright or proprietary aspects of the items listed above or the supporting Westinghouse affidavit should reference CAW-12-3414 and should be addressed to J. A. Gresham, Manager, Regulatory Compliance, Westinghouse Electric Company, Suite 428, 1000 Westinghouse Drive, Cranberry Township, Pennsylvania 16066.